The Effects of K-Metasomatism on the Mineralogy and Geochemistry of Silicic Ignimbrites near Socorro, New Mexico

by

David J. Ennis

A thesis submitted to the Department of Earth and Environmental Science in partial fulfillment of the requirements for the degree of Master of Science in Geochemistry

New Mexico Institute of Mining and Technology

Socorro, New Mexico

August, 1996

Abstract

K-metasomatism of Cenozoic rocks, including the upper Lemitar and Hells Mesa silicic ignimbrites, has occurred near Socorro, New Mexico, likely as the result of the downward percolation of alkaline, saline brines in a hydrologically closed basin. One result of K-metasomatism is the dissolution of Na-rich phases, primarily plagioclase, and the formation of secondary mineral phases. Based on XRD and semi-quantitative clay mineral analysis, the alteration assemblage produced by alteration of plagioclase consists of adularia, quartz, mixed layer illite-smectite (I/S), kaolinite, discrete smectite and illite, minor calcite and barite. Some remnant plagioclase also remains as a result of incomplete dissolution. Kaolinite and barite likely result from localized hydrothermal events that are superimposed on the metasomatic alteration. A hydrothermal origin for kaolinite is suggested due to acidic conditions necessary for its formation and stability whereas K-metasomatism in the Socorro area is believed to be an alkaline alteration process. Adularia, a low-temperature K-feldspar, is the dominant mineral produced during K-metasomatic alteration. Scanning electron microscope (SEM) and electron microprobe analysis indicate the stability of mixed-layer I/S and discrete smectite in the assemblage. The formation of discrete smectite within the assemblage during K-metasomatism may have occurred during periods of low cation / H^+ ratios in the alkaline, saline brine. Upon an increase in the cation / H^+ ratio, possibly due to an increase in evaporation of the alkaline lake, the solution may have become sufficiently concentrated to cause illitization of smectite resulting in the formation of mixed-layer I/S within the assemblage. Data also suggests formation of the alteration assemblage as a result of coprecipitation, although

direct evidence for this is elusive. Electron microprobe backscattered images and element maps strongly suggest a dissolution-precipitation reaction for K-metasomatism in the Socorro area as indicated by the presence of dissolution embayments in plagioclase crystals, the presence of crystalline adularia, and the common occurrence of authigenic clay minerals in the assemblage.

In addition to changes in the mineralogy, K-metasomatism also caused significant chemical modification of the silicic ignimbrites. Adularia abundance positively correlates with K_2O and Rb content of whole rock samples, whereas there is a negative correlation for Na_2O, CaO, and Sr. The correlation between Rb and K_2O suggests that Rb is enriched during alteration due to substitution for K in the crystal lattice of adularia. High concentrations of elements such as Ba, As, Sb, Pb and Cs likely reflect enrichment due to hydrothermal overprinting, however low levels of As and possibly Ba and Sb are related to enrichment through K-metasomatism. Several major element oxides and trace elements such as SiO_2, TiO_2, Al_2O_3, Y, Zr, and Nb show no systematic variation in K-metasomatized rocks, thus suggesting that no mass gain or loss occurred during metasomatism thereby, allowing for evaluation of primary compositional zonation of the upper Lemitar and Hells Mesa Tuffs.

Rare earth element (REE) concentrations also show variability in the two silicic ignimbrites as a result of alteration, which is dissimilar to other studies of K-metasomatism. Notably, middle and heavy REE are depleted in the upper Lemitar Tuff and enriched in the Hells Mesa Tuff, whereas light REE show little to no systematic variation. Data from this study suggest attempted partial equilibration between the

mineral assemblage and the altering fluid as the most likely mechanism for redistribution of REE within the units. Enrichment and depletion of REE in the alteration assemblage suggests that the initial REE content of plagioclase, relative to the fluid REE content, may have been responsible for the resultant change in REE concentration. Initial data imply incorporation of REE into clay minerals, although this is somewhat speculative.

Stable isotope data collected on both whole rock and separated samples indicate significant enrichment of $\delta^{18}O$, however the mechanism responsible for this enrichment is not conclusive due to poor temperature constraints. The $\delta^{18}O$ values obtained are consistent with either low-temperature equilibration with meteoric water or high-temperature equilibration with an isotopically heavier water. However, preliminary temperature data and additional geologic constraints suggest a low-temperature regime for the Socorro K-anomaly.

Acknowledgements

I gratefully acknowledge my advisors Nelia Dunbar and Andrew Campbell as well as the rest of my committee, Chuck Chapin and Peter Mozley, all of whom provided encouragement, support, and helpful discussions. I especially thank Nelia for many reviews of the manuscript and Andy for constructive suggestions. I am also thankful to the New Mexico Bureau of Mines and Mineral Resources and Director Chuck Chapin for providing financial support and for allowing use of official vehicles for field and analytical work.

My appreciation also goes to Richard Chamberlain, George Austin, Chris McKee, and Mike Spilde at the University of New Mexico for SEM and Electron Microprobe assistance. A special thanks to Phil Kyle who went beyond the call of duty to help me get XRF and INAA data in a timely fashion. XRF analysis was done at the New Mexico Tech X-Ray Fluorescence Facility for which partial funding was provided by NSF grant EAR93-16467. Wilma and Clint Kelly allowed access to their private land in the Lemitar Mountains.

A hardy handshake to those who have helped me in the field: Robert 'Geobob' Appelt, Steve 'maximum grade, minimal effort' Deal, Tim Pease, Hal Newell, and Dan Miggins. Thanks also goes to my bullpen officemates Geobob and Tim for much needed slacking and for helping me 'get metasomatized' when necessary.

I am also thankful to my parents and family for their continued encouragement and support. Finally, my thanks to Melissa for her patience, understanding, and dedication throughout the years.

Table of Contents

List of Figures

List of Tables

Introduction

A number of areas of the western United States, in particular areas of basin and range extension, show characteristics of surface enrichment of K that appears to postdate rock deposition (Duval, 1990). Many of these areas, including the area around Socorro, New Mexico, are thought to be caused by K-metasomatism (Chapin and Lindley, 1986), which is a secondary alteration process caused by interaction between a K-rich fluid and the surrounding rock. During K-metasomatism, potassium and various elements become concentrated while other elements are depleted in the altered rock. Commonly associated with this type of alteration is the deposition of elements of economic interest, which has been recognized in some areas (Glazner, 1988; Roddy et al., 1988) including the Socorro area (Eggleston et al., 1983). However, the chemical processes and composition of the altering fluid in the Socorro area are poorly understood.

The origin of K-metasomatism has been explained through many different models including a magmatic origin (Shafiquallah et al., 1976; Rehrig et al., 1980); as a result of hydrogen metasomatized basement rocks from deep within the rock complex (Glazner, 1988); or from the percolation of low temperature alkaline, saline waters within a hydrologically closed basin (Chapin and Lindley, 1986; Leising et al., 1995; Turner and Fishman, 1991). The aim of this study is to investigate the mineralogical and chemical alteration that occurs within two rhyolitic ignimbrite sheets, the upper Lemitar and the Hells Mesa Tuffs, as a function of intermediate to advanced degrees of K-metasomatism. Specifically, the objective is to study the mobility of major and trace elements with respect to the alteration assemblage formed during K-metasomatism. The upper Lemitar and

Hells Mesa ignimbrites are particularly appropriate because these units are quite voluminous and extend into and beyond the K-anomaly, thus providing the opportunity to systematically study the alteration in areas where the ignimbrites are unaltered, partially altered, and highly altered (Chapin and Lindley, 1986).

Background on K-Metasomatism

Many areas that have undergone regional crustal extension show evidence of K-metasomatism of volcanic and sedimentary rocks along regional, low-angle normal faults or 'detachment faults' (Davis and others, 1986). Evidence for K-metasomatism associated with regional extension is reported by Brooks (1986) at Picacho Peak, Roddy et al. (1988) in the Harcuvar Mountains in Arizona, and by Glazner (1988) in the Sleeping Beauty area, Central Mojave Desert. Glazner (1988) concludes that the added K in the Sleeping Beauty area is a result of circulating meteoric waters picking up K from basement rocks in exchange for H^+. The circulating water then deposits K and receives Na and Ca in exchange. Na and Ca are eventually removed from the system via surface hot springs.

The Socorro K-anomaly is interpreted to be the result of widespread alteration by alkaline, saline water derived from a large playa lake (Chapin and Lindley, 1986) for several reasons. First, the large areal extent affected by K-alteration is difficult to explain as a result of hydrothermal alteration. Although localized areas of hydrothermal activity are known to exist in the Socorro K anomaly, the magnitude of a magmatic system necessary to cause such a large alteration is not known to exist in the time frame when K-metasomatism was thought to be active. Based on $^{40}Ar/^{39}Ar$ radiometric dating, K-

metasomatism is confirmed to have occurred between 7.4 and 8.7 Ma, but possibly started as early as 15 Ma (Dunbar et al., 1994). In addition, the K-metasomatized rocks in the Socorro area are enriched in $\delta^{18}O$ (Chapin and Lindley, 1986; Dunbar, 1994), which is not indicative of fluids associated with a magmatic system, for most hydrothermal events tend to result in host rock depletion of $\delta^{18}O$. Lastly, the presence of thick playa deposits containing gypsum within the Socorro area suggest the occurrence of a long-lived alkaline, saline lacustrine environment. Once the closed lacustrine environment was established, the metasomatizing fluids may have been transported by vertical advection caused by salinity-induced density convection (Leising et al., 1995).

The potassic alteration is chemically and mineralogically distinctive, yet subtle (Agron and Bentor, 1981). The alteration process involves the selective replacement of plagioclase and other K-poor phases resulting in a metasomatically produced mineral assemblage consisting of K-feldspar (specifically adularia) + quartz ± montmorillonite ± illite ± mixed layer illite-montmorillonite. Adularia ($KAlSi_3O_8$) is a colorless, translucent variety of K-spar commonly found as pseudo-orthorhombic crystals (Deer, Howie, and Zussman, 1992). Some samples contain remnant plagioclase due to incomplete dissolution during alteration. Rocks affected by K-metasomatism commonly have a characteristic red-brown color due to the oxidation of groundmass magnetite resulting in the formation of hematite (Lindley, 1985).

Geologic Background

K-Metasomatic Alteration Area

The K-anomaly near Socorro, New Mexico is located in the northeast corner of the Mogollon-Datil volcanic field and is approximately L-shaped with an area of roughly 40-50 km on a side and 20 km in width (Figure 1). The area contains a sequence, oldest to youngest, of five silicic ignimbrites interbedded with mafic lava flows: Hells Mesa, La Jencia, Vicks Peak, Lemitar, and South Canyon Tuffs. Together, the stratigraphic thickness of the tuffs is approximately 500 m with ages ranging from Oligocene to early Miocene (Chapin and Lindley, 1986). Overlying the ignimbrites are volcaniclastic sedimentary rocks and fine-grained playa deposits known collectively as the Popotosa Formation (Osburn, 1978). Stratigraphically, the K alteration is restricted to units from the Hells Mesa Tuff through the basal Popotosa. Several thin layers of volcanic ash in the overlying playa clay deposits appear to be K- metasomatized, while a 4 Ma basalt flow, which overlies the playa clays, is not affected by the alteration (Osburn and Chapin, 1983). Vertical controls for K-metasomatism appear to be permeability and composition of the host rocks, whereas horizontal controls were likely permeability, salinity, and possibly the temperature of the altering fluids (Chapin and Lindley, 1986). Several areas of hydrothermal activity are known to overprint the K-metasomatic alteration including the Luis Lopez manganese district, Socorro Peak district, and the Lemitar and Magdalena Mountains districts.

The Socorro K-metasomatized area was recognized by D'Andrea-Dinkelman and others (1983) to coincide spatially with the Rio Grande rift valley, an area

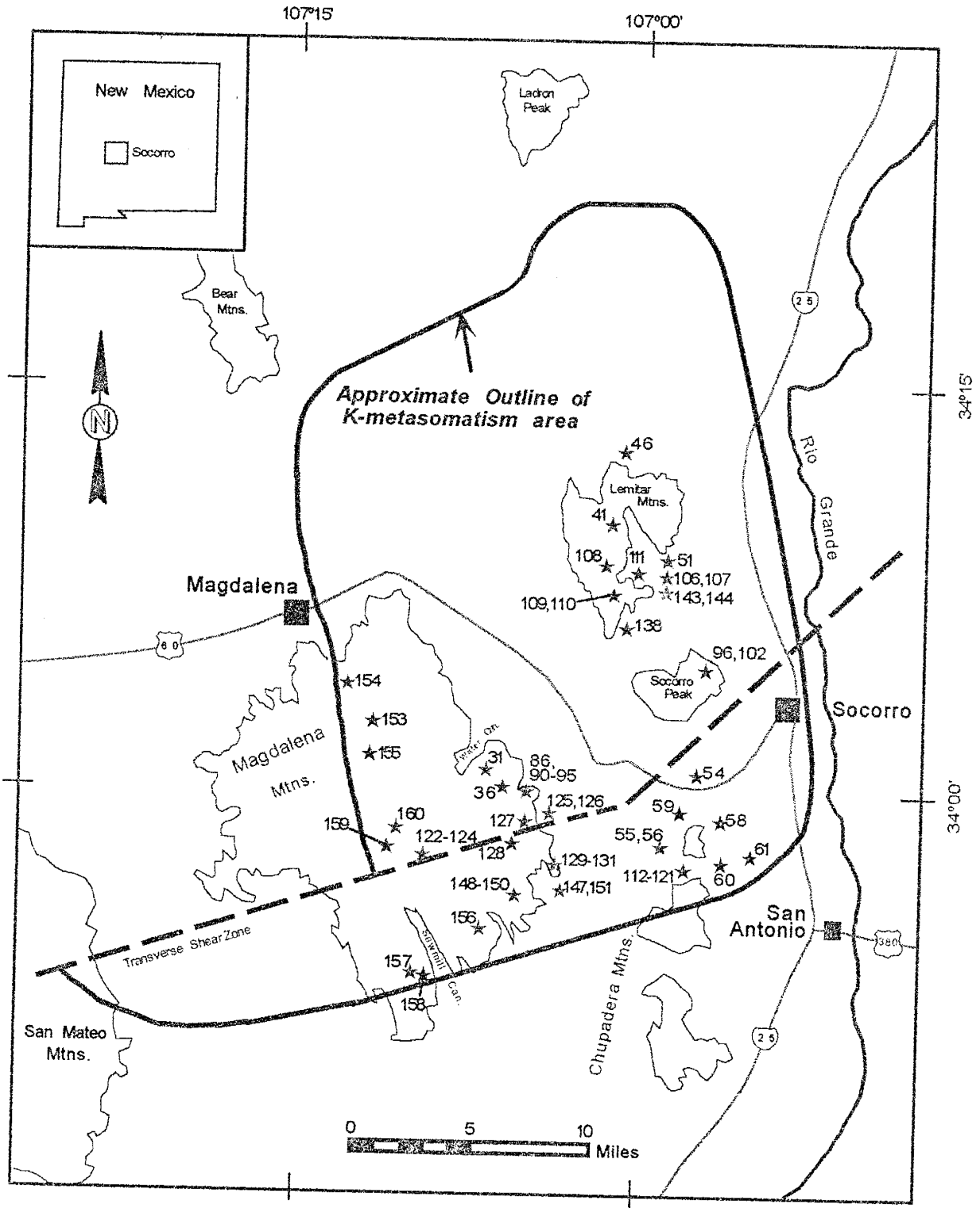

Figure 1: Map of the Socorro K-metasomatism area after Lindley (1985). Red stars: upper Lemitar Tuff samples, Blue stars: Hells Mesa Tuff samples. Samples numbered with a hyphen are inclusive; i.e. 112 through 121.

of unusually high crustal extension (20-100%) in which domino-style normal faulting and strong rotation of beds (25-70°) occurs throughout. Chapin et al. (1978) have recognized two domains of domino-style fault blocks in the metasomatized area: the northern portion dips to the west and the southern section is east-dipping (See Figure 1). The two domains are separated by a transverse shear zone (the Socorro accommodation zone) which is a null line across which the direction of tilting changes (Chapin, 1983). This style of extension is commonly associated with K_2O enrichment as noted by Roddy et al. (1988), Glazner (1988), and Brooks (1986).

Highly metasomatized volcanic rocks in the Socorro, New Mexico area are chemically distinctive. K_2O contents are as high as 13.5 wt. % while Na_2O, CaO and MgO are typically each depleted to 1 wt. % or less (Chapin and Lindley, 1986). K_2O/Na_2O ratios have been found to be as high as 14.2 within the anomaly, thus providing a useful index to the degree of K-metasomatism. Other chemical changes accompanying K-metasomatism in the Socorro area include increases in Rb and Ba along with decreases in Sr, Mn and Mg (Chapin and Lindley, 1986). Isotopically, $\delta^{18}O$ increases in whole rock rhyolitic tuffs from approximately +8 to +10 per mil, typical of unaltered rock, to +11 to +13 per mil within the metasomatized area. Phenocrystic quartz and sanidine retain their magmatic values of approximately +8 and +7 per mil, respectively, indicating that these minerals are basically unaffected by the K-metasomatic alteration (Chapin and Lindley, 1986).

The Socorro K-anomaly provides an excellent opportunity to study the alteration due to its size, which is approximately 1800 km^2, and the fact that five regional ash flow

tuffs extend into and beyond the anomaly, thus providing the opportunity to systematically study the alteration in areas where the ash-flows are unaltered, partially altered and highly altered (Chapin and Lindley, 1986).

Ignimbrites

Lemitar Tuff

The Lemitar Tuff was emplaced at 28 Ma ± 0.08 (McIntosh et al., 1990) and is present throughout the Socorro area. The Lemitar Tuff is a multiple-flow, compositionally zoned, rhyolitic ignimbrite (Chapin et al., 1978) consisting of two members. The lower member is a crystal-poor, light-gray to pale-red unit, whereas the upper member is a crystal-rich, medium-red unit (Osburn, 1978). The upper member of the Lemitar Tuff is of the most interest for this study due to the crystal-rich nature of this unit and the presence of plagioclase, a phase that is strongly altered during metasomatism. The vertical zonation of phenocrysts within the Lemitar Tuff is very distinct and is often the most diagnostic feature of the ignimbrite (Ferguson, 1985). The upper member grades from 17 percent total phenocrysts at the base to between 30 and 40 percent phenocrysts near the top, with sanidine being the dominant phenocryst, ranging from 12 to 25 percent of the total phenocrysts present (D'Andrea, 1981; Ferguson, 1985). Plagioclase is relatively abundant in the upper member and averages 10 percent of the total phenocrysts present, but it is often as plentiful as 15 percent. The basal portion of the upper member tends to contain between 5 to 10 percent plagioclase. Quartz is present in as much as 10 percent of the total phenocrysts in the upper member and is typically subhedral to

rounded. Biotite, magnetite, clinopyroxene, sphene, and zircon are also found within the upper member, but only in minor to trace amounts (D'Andrea, 1981).

Hells Mesa Tuff

The Hells Mesa Tuff is a crystal-rich, densely welded, simple cooling unit of rhyolitic to quartz latitic composition. Chapin et al. (1978) found the Hells Mesa Tuff to be reversely zoned with a mafic, quartz-poor base grading into a more silicic, quartz-rich upper portion. This ash-flow tuff contains both plagioclase and K-feldspar, and was emplaced at 32.06 Ma ± 0.10 (McIntosh et al., 1990). The Hells Mesa Tuff has been estimated to contain 35 to 45 percent phenocrysts with 10 to 30 percent of those being sanidine. Plagioclase represents 4 to 10 percent of the total phenocrysts present and often averages approximately 8 percent (Deal, 1973). Up to 12 percent of the phenocrysts may be quartz which is typically found to be sub-angular to rounded in shape (Lindley, 1979). Present in minor to trace quantities are biotite, clinopyroxene, sphene, and lithic fragments (D'Andrea, 1981).

Areas of Hydrothermal Alteration

Luis Lopez Manganese District

The Luis Lopez manganese district, located in the northern Chupadera Mountains, southwest of Socorro, New Mexico (See Figure 1), is located on an intra-rift horst consisting of lavas and ash-flow tuffs of mafic to felsic composition. The Luis Lopez manganese district is peripheral to a zone of red alteration, which shows a distinct

depletion in MnO; from .05% in unaltered rocks to .005% in altered rocks (Eggleston et al., 1983). This zone of red alteration is overprinted on the regional K-metasomatism anomaly. Psilomelane is the primary manganese phase in the Luis Lopez district. The mineralization occurs as open-space fillings in fault breccias and fault openings (Norman and others, 1983). Structural evidence suggests the manganese was deposited between 7 and 3 Ma (Eggleston et al., 1983; Chamberlin, 1980). The host rocks in the northern portion of the Luis Lopez manganese district are the upper and lower members of the Lemitar Tuff, while the Hells Mesa Tuff is the host rock in the southern portion of the district. Vein-related, wall-rock alteration is notably absent in all of the deposits in the district (Eggleston et al., 1983; Norman et al., 1983).

Roy (1981) states that psilomelane generally occurs either in surface environments, in the shallow, low-temperature part of veins or in thermal spring deposits. Norman et al. (1983) propose that the Luis Lopez district is the surface expression of an extensive hydrothermal system. A hydrothermal system is indicated by the size of the district, the common occurrence of manganese oxides high in hydrothermal systems, the report of anomalous Ag and W in the deposits (Willard, 1973), and a distinct association of manganese with other precious mineralization such as gold-silver and molybdenum-tungsten. The hydrothermal alteration responsible for the formation of the Luis Lopez manganese district is younger than the K-metasomatic event and therefore overprints the regional K-anomaly (Eggleston et al., 1983; Norman et al., 1983). Gangue minerals associated with the manganese deposits include calcite, hematite, and quartz with rare barite and fluorite (Norman et al., 1983).

Socorro Peak District

The major ore deposits of the Socorro Peak district contain silver-bearing minerals and occur as veins along faults in the Socorro Peak Rhyolite (late Miocene) and the underlying Popotosa Formation (North, 1983). In comparison to the Luis Lopez manganese district, much less has been reported on the Socorro Peak district, although it is known that this district was an important producer of silver in the 1880's. The major ore mineral of the district is chlorargyrite (AgCl) which contains significant bromine. A small amount of galena is present with gangue minerals including barite and quartz with minor amounts of fluorite, calcite and manganese oxides (Lasky, 1932).

Magdalena Mountains (Water Canyon) District

Within this district, North (1983) notes at least three types of deposits: (1) veins associated with volcanic rocks, (2) vein, replacement, and skarn deposits in limestone, and (3) veins along faults between Paleozoic and Precambrian rocks. Mineralization is restricted to the north side of the South Canyon fault in the Hells Mesa Tuff and in white rhyolite dikes (Krewedl, 1974). The dominant sulfide is pyrite with minor amounts of chalcopyrite, galena, and sphalerite.

Lemitar Mountains District

The precious metal deposits of the Lemitar Mountains district occur as hydrothermal veins that tend to fill areas of high permeability. The deposits are likely

related to Tertiary igneous activity, although no large Tertiary intrusive rocks are exposed near the deposits (North, 1983). The majority of the mineralization consists of galena and malachite in a gangue of quartz, barite, fluorite, and calcite usually along the unconformable contact of Precambrian rocks and Paleozoic sediments.

Sampling and Analytical Methods

Sampling and Sample Preparation

Two silicic ignimbrites, the Hells Mesa Tuff and the upper Lemitar Tuff, were sampled in various areas of the K anomaly (See Figure 1). A total of 63 samples were collected, ranging in degree of alteration from nearly pristine to highly metasomatized. Where feasible, altered plagioclase was carefully hand-picked or drilled out from the interior of former plagioclase phenocrysts using a Foredom hand drill. Selective sampling of plagioclase phenocrysts, and other low-K phases, which typically show significant degrees of alteration within the metasomatized area, allow evaluation of the mineralogy produced by K-metasomatism. Four unaltered samples, two from each tuff unit, were examined in thin section in order to assess the degree to which plagioclase has been altered through weathering and diagenesis. Altered plagioclase was drilled out of a total of 41 samples. The removed, altered plagioclase crystals are hereafter called the 'separated samples.' Whole rock samples were crushed in a jawcrusher to approximately pebble sized grains then milled in a TEMA grinder with a tungsten-carbide inner container to <200 mesh.

Mineralogy

In order to determine the mineral assemblage present each separated sample was analyzed on a Rigaku DMAX-I X-ray diffractometer with Ni-filtered CuKα_1 (=1.5418 Å) radiation and JADE pattern-processing software. The receiving and scattering slits of the Rigaku XRD are, respectively, $^1/_2°$ and 4°. An initial 2θ angle of 2° and a final angle of

70° was used with the goniometer stepping at a rate of .05° every second. Operating conditions were an accelerating voltage of 40 kV and a sample current of 25 mA using a copper target. For XRD analysis, altered plagioclase was placed in an aluminum sample holder as an unoriented mount. Where applicable, semi-quantitative clay mineral analysis was performed on separated samples using three scans for each sample: airdried, saturated with ethylene glycol, and heated at 375°C for 30 min. The semi-quantitative nature of the technique allows for the determination of clay minerals to parts in ten (Austin per. comm.,1992). Scanning electron microscopy (SEM) analysis was performed on six carbon-coated sample chips using a Hitachi S450 equipped with an energy dispersive spectrometer (EDS).

Geochemistry

Two carbon-coated polished thin sections were examined at the University of New Mexico using a JEOL 733 electron microprobe (EMP) equipped with five wavelength dispersive spectrometers (WDS), one EDS, and one backscatter electron detector (BSE). Operating conditions for the EMP during analyses were an accelerating voltage of 15 kV, a beam diameter of 1-10 μm, a beam current of 20 nA and a count time of approximately 45 s. Standards used to calibrate the microprobe for this study include orthoclase (K), albite (Na, Al, and Si), olivine (Fe), and diopside (Mg and Ca). Element distribution maps were also obtained for the two samples with the microprobe.

X-ray fluorescence (XRF) analysis was performed on whole rock samples in order to determine the major and minor element chemistry. Analysis followed the procedure of

Norrish and Chappell (1977) using a Rigaku 3062 instrument at both the New Mexico Institute of Mining and Technology X-Ray Fluorescence Facility and the University of New Mexico. XRF operating conditions for the x-ray beam were 40 kV and 25 mA at both locations. Instrumental neutron activation analysis (INAA) was performed on whole rock and separated samples in order to determine trace element geochemistry of the samples. Whole rock samples were analyzed at X-Ray Assay Laboratories while analysis of the separated samples was performed at New Mexico Institute of Mining and Technology. Stable isotope geochemistry was performed on 13 separated samples at the New Mexico Institute of Mining and Technology.

RESULTS

Mineralogy

Mineral Abundances and Morphology

Fresh upper Lemitar and Hells Mesa Tuff samples examined in thin section show no significant signs of plagioclase alteration. One unaltered Hells Mesa Tuff sample does show a slight amount of plagioclase replacement by clay or possibly calcite, however, it is minor. Due to the unaltered nature of plagioclase in fresh upper Lemitar and Hells Mesa Tuff samples, the mineralogy found in the hand-picked (separated) samples is attributable to an alteration process other than weathering. The mineral assemblage of the hand-picked material from relict plagioclase grains was determined by XRD, semi-quantitative clay mineral analysis, and SEM investigation and was found to consist of variable combinations of adularia, quartz, kaolinite, mixed-layer illite-smectite (I/S), discrete smectite, discrete illite, remnant plagioclase and occasionally calcite and barite.

Adularia, a low-temperature potassic feldspar, is present in all 41 of the separated samples, in varying amounts (Table 1; Figure 2). In all samples examined using SEM, adularia consistently displays euhedral habit, indicative of an authigenic origin. Fine-grained quartz is also present in all 41 separated samples and is recognized by both XRD and SEM analysis. Typically, quartz displays an amorphous, globular habit when viewed by SEM. Residual plagioclase was found in 17 of the 41 separated samples and may be related to incomplete alteration. When viewed by SEM, remnant plagioclase consistently appears partially dissolved, indicating that it is chemically unstable (Figure 2). The unaltered nature of plagioclase prior to metasomatism suggests that it is chemically

Relative Percentages of Minerals in the Alteration Assemblage

Sample #	% Adul	% Plag	% Clay	Clay (ppt)	Sample #	% Adul	% Plag	% Clay	Clay (ppt)
KM-36*	67	0	33	Mx=6, Sm=3, I=1	KM-113	50	0	50	K=10
KM-41	78	11	11	K=10	KM-114	75	0	25	K=10
KM-46*	33	67	0	N/A	KM-115	67	0	33	K=10
KM-51*	50	0	50	Sm=10	KM-116	50	25	25	K=9, Mx=1
KM-54	50	0	50	Mx=8, Sm=1, K=1	KM-127	86	0	14	K=10
KM-55	89	0	11	Mx=9, I=1	KM-128	67	0	33	K=7, Mx=2, Sm=1
KM-56	91	0	9	Mx=10	KM-129	50	50	0	N/A
KM-58	67	0	33	K=9, Mx=1	KM-131	25	50	25	(flocculation)
KM-59	50	0	50	K=10	KM-144	89	0	11	Mx=7, K=2, Sm=1
KM-60	29	14	57	K=9, I=1	KM-148	20	80	0	N/A
KM-61*	25	25	50	K=7, Sm=3	KM-149	33	67	0	N/A
KM-86	75	0	25	K=9, Mx=1	KM-150	25	75	0	N/A
KM-90	83	0	17	(flocculation)	KM-153	100	0	0	N/A
KM-91	29	14	57	(flocculation)	KM-154	75	0	25	Mx=7, I=3
KM-94	33	0	67	Mx=7, I=2, Sm=1	KM-155	33	0	67	I=5, Mx=4, K=1
KM-95	86	0	14	K=7, Mx=3	KM-156	100	0	0	N/A
KM-96*	50	0	50	Mx=6, I=4	KM-157	12	38	50	K=6, Sm=4
KM-102	67	0	33	Mx=7, I=3	KM-158	57	29	14	K=6, Sm=4
KM-107	80	20	0	N/A	KM-159	83	0	17	I=5, Mx=5
KM-111*	55	27	18	Sm=9, Mx=1	KM-160	75	0	25	I=5, Mx=5
KM-112	75	0	25	K=10					

Table 1: Relative percentages of minerals within the alteration assemblage. Percentages are estimated using ratios of peak area from XRD patterns. Sm=smectite, Mx=mixed layer illite-montmorillonite, I=illite, K=kaolinite, N/A=not applicable due to absence of clay. 'Flocculation' indicates that clay is present in the alteration assemblage, however, semi-quantitative analysis was not able to be performed on that sample. * indicates samples examined by SEM.

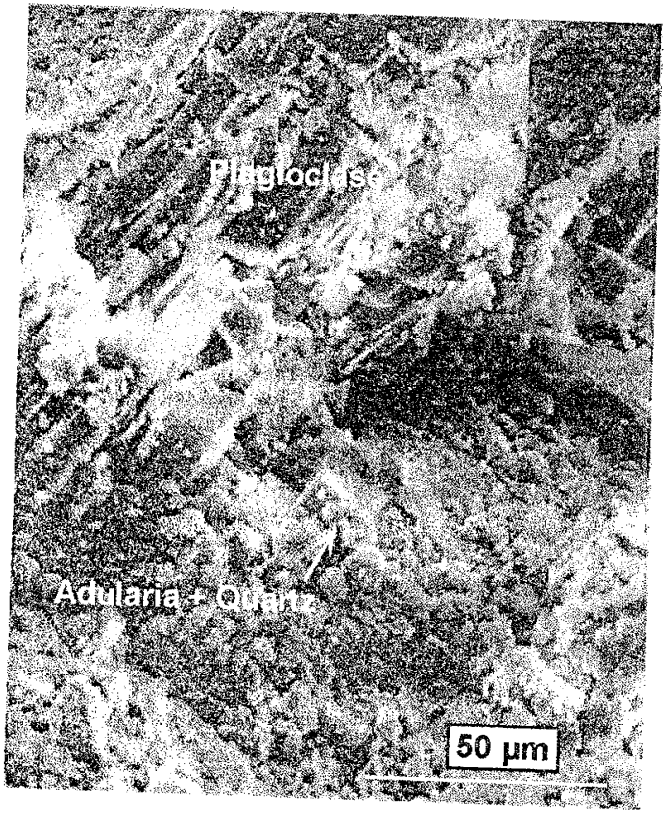

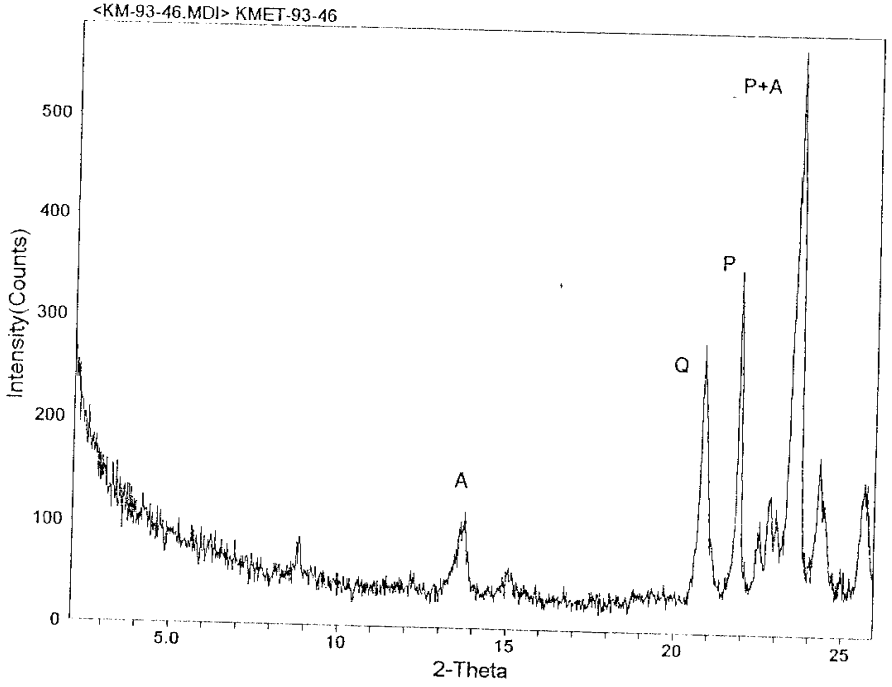

Figure 2: SEM photo of partially dissolved plagioclase with adularia and quartz. XRD pattern shows this same assemblage; plagioclase (P) at ~22.0° 2-Theta, adularia (A) at ~14.5° 2-Theta, and quartz (Q) at ~20.8° 2-Theta. Overlap of plagioclase and adularia at ~23.5° 2-Theta.

unstable during the conditions imposed during potassic alteration.

The alteration mineral assemblage also contains various amounts and types of clay minerals as determined by semi-quantitative clay analysis and reported in parts per ten of the total amount of clay present (Table 1). Clay minerals are commonly found in direct association with euhedral adularia and remnant plagioclase (Figure 3). The most common clay types are kaolinite and mixed-layer I/S with each being present in 19 of the separated samples. When present, kaolinite is typically a major clay constituent; 16 of the 19 samples have ≥5 parts per ten kaolinite. Kaolinite is observed as euhedral books in direct association with adularia, which appears to contain the imprint of the kaolinite books (Figure 4). Mixed-layer clay is also a major clay component and is found in quantities ≥5 parts per ten in 11 of the 19 separated samples. From Figure 5, the mixed-layer clay present appears to be either metastable or near equilibrium with adularia, for both minerals show no apparent indication of dissolution when in the same assemblage.

In contrast to the relatively large quantities and frequent occurrence of kaolinite and mixed-layer I/S, significant abundances of discrete smectite and discrete illite are relatively uncommon in the alteration assemblage. Large quantities of discrete smectite are extremely rare in the alteration assemblage with only 2 of the 41 separated samples having ≥5 parts per ten smectite, yet trace quantities are found in 12 samples. When present, smectite tends to be subhedral and typically coats euhedral adularia crystals (Figure 6). Discrete illite is equally scarce with only 3 samples containing ≥5 parts per ten illite in the alteration assemblage and trace amounts in 9 of the 41 samples. Table 1 contains the relative percentages of the minerals present within the alteration assemblage

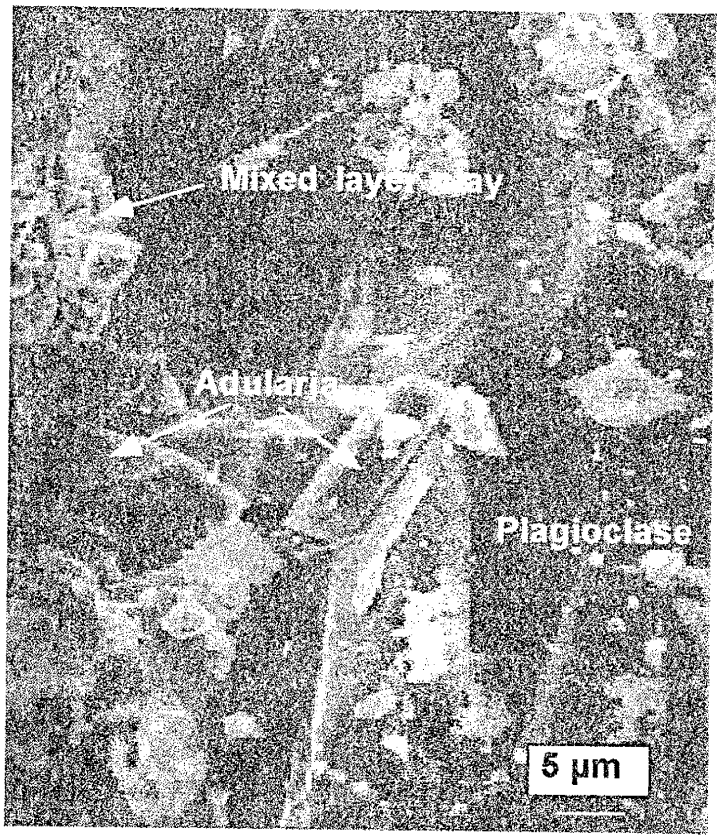

Figure 3: SEM photo of plagioclase + adularia + mixed-layer I/S.

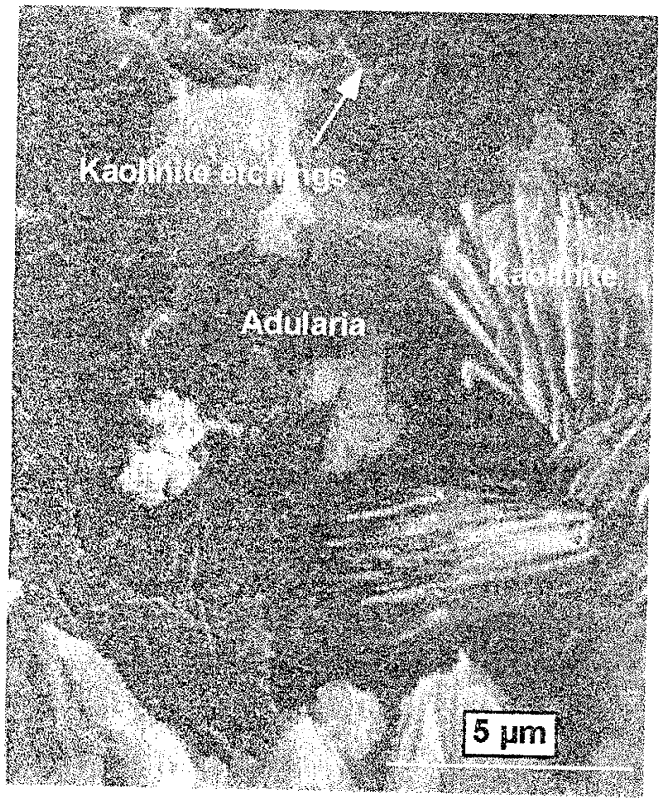

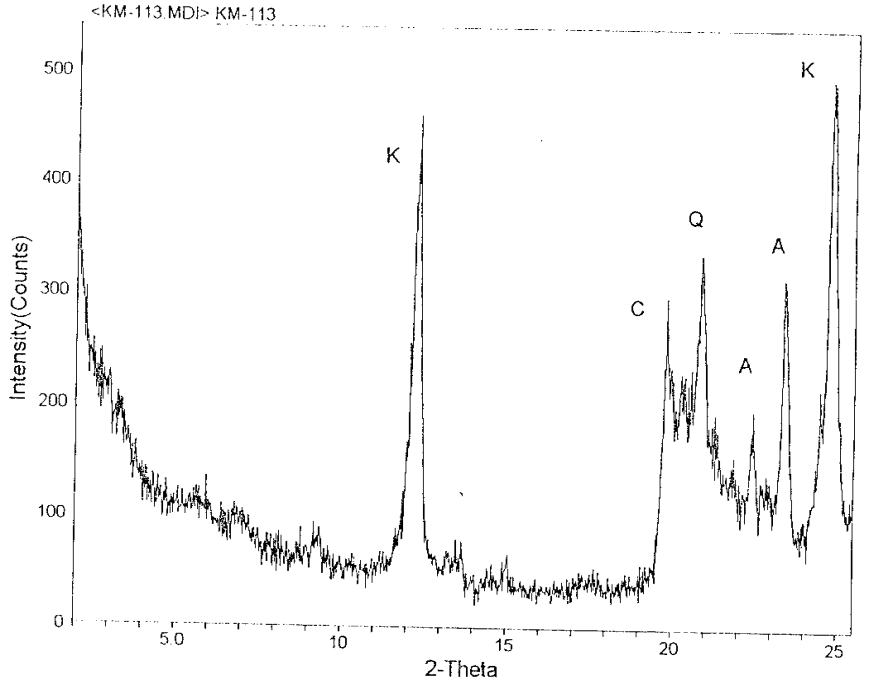

Figure 4: SEM photo of adularia and kaolinite books. XRD pattern shows kaolinite at characteristic 2-Theta angle of 12.4°; K=kaolinite, C=general clay peak, Q=quartz, A=adularia.

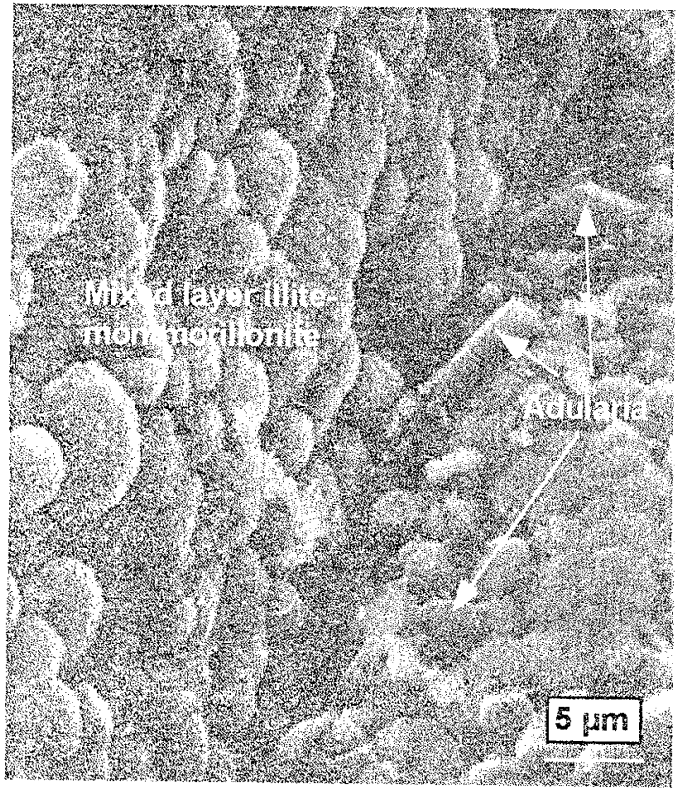

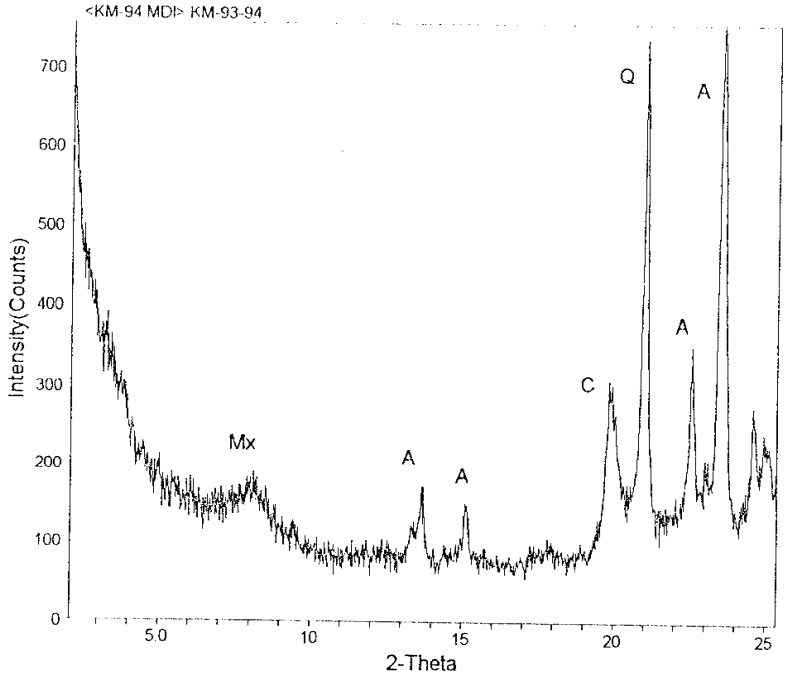

Figure 5: SEM photo of mixed-layer I/S and euhedral adularia. XRD pattern shows this same assemblage; Mx=mixed-layer I/S, A=adularia, C=general clay peak, Q=quartz.

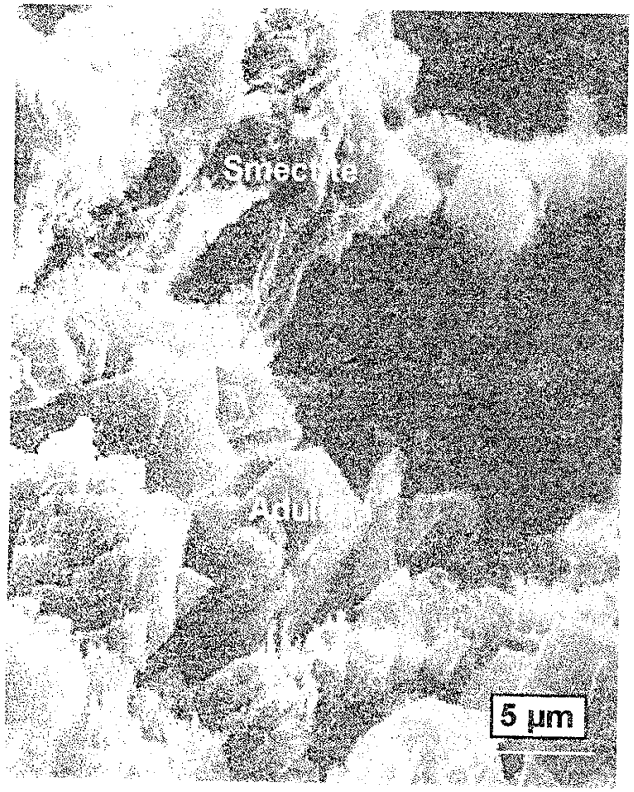

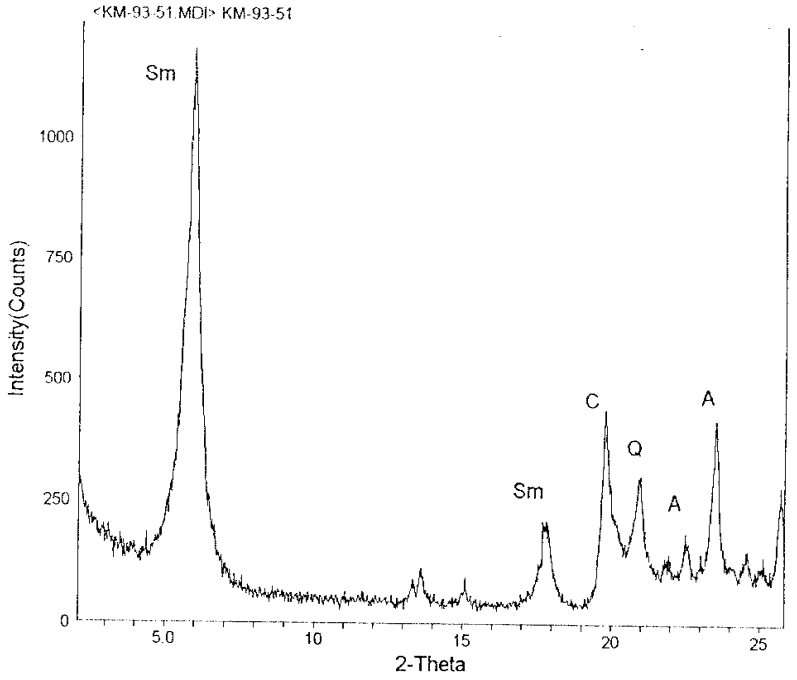

Figure 6: SEM photo of euhedral adularia and smectite. XRD pattern shows a distinctive smectite peak at approximately 6.0° 2-Theta; Sm=smectite, C=general clay peak, Q=quartz, A=adularia.

along with the types of clay minerals present for each sample examined.

The presence of calcite in the alteration assemblage has not been documented previously, but in this study, calcite appears to be present in at least 4 of the separated samples. Calcite is reliably detected only through thin section or microprobe analysis, for XRD did not consistently detect its presence. However, when present, calcite is extremely fine-grained and found in exceedingly small amounts. Barite is also found within the alteration assemblage of a few samples collected in the vicinity of the Luis Lopez manganese district, therefore suggesting a hydrothermal source.

Backscattered Images, Element Mapping, and Chemical Analyses

The backscattered image of a polished thin section of KM-54 (Figure 7), from the Hells Mesa Tuff, shows a sharp boundary between the minerals in the alteration assemblage and residual plagioclase. An enlargement of the plagioclase embayment in KM-54 clearly shows additional, smaller embayments at the margin between plagioclase and the alteration phases (Figure 8). The most interesting elements mapped for KM-54 are also shown in Figure 7 where brightness is indicative of higher concentrations of a particular element. The K-map for this sample shows adularia as the dominant K-rich phase in the alteration assemblage, although the clay matrix is somewhat K-rich, thus implying a mixed-layer clay. This is supported by semi-quantitative clay analysis which resolved mixed-layer I/S to be the dominant clay mineral present in this sample. The Ca-map demonstrates the presence of extremely fine-grained calcite within the alteration assemblage.

Element Map for KM-54

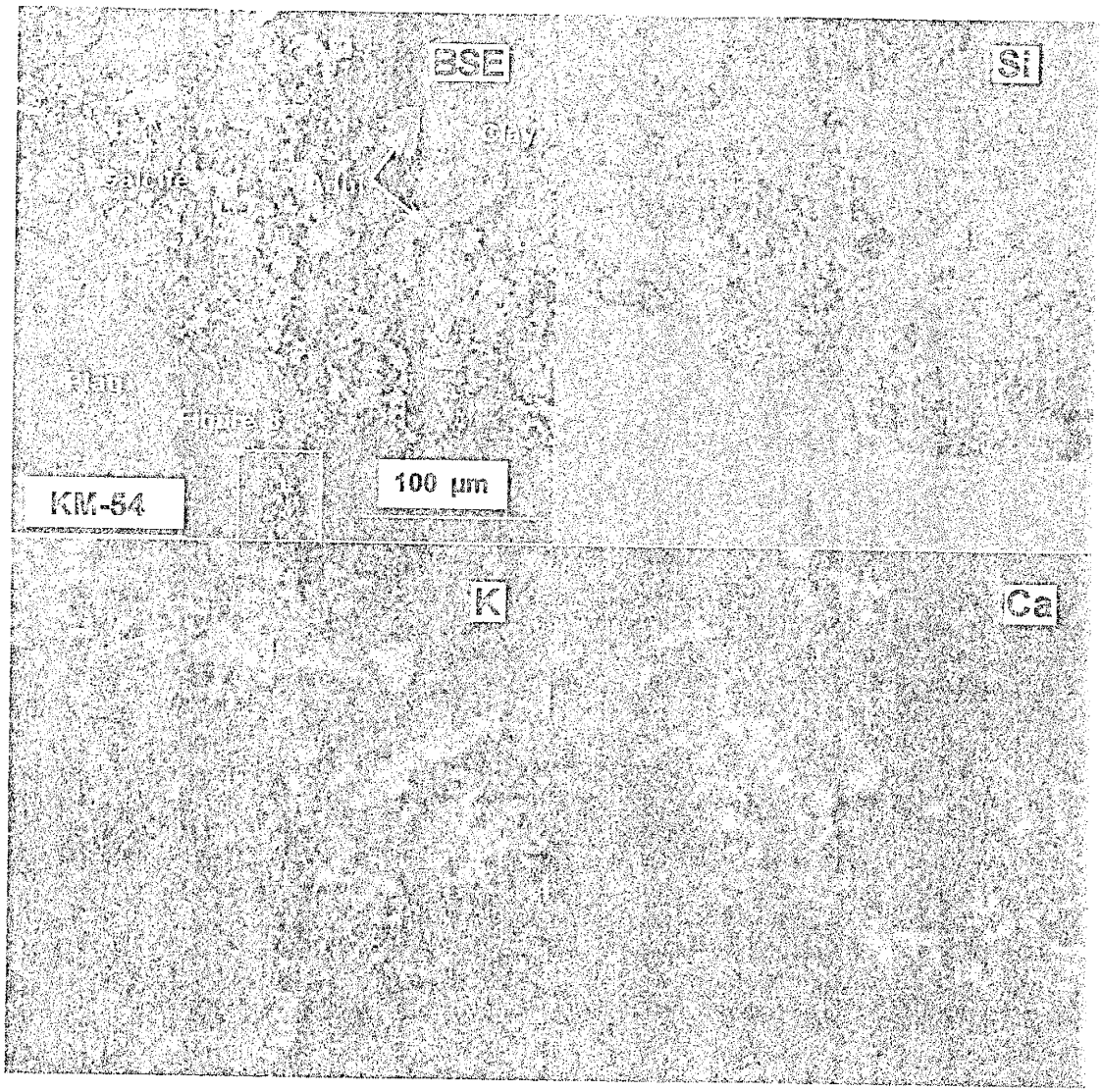

Figure 7: Electron microprobe back-scattered (BSE) image with element maps for silica, potassium and calcium where brightness is indicative of higher concentrations. A magnified view of the plagioclase embayment is shown in Figure 8.

Enlargement of Embayment in Plagioclase
from KM-54

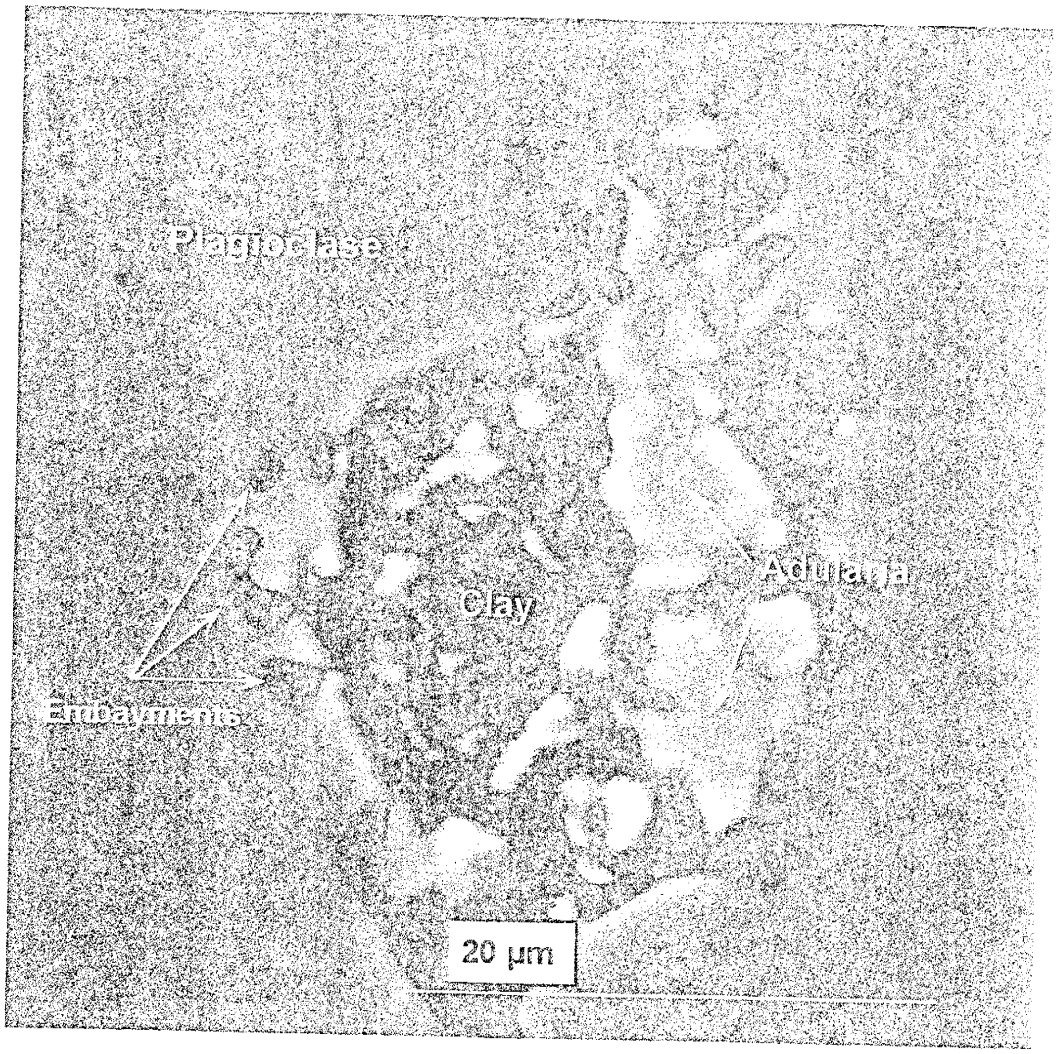

Figure 8: Electron microprobe back-scattered image. Enlargement of plagioclase embayment indicated on Figure 7. Note small dissolution textures within the main embayment as well as the presence of clay in direct association with plagioclase.

Element mapping of KM-51 from the upper Lemitar Tuff shows the matrix of smectite to be Mg-rich (Figure 9). As expected for discrete smectite, the K-map depicts that this clay is K-poor, leaving adularia as the only K-bearing phase present within the alteration assemblage. Calcite does not appear to be present in this sample, possibly indicating that its presence is a limited occurrence within the K-metasomatized area. Only one small grain of residual plagioclase was found within the alteration assemblage, suggesting a significant degree of metasomatism has occurred to this sample.

Average chemical compositions of adularia and plagioclase from the Hells Mesa and upper Lemitar Tuffs, determined by electron microprobe analysis, are given in Table 2 below. Plagioclase from the Hells Mesa Tuff is significantly more calcic in composition whereas upper Lemitar Tuff plagioclase is slightly more sodic. No noticeable difference in adularia composition is recognized between the Hells Mesa and upper Lemitar Tuffs.

Mineral	Na_2O	MgO	Al_2O_3	SiO_2	K_2O	CaO	FeO
Adularia	0.1 ±.01	0.02 ±.008	17.8 ±.10	66.0 ±.37	16.5 ±.09	0.05 ±.01	0.05 ±.02
HM plag	8.5 ±.06	0.01 ±.008	22.3 ±.12	62.8 ±.37	0.97 ±.02	4.4 ±.05	0.23 ±.03
UL plag	9.6 ±.07	0.14 ±.01	19.5 ±.11	67.9 ±.39	0.08 ±.01	0.62 ±.02	0.09 ±.03

Table 2: Average compositions of adularia (thirteen total analyses) and plagioclase (six total analyses of Hells Mesa Tuff plagioclase and one analysis of upper Lemitar Tuff plagioclase) via the electron microprobe. All elements and errors are measured in wt. % oxide. HM=Hells Mesa Tuff; UL=upper Lemitar Tuff

Element Map for KM-51

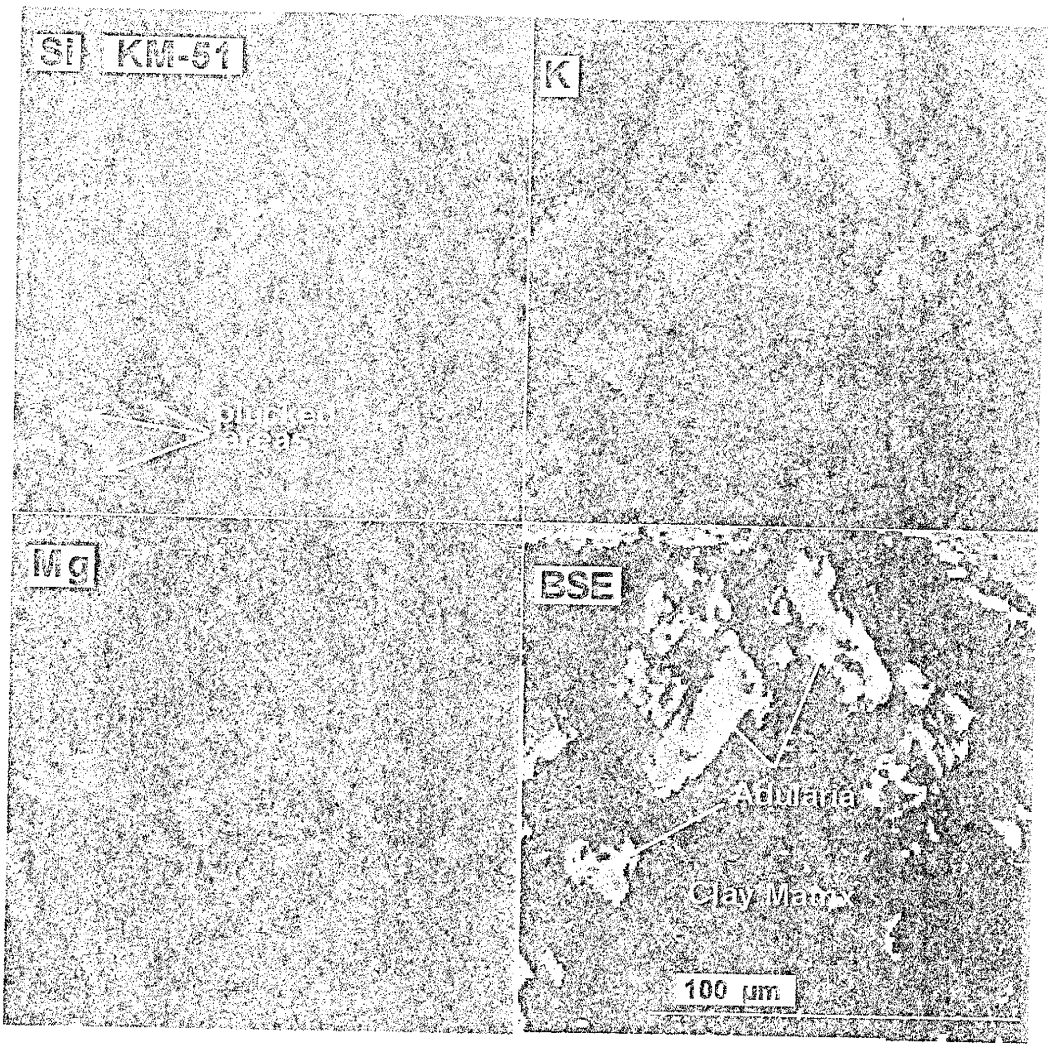

Figure 9: Electron microprobe back-scattered image (BSE) for adularia + smectite with element maps for silica, potassium, and magnesium (brightness indicates higher concentrations). Note Mg-rich smectite. Plucked areas are due to sample preparation.

Geochemistry

Whole Rock - Upper Lemitar and Hells Mesa Tuffs

Major Elements

The geochemical signature of upper Lemitar and Hells Mesa Tuff samples collected in this study show significant effects of K-metasomatism (Figure 10). Despite the overall similarity, there are systematic differences between the two units. Altered upper Lemitar ignimbrite samples generally contain >66 wt. % SiO_2, 3.6 - 12.2 wt. % K_2O, and 1.0 - 4.7 wt. % Na_2O, while the Hells Mesa Tuff contains >71 wt. % SiO_2, 5.1 to 8.8 wt. % K_2O and 0.6 to 3.1 wt. % Na_2O. Fresh equivalent SiO_2 values for the upper Lemitar Tuff are ~69 wt. % and for the Hells Mesa Tuff are ~72 wt. %, with unaltered K_2O and Na_2O values for the two units averaging ~5 wt. % K_2O and ~4 wt. % Na_2O. K_2O/Na_2O ratios within the K anomaly are generally high (0.77 - 9.69 for the upper Lemitar Tuff and 1.8 - 14.2 for the Hells Mesa Tuff) and are typically characterized by K_2O enrichment and Na_2O depletion within the altered region. Two upper Lemitar Tuff vitrophere samples (K_2O/Na_2O ratios of 0.77 and 1.2) collected within the altered zone show little signs of potassic alteration as indicated by the low K_2O/Na_2O ratios. Only one non-vitrophere upper Lemitar Tuff sample (KM-148) collected within the study area appears to be relatively unaltered. This sample has K_2O and Na_2O values comparable to upper Lemitar Tuff fresh equivalent values and a K_2O/Na_2O ratio of 1.3. Nockolds and others (1978) state that unaltered rhyolite samples typically have a $K_2O/Na_2O < 2$, further indicating KM-148 has not been greatly affected by K-metasomatism.

Upper Lemitar Tuff samples appear to show two different, distinct trends on a

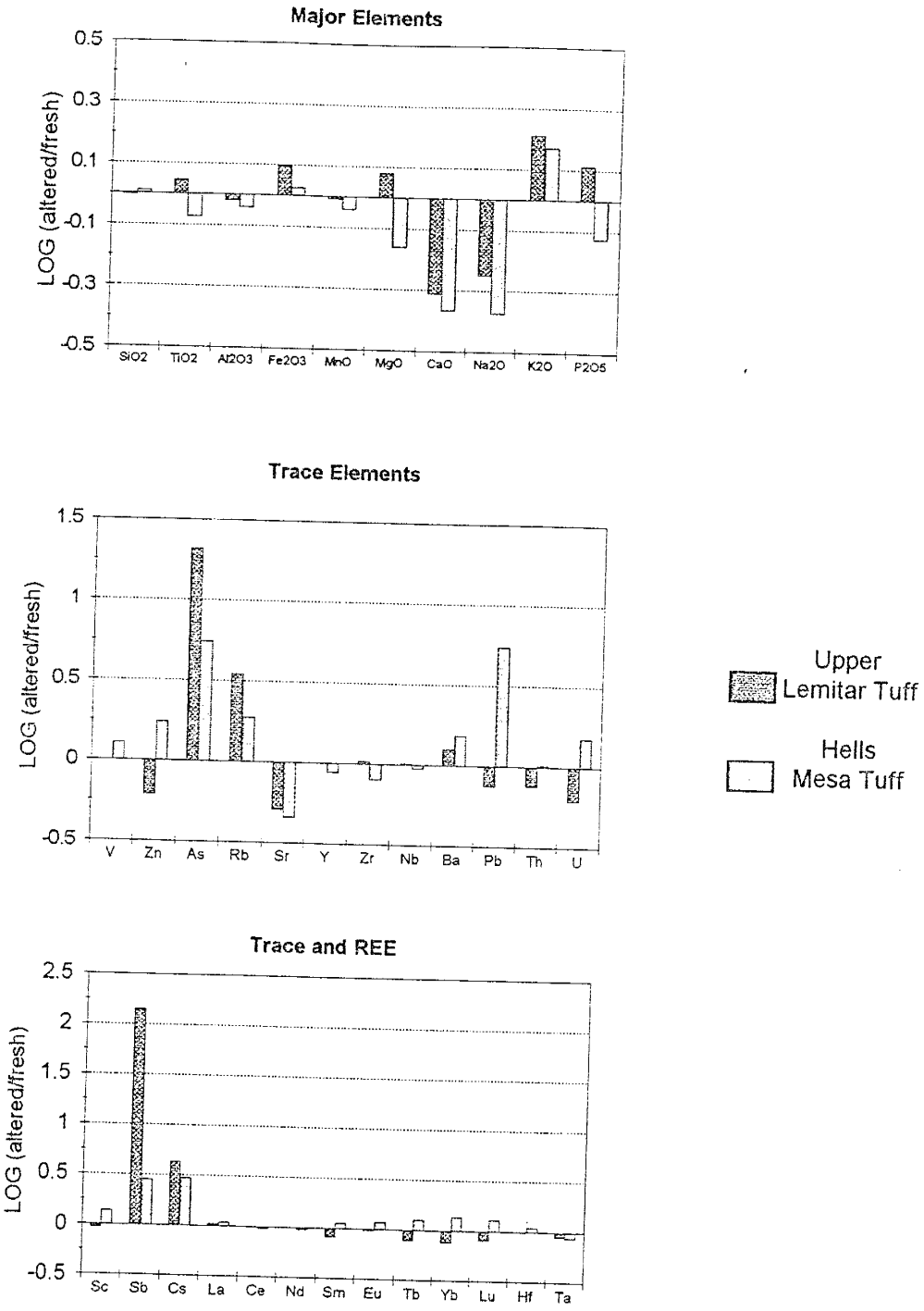

Figure 10: Enrichment/depletion diagrams for major and trace elements. The enrichment/depletion factors are based on averages of 6 and 4 unaltered upper Lemitar and Hells Mesa Tuff samples, respectively.

mole K^+ vs. mole Na^+ diagram, whereas Hells Mesa Tuff samples display only one distinct trend (Figure 11). The upper Lemitar Tuff trend defined as UL1 on Figure 11 has a slope of -0.96, which is very close to -1.0, therefore suggesting the number of moles of K gained by the system is equivalent to the number of moles of Na lost by the system. The upper Lemitar Tuff trend defined as UL2 has a slope of -0.83 on this same diagram. The difference in trends is most likely related to compositional zonation of the upper Lemitar Tuff as discussed in a subsequent section. Hells Mesa ignimbrite samples produce a slope of -1.08, reflecting a 1:1 ratio of K gain vs. Na loss by the metasomatic system.

The CaO concentration of the upper Lemitar and Hells Mesa Tuffs can be quite variable, yet overall depletion of CaO is apparent when compared to average fresh rock values (Figure 10). CaO content for the two units range from 0.1 to 1.8 wt. %; fresh CaO values are approximately 1.15 wt. % for both units. Unaltered samples typically have a K_2O/CaO ratio between 4.25 - 4.7, while K_2O/CaO ratios for metasomatized upper Lemitar Tuff samples are 2.0 - 45.9 and between 4.0 - 87.4 for the Hells Mesa Tuff. In order to produce a K_2O/CaO ratio as high as 87.4, it is clear that K_2O content must increase while CaO concentration becomes depleted during alteration. Most of the upper Lemitar Tuff samples and all of the Hells Mesa Tuff samples collected within the alteration area fall into the "K_2O metasomatized ash-flow tuff" region on a K_2O-CaO-Na_2O diagram (Figure 12) defined by D'Andrea-Dinkelman (1983). KM-148, however, falls into the "fresh ash-flow tuff" field, further exemplifying the relatively unaltered nature of this sample. Two other samples, upper Lemitar Tuff vitropheres, fall into this field as well.

Other major elements found to be slightly variable between the upper Lemitar and

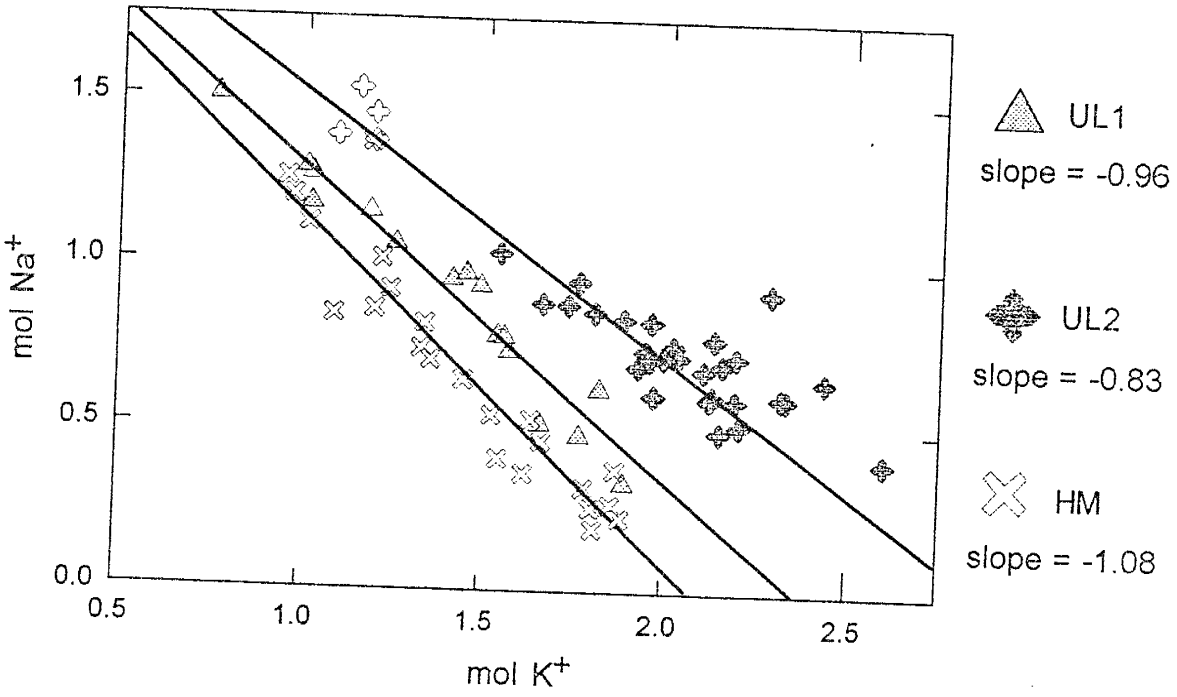

Figure 11: mol K^+ vs. mol Na^+ for upper Lemitar and Hells Mesa Tuff whole rock samples. Upper Lemitar samples show two trends (UL1 and UL2) while the Hells Mesa Tuff (HM) only shows one. Open symbols indicate unaltered samples collected outside of the K-anomaly.

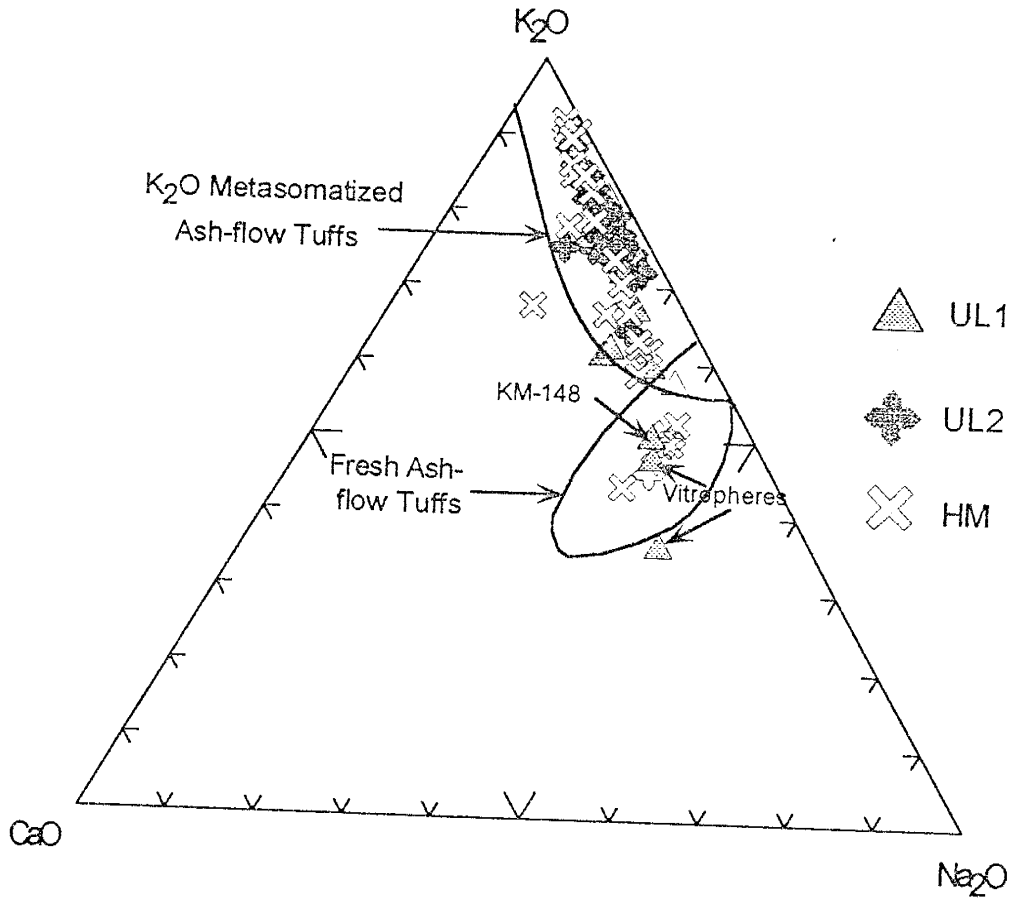

Figure 12: Ternary diagram from D'Andrea (1981) showing metasomatized and fresh fields for ignimbrites. Most upper Lemitar (UL1 and UL2) and Hells Mesa (HM) Tuff samples plot in the metasomatized field; KM-148 plots in the fresh field. Open symbols indicate unaltered samples.

Hells Mesa Tuffs include MgO and P_2O_5 (Figure 10). The remaining major elements, SiO_2, TiO_2, Al_2O_3, Fe_2O_3, and MnO, show neither significant enrichment nor depletion as a result of K-metasomatism. Major element data for the upper Lemitar Tuff, specifically the oxides SiO_2, TiO_2, and Fe_2O_3, indicate that compositional zonation may play an important factor when assessing the effects of K-metasomatism on this unit. No discernible difference in SiO_2, TiO_2, and Fe_2O_3 content is apparent within the Hells Mesa Tuff data set.

Trace Element Whole Rock Concentrations Consistently Enriched or Depleted

A number of trace elements in altered upper Lemitar and Hells Mesa whole rock samples show consistent enrichment or depletion as a result of K-metasomatism, when compared to fresh samples (Figure 10). Metasomatized upper Lemitar Tuff samples show enrichment of Rb with a range of 136 to 535 ppm, while Sr is depleted and displays a range from 47 to 391 ppm (fresh upper Lemitar Tuff samples typically average 136 ppm Rb and 245 ppm Sr). The Hells Mesa Tuff also shows enrichment of Rb, which ranges from 251 to 424 ppm Rb, and depletion of Sr, typically varying in concentration between 16 to 230 ppm. In accordance with Rb enrichment and Sr depletion, Rb/Sr ratios are generally high in altered tuff samples; 0.82 to 6.8 for the upper Lemitar Tuff and 1.1 to 19.4 for the Hells Mesa Tuff. KM-148, from the upper Lemitar Tuff, has a Rb/Sr ratio of only 0.82, again suggesting this sample has not undergone significant degrees of K-metasomatism.

In addition to Rb enrichment, Ba, As, Sb, and Cs also show significant increases in concentration within altered samples when compared to fresh upper Lemitar and Hells Mesa Tuff samples. Ba and As can be quite enriched in altered samples with As values ranging from <3 to 90.6 ppm and Ba from 275 to 2687 ppm in whole rock upper Lemitar and Hells Mesa Tuff samples. Sb is also enriched and displays a range in concentration from <0.2 to 130 ppm within the upper Lemitar Tuff. Sb has a significantly smaller range within the Hells Mesa Tuff (0.3 to 7.0 ppm), yet still displays enrichment over unaltered samples. Cs ranges from 1.0 to 88.0 ppm within the upper Lemitar Tuff with the two vitrophere samples, KM-106 and KM-110, containing the highest concentrations (88.0 and 77.0 ppm, respectively). Hells Mesa Tuff whole rock samples range between 3.0 and 22.0 ppm Cs, which is less than that found for the upper Lemitar Tuff.

It appears that hydrothermal input may account for several trace elements which show significant enrichment or depletion on Figure 10. For example, samples KM-55 and KM-56, collected near the Luis Lopez manganese district, contain extremely elevated levels of As (77.3 ppm and 90.6 ppm respectively), which contributes significantly to the enrichment factor for the upper Lemitar Tuff. Similarly, samples KM-128 and KM-138 from the upper Lemitar Tuff contain high levels of Sb (130 ppm Sb each) and thus also likely represent a significant hydrothermal overprint. In addition, samples containing a high whole rock concentration of Ba may represent samples affected by hydrothermal alteration.

Trace Element Whole Rock Concentrations Unchanged Upon Alteration

Although some trace elements show consistent enrichment or depletion within K-metasomatized upper Lemitar and Hells Mesa Tuff samples, the majority appear to be unaffected by the alteration. The trace elements V, Ga, Y, Zr, Nb, Pb, Th, Sc, La, Ce, Nd, Hf, and Ta show little variation on enrichment / depletion diagrams (Figure 10), likely indicating that these elements are unaffected by K-metasomatism. The light rare earth elements (LREE) commonly display somewhat variable concentrations (Figure 13), yet no net enrichment or depletion when compared to fresh samples. Generally, the elements Ga, Y, Zr, and Nb are considered to be immobile during secondary alteration processes (Winchester and Floyd, 1977) and can also be used to evaluate the degree or presence of compositional zonation within an ignimbrite (Hildreth, 1979). A small number of Hells Mesa Tuff samples, (i.e. KM-96 and KM-102 from Socorro Peak and KM-155 from the Magdalena Mountains), have considerably elevated Pb concentrations due to collection of these samples near hydrothermally affected areas. These outlier samples contribute significantly to the enrichment factor calculated for the Hells Mesa Tuff (Figure 10).

Trace Element Whole Rock Concentrations Markedly Different Between the Upper Lemitar and Hells Mesa Tuffs

Several trace elements within the upper Lemitar and Hells Mesa Tuffs show distinctly different trends upon K-metasomatic alteration. The elements Zn, U, Sm, Eu, Tb, Yb, and Lu all display depletion in the upper Lemitar Tuff, but enrichment in the Hells Mesa Tuff (Figure 10). Although the magnitude of enrichment or depletion of these

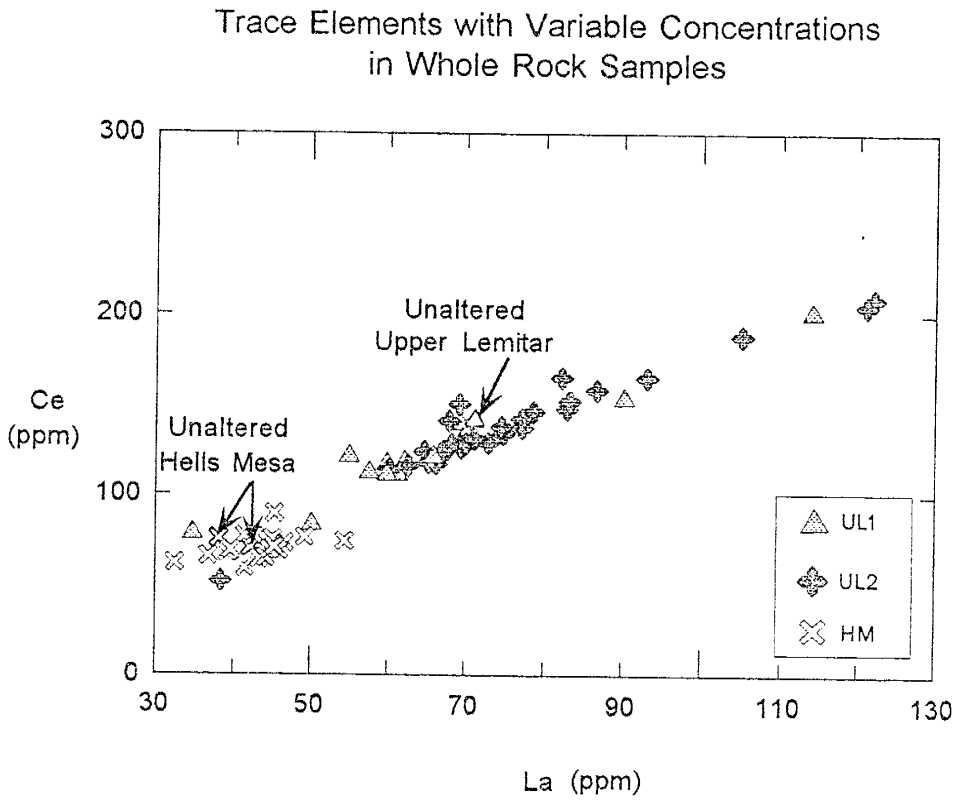

Figure 13: Light rare earth element variability within upper Lemitar (UL1 and UL2) and Hells Mesa (HM) Tuff whole rock samples. Open symbols represent unaltered samples collected outside the K-anomaly.

elements is relatively minor, the trend is fairly striking, especially within the heavy rare earth elements (HREE). Altered upper Lemitar whole rock samples range from 2.1 to 6.8 ppm Yb and 0.3 to 1.0 ppm Lu; fresh values are ~6.9 ppm Yb and ~0.9 ppm Lu. Hells Mesa Tuff samples collected from within the K-anomaly range from 1.9 to 5.0 ppm Yb and 0.3 to 0.7 ppm Lu with fresh Hells Mesa Tuff samples containing ~1.8 ppm Yb and ~0.3 ppm Lu (Figure 14a). The REEs Sm, Eu, and Tb display somewhat variable concentrations when compared to unaltered samples (Figure 14b), yet show net depletion in the upper Lemitar Tuff and enrichment in the Hells Mesa Tuff whole rock samples (Figure 10).

Separated Sample Neutron Activation Analysis

Geochemical investigation of separated samples from relict plagioclase crystals allows the chemistry of the alteration assemblage to be examined in detail. However, an appropriate 'unaltered' composition for plagioclase, especially for trace and REE, can be difficult to determine. Separated plagioclase was obtained for KM-148, however, this sample appears to show only a slight degree of metasomatism based on evidence discussed previously. This sample is therefore used in comparison to the other upper Lemitar Tuff separated samples collected for this study. KJH-26 consists of separated plagioclase crystals from an unaltered Hells Mesa Tuff sample, which was collected outside of the K anomaly. As a result, it appears reasonable to use this sample as a comparison for values obtained from Hells Mesa Tuff separated samples collected within the metasomatized area.

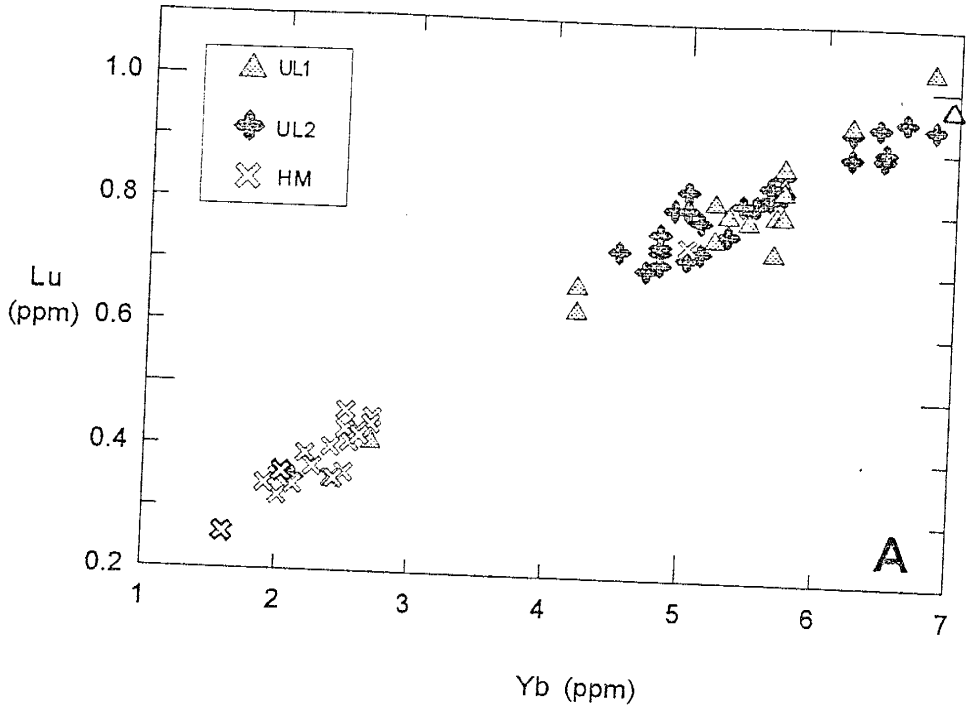

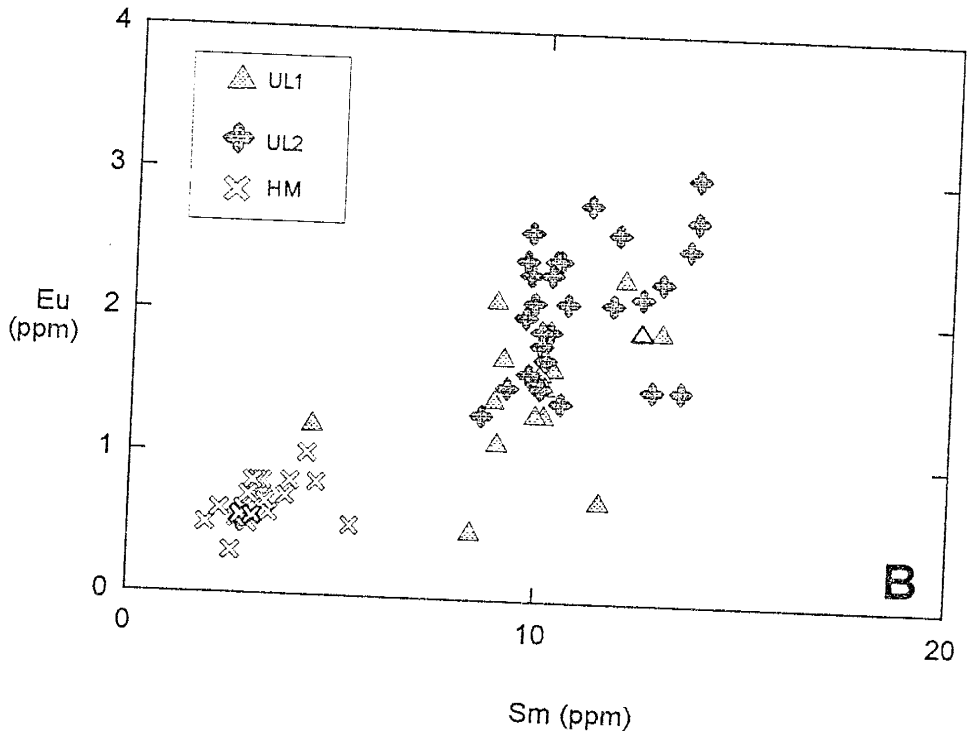

Figure 14a and b: Rare earth element variation within whole rock upper Lemitar (UL1 and UL2) and Hells Mesa (HM) Tuff samples. Open symbols indicate unaltered samples collected outside of the K-anomaly.

Elements Concentrations that are Consistently Enriched or Depleted Upon Alteration

When compared to the separated sample chemistry of KM-148 and KJH-26, several elements in the separated samples show consistently elevated concentrations including Sc, Co, Zn, As, Br, Rb, Sb, Cs, and Ba (Figure 15). Rb in the upper Lemitar Tuff separated samples ranges from 110 to 854 ppm, As from 0.8 to 108.6 ppm, and Sb from 0.1 to 9.7 ppm. KM-148, representing relatively unaltered material for the upper Lemitar Tuff, has 141 ppm Rb, 0.06 ppm Sb, and As was not detected. In the Hells Mesa Tuff separated samples, Rb varies between 93 to 508 ppm, As from 1.8 to 40.1 ppm and Sb from 0.10 to 8.55 ppm. KJH-26, used in comparison to the remaining Hells Mesa Tuff separated samples, contains only 1.0 ppm Rb, 0.01 ppm Sb, and As was not determined. Figure 15 does not reflect As enrichment or depletion because this element was not detected in either KJH-26 or KM-148. However, As is interpreted to be enriched upon alteration as indicated by the relatively high values found in the separated samples.

Another element displaying enrichment is Ba, which is extremely variable in the separated samples of both units and, in some cases, can be extremely concentrated. For instance, Ba concentration varies dramatically between 112 to 38,899 ppm for the two units (KM-56 from the upper Lemitar Tuff contains 25,051 ppm Ba and KM-115 from the Hells Mesa Tuff contains 38,899 ppm Ba), clearly demonstrating its variability. High concentrations of Ba within the separated samples are likely indicative of a hydrothermal source, for both KM-56 and KM-115 were collected in the vicinity of the Luis Lopez

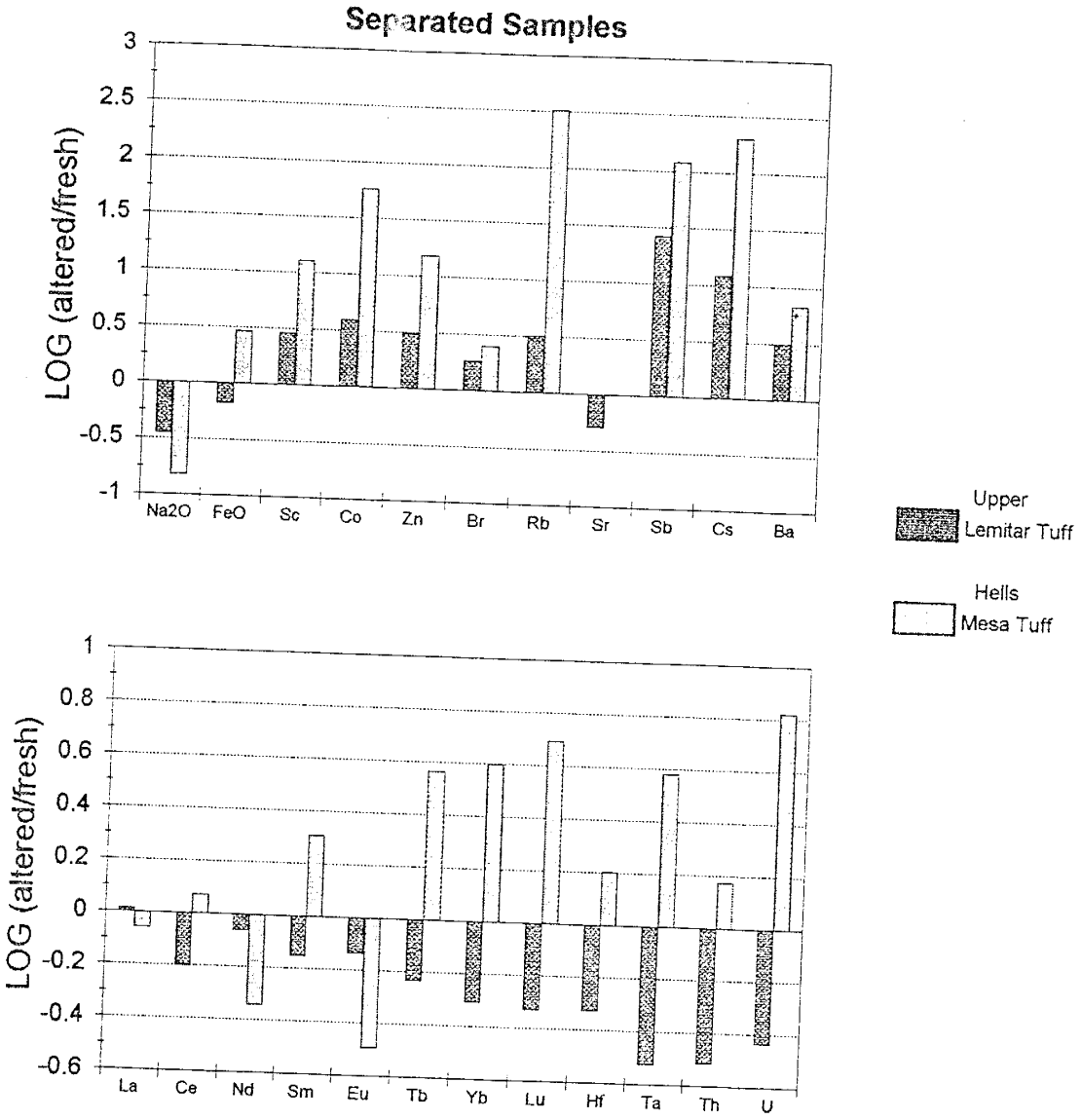

Figure 15: Enrichment/depletion diagrams for elements within the separated samples of the upper Lemitar and Hells Mesa Tuffs. Unaltered samples used to calculate the enrichment/depletion factors were KM-148 (upper Lemitar Tuff) and KJH-26 (Hells Mesa Tuff).

manganese district. In addition, elevated concentrations of As are generally believed to be associated with hydrothermal input.

Several elements within the separated samples of the upper Lemitar and the Hells Mesa Tuffs do not show enrichment, but rather depletion upon K-metasomatic alteration. Na_2O, Sr, and Eu are the only elements found in the separated samples to show convincing depletion, likely as a result of plagioclase dissolution due to the compatible nature of these elements in plagioclase (McBirney, 1993; Figure 15). Na_2O within the separated samples of both units ranges from 0.10 to 5.36 wt. % with KJH-26 containing 6.86 wt. % and KM-148 having 4.86 wt. % Na_2O. Values for Sr in the separated samples are 35 to 599 ppm. KJH-26 was not analyzed for Sr, hence no enrichment or depletion factor was able to be calculated for Hells Mesa Tuff separated samples on Figure 15, but KM-148 contains 449 ppm Sr and reflects overall depletion of Sr within the upper Lemitar Tuff.

Element Concentrations that are Variable or Unchanged Upon Alteration

The concentrations of the elements La, Ce, and Nd are variable within the separated samples of the upper Lemitar and Hells Mesa Tuffs when compared to the unaltered samples KM-148 and KJH-26. Separated samples from the upper Lemitar Tuff contain 3.5 to 70.0 ppm La, 4.9 to 140.2 ppm Ce, and 7.4 to 56.0 ppm Nd. The Hells Mesa Tuff separated samples display 7.9 to 69.4 ppm La, 20.2 to 83.9 ppm Ce, and 2.9 to 42.8 ppm Nd. When these values are compared to the LREE chemistry of KM-148 and KJH-26, which contains 27.5 ppm La, 103.4 ppm Ce, 28.4 ppm Nd and 22.3 ppm La,

32.4 ppm Ce, 9.6 ppm Nd respectively, the variable nature of these elements becomes evident (Figure 16). Figure 15 also shows inconsistent behavior of these LREE, for La appears to be unaffected by the alteration, while Ce and Nd show differing enrichment / depletion trends. The discordant trends of LREE within the separated samples is similar to that found in whole rock samples as discussed previously, possibly indicating that these elements are not significantly affected by K-metasomatic alteration.

Element Concentrations that are Markedly Different Between the Upper Lemitar and Hells Mesa Tuffs

A number of components, such as FeO, Sm, Tb, Yb, Lu, Hf, Ta, Th, and U are depleted within the upper Lemitar Tuff separated samples when compared to KM-148, but are enriched within the Hells Mesa Tuff separated samples when compared to KJH-26 (Figure 15). Of particular interest is the apparently different trends of the REE within the upper Lemitar and Hells Mesa Tuffs upon potassic alteration. The middle and HREE are found to most clearly represent the differences. In the upper Lemitar Tuff separated samples, Tb ranges from 0.05 to 2.3 ppm, Yb from 0.3 to 5.6 ppm, and Lu ranges from 0.04 to 0.80 ppm. When compared to the separated chemistry of KM-148 (containing 1.4 ppm Tb, 4.9 ppm Yb, and 0.7 ppm Lu), enrichment is clearly indicated. Depletion of these same elements within the Hells Mesa Tuff is demonstrated when a comparison is made between altered separated samples and the unaltered sample KJH-26. The Hells Mesa Tuff separated samples contains between 0.15 to 0.8 ppm Tb, 0.6 to 4.2 ppm Yb, and 0.1 to 1.9 ppm Lu with KJH-26 containing 0.1 ppm Tb, 0.4 ppm Yb, and 0.1 ppm Lu

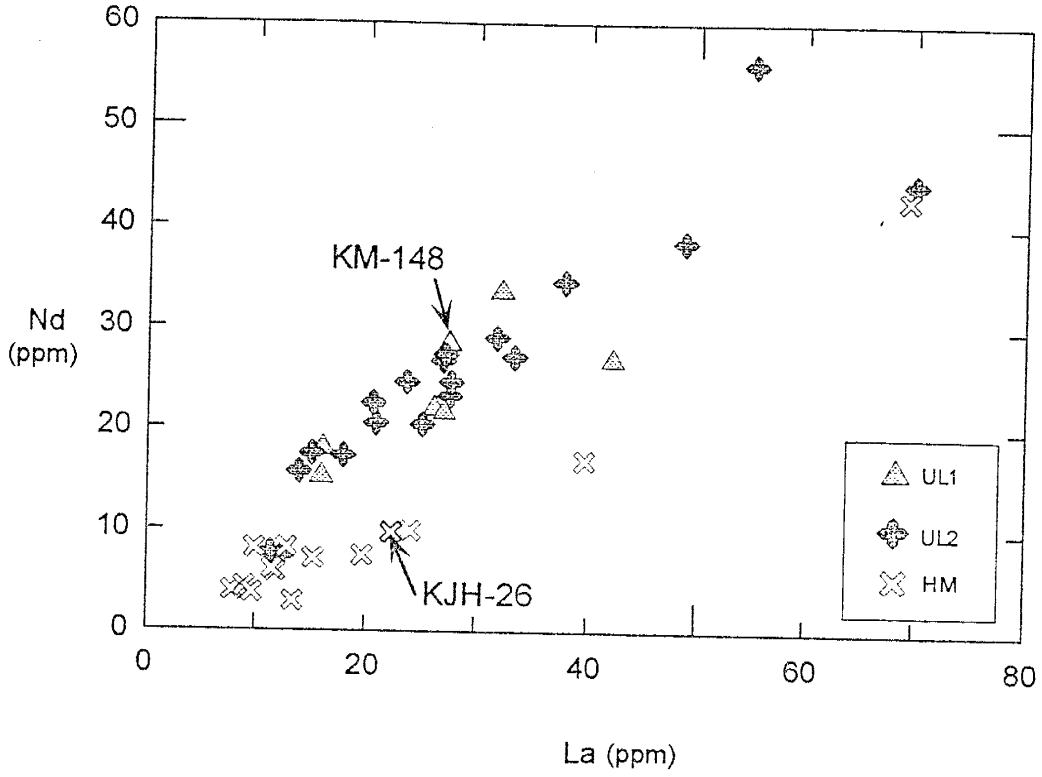

Figure 16: Rare earth element variation within the separated, altered plagioclase samples in relation to unaltered plagioclase from the upper Lemitar (UL1 and UL2) and Hells Mesa (HM) Tuffs (KM-148 and KJH-26, respectively).

(Figure 17a and b). The enrichment of these elements within the upper Lemitar Tuff separated samples and the depletion within the Hells Mesa Tuff separated samples is similar to the trends found in whole rock analyses (compare Figures 10 and 15).

Stable Isotopes

Stable isotope analyses were performed for a total of 12 whole rock samples and 13 separated samples, including unaltered plagioclase from sample KJH-26. All samples were analyzed for $\delta^{18}O$ values relative to SMOW. Whole rock $\delta^{18}O$ ranges from +7.0 to +14.3 per mil and the 13 separated samples range from +6.3 to +14.1 per mil (Table 3). Sample KJH-26 consists of separated plagioclase crystals from an unaltered Hells Mesa Tuff sample collected outside of the K anomaly and has a $\delta^{18}O$ value of +6.3 per mil. This sample has the lowest value of $\delta^{18}O$ within the sample set and likely represents the isotopic composition of plagioclase before alteration. Taylor (1968) states that most unaltered volcanic rocks have $\delta^{18}O$ values of +5 to +10 per mil, which also helps confirm its origin as a primary, unaltered sample. Because this sample isotopically and mineralogically resembles unmetasomatized material, this sample is therefore used as a comparison for values obtained from separated samples collected within the metasomatized area.

The separated samples for KM-31, -36, -41, -51, -60, and -61 all appear to be quite enriched in $\delta^{18}O$ with a range from +9.7 to +14.1 per mil. Similarly, whole rock $\delta^{18}O$ values for these same samples range from +9.9 to +14.3 per mil. The KM-41 separated sample, which consists almost entirely of adularia and quartz, with very minor

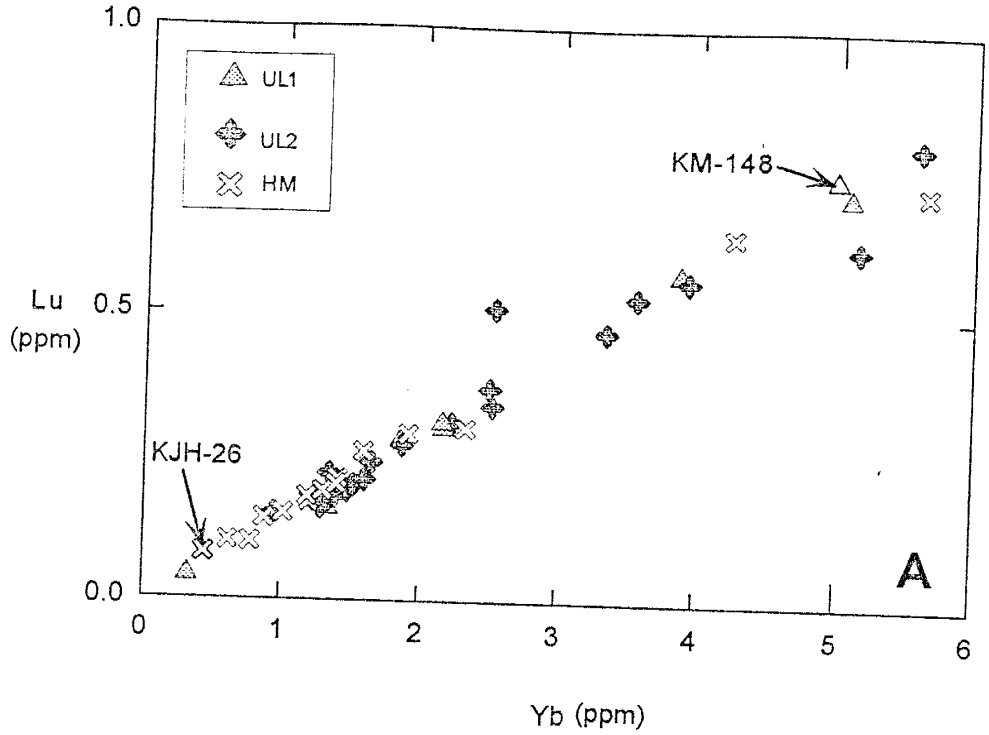

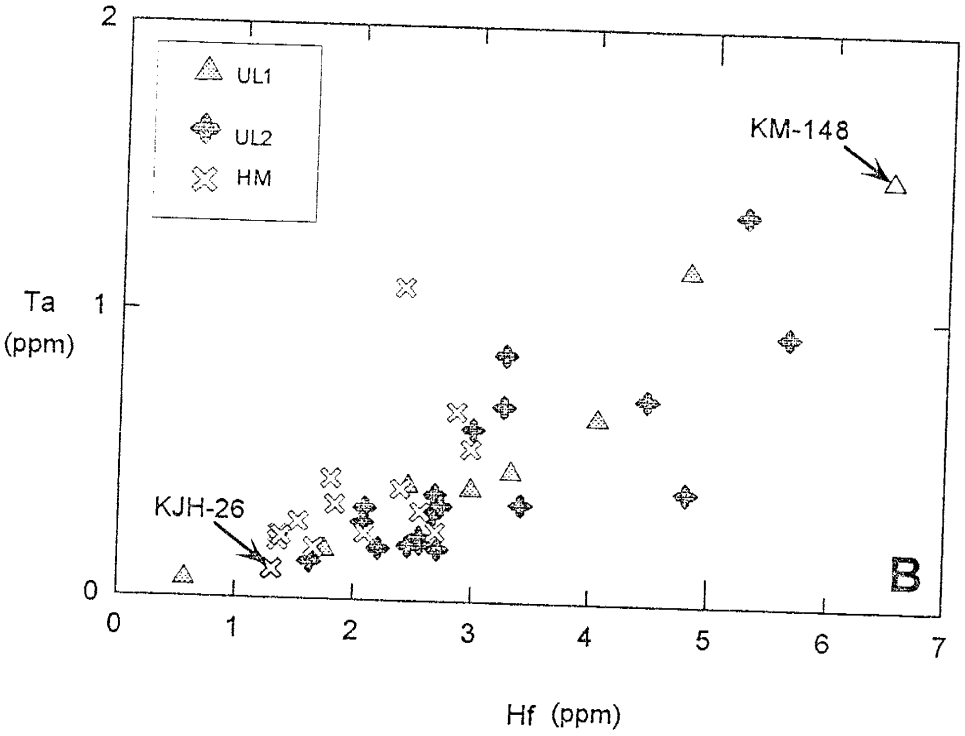

Figure 17a and b: Heavy rare earth element and trace element trends in the separated samples from the upper Lemitar (UL1 and UL2) and Hells Mesa (HM) Tuffs compared to unaltered plagioclase (KM-148 and KJH-26).

Sample #	$\delta^{18}O$ Value (Whole Rock)	$\delta^{18}O$ Value (Separated Samples)
KJH-26	N/A	6.3
KM-31	14.3	9.7
KM-36	10.9	11
KM-41	11.7	14.1
KM-46	13.6	12.6
KM-51	10.1	13.6
KM-54	8.4	8.5
KM-55	8.6	8.2
KM-56	9.9	8.2
KM-58	7	8.6
KM-59	10.8	9.1
KM-60	9.9	11.9
KM-61	10.2	10.2

Table 3: Isotopic composition of 12 separated and whole rock samples collected from within the Socorro K-anomaly, and one unaltered plagioclase sample, KJH-26, collected from outside the alteration. N/A=not applicable (sample consists only of separated plagioclase). All $\delta^{18}O$ values relative to SMOW.

kaolinite and remnant plagioclase, represents the largest value of $\delta^{18}O$ of the separated samples (+14.1 per mil). When compared to KJH-26, the $\delta^{18}O$ value of this separated sample is almost 8 per mil greater, indicating a significant amount of enrichment.

Several samples collected from the K anomaly appear to reflect hydrothermal overprinting. For instance, KM-54, -55, -56, -58, and -59 were all collected from the Luis Lopez manganese district in the northern Chupadera Mountains (See Figure 1), a known area of hydrothermal activity which has been described as epithermal in nature (Norman et al., 1983; Eggleston, 1983). The $\delta^{18}O$ values for these separated samples are all extremely similar, with a range of only +8.2 to + 9.1 per mil. Whole rock values for these same samples appear show no significant deviation from the separated sample $\delta^{18}O$ values (Table 3). The values obtained from these samples are significantly lower than those obtained for samples KM-31, -36, -41, -51, -60, and -61, therefore possibly reflecting the influence of hydrothermal alteration upon these samples.

DISCUSSION

Pre-alteration chemical composition of the Upper Lemitar Tuff

The two silicic ignimbrites studied, the upper Lemitar and Hells Mesa, along with all overlying units, have undergone significant degrees of K-metasomatism resulting in the modification of the mineralogy, chemistry, and isotopic compositions of these units. In order to assess the effects of potassic alteration on the units, it is important to have a clear understanding of the initial chemical composition of the two ignimbrites. Upon examination of Figure 11, it appears that altered upper Lemitar Tuff samples show two distinct trends, which contrasts with the single trend shown by Hells Mesa Tuff samples. Previous studies have shown the upper Lemitar ignimbrite to be compositionally zoned (Chapin and others, 1978), and it is conceivable that chemical zones within the unit may produce slightly different trends upon alteration. To test this, 'outliers' from the main group of upper Lemitar Tuff samples on Figure 11 were designated as UL1 while the remaining upper Lemitar samples were denoted as UL2. This resulted in the artificial formation of two groups of upper Lemitar Tuff samples which were then compared to assess if the groups are distinguishable based on additional chemical criteria.

The major elements SiO_2, TiO_2, and Fe_2O_3 have been used effectively as indicators of gradients associated with continuous eruption of ignimbrites from silicic magma chambers (i.e. Hildreth, 1979; Briggs et al., 1993). Because these elements appear to show neither enrichment nor depletion during metasomatism, it is possible to evaluate chemical zonation within the upper Lemitar Tuff based on these elements. UL1 samples typically have a higher SiO_2 content and a lower TiO_2 and Fe_2O_3 content compared to UL2

samples (Figure 18a and b). Hildreth (1979) found that with progressive tapping of a magma chamber, SiO_2, TiO_2, and total Fe content usually drop, thus providing evidence that UL1 samples were erupted early in the sequence while UL2 samples are from ensuing stages of eruption.

In addition to major elements, trace elements also demonstrate the chemically zoned nature of the upper Lemitar Tuff. The elements Zr, Nb, and Y appear to show no systematic variation during metasomatism (Figure 10) and can be used to further address the possibility of compositional zonation within the upper Lemitar Tuff (Winchester and Floyd, 1977; Hildreth, 1979; Stix et al., 1988). Based on these elements, the two groups of upper Lemitar Tuff samples appear to be distinct (Figures 19a and b). Although there is no noticeable difference in Y concentration between the two groups, UL2 samples generally have a higher Zr content compared to UL1 samples. Furthermore, UL1 samples tend to be slightly more enriched in Nb compared to UL2 samples. These results indicate that UL1 samples are representative of material produced early in the eruptive sequence while UL2 samples are late in the sequence (Hildreth, 1979), supporting the conclusions based on major element data as discussed previously. Based on major and trace element data for the upper Lemitar ignimbrite, it seems reasonable to attribute the two separate trends seen in Figure 11 to primary chemical zonation within this unit.

Mineralogy and Geochemistry

During K-metasomatism of silicic ignimbrites in the study area, plagioclase phenocrysts were replaced by an assemblage dominantly composed of adularia, quartz,

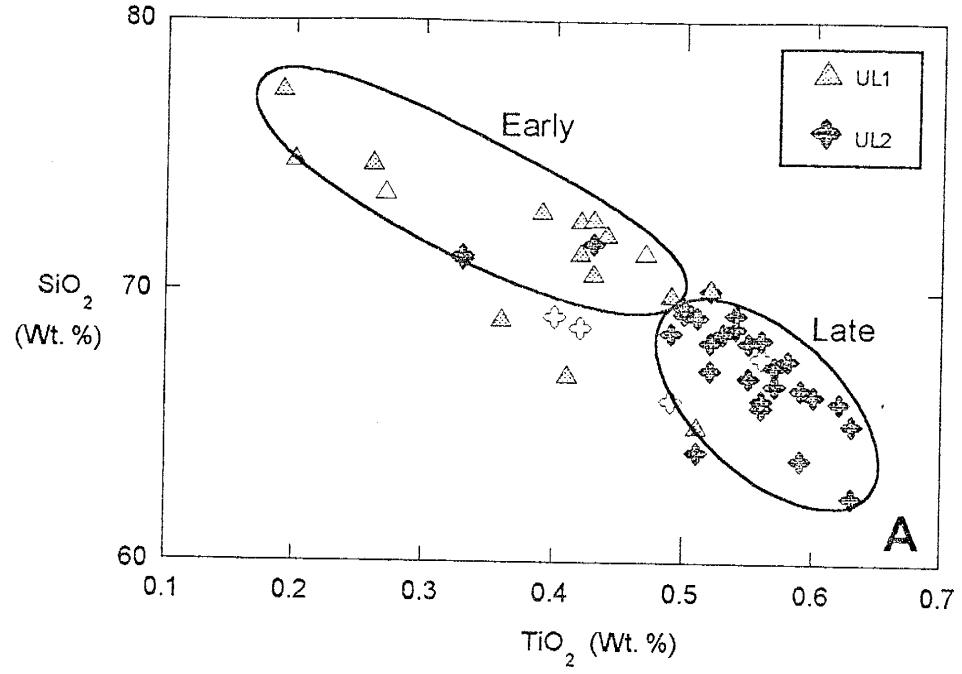

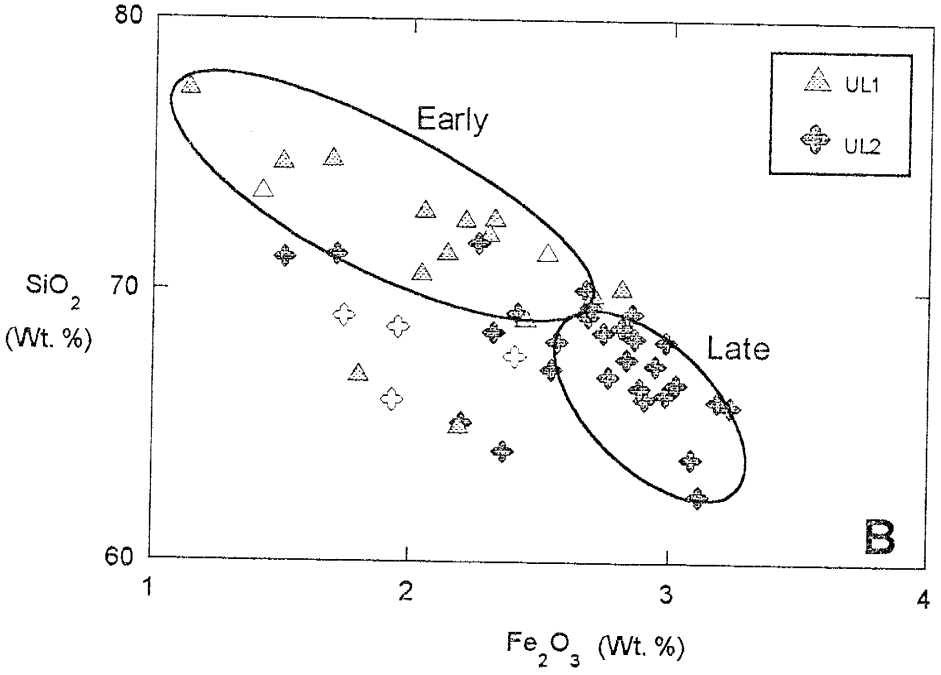

Figure 18a and b: Major element, primary variation between the two groups of upper Lemitar Tuff whole rock samples (UL1 and UL2). Open symbols indicate unaltered whole rock upper Lemitar Tuff samples. See text for explanation.

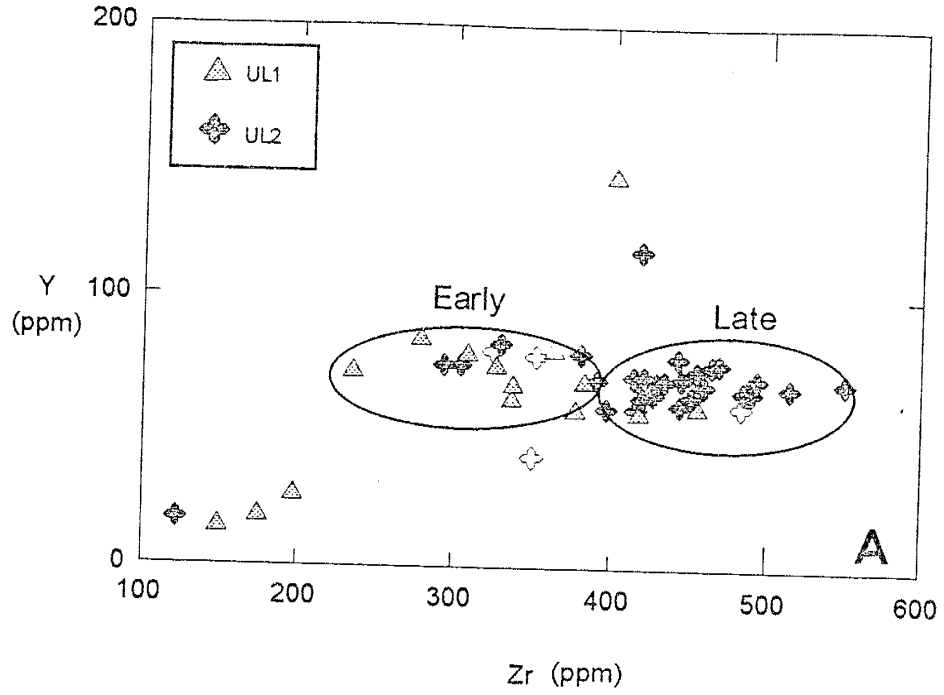

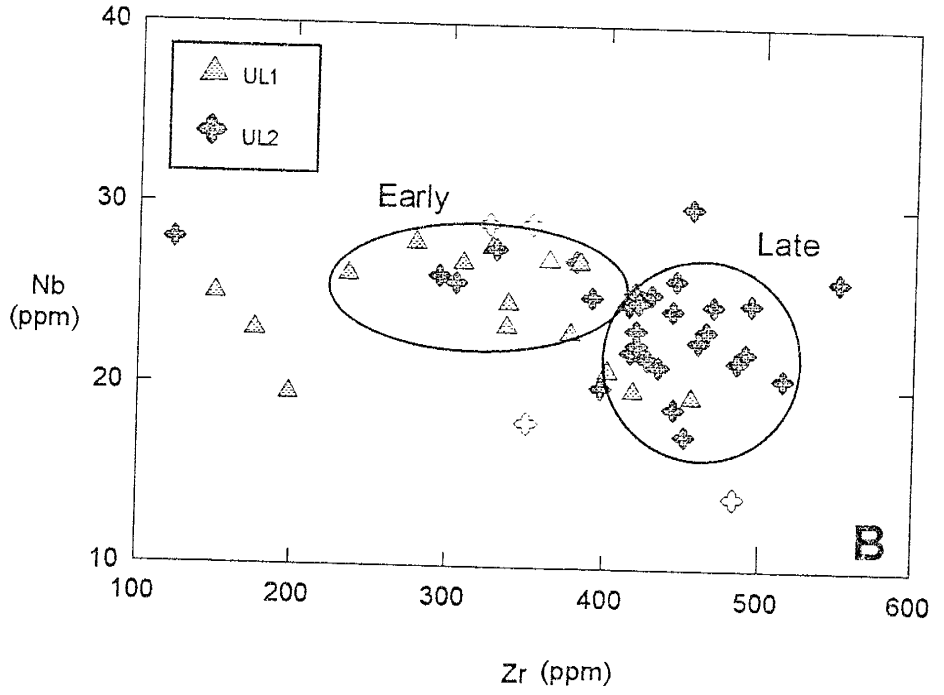

Figure 19a and b: Trace element variation between the two groups of upper Lemitar Tuff whole rock samples (UL1 and UL2). Open symbols indicate unaltered samples.

and a variety of clay minerals. Although clay minerals such as smectite and kaolinite commonly replace plagioclase during diagenesis and weathering, fresh samples examined in thin section indicate plagioclase has not undergone a significant degree of alteration due to these processes. The mineralogy produced through plagioclase dissolution is therefore attributable to other alteration processes. Our study of the morphology and chemistry of the primary and secondary phases, plus chemical composition of altered whole rock samples, allows the chemical and mineralogical affects of alteration to be assessed in detail. In addition to K-metasomatic alteration, the Socorro area has also undergone several, relatively small-scale epithermal alteration events. The Luis Lopez manganese district in the northern Chupadera Mountains, southwest of Socorro is a well documented example of one such hydrothermal event (i.e. Eggleston et al., 1983; Norman et al., 1983). It is important to note that because many of these localized hydrothermal events are superimposed or overprinted on the regional K-metasomatic event, a spatial relationship between multiple alteration episodes has been created. The separation of the effects of K-metasomatism from local hydrothermal events is certainly a complication in this study; however, because the chemistry, mineralogy, and physical conditions associated with these different alteration types is relatively unique, we feel it is possible to distinguish between them.

Adularia

The dominant K-bearing phase produced by alteration is adularia, a low-temperature feldspar structurally resembling orthoclase. Adularia has been interpreted by

other workers as secondary in nature, formed upon alteration of the silicic ignimbrite units rather than resulting from primary magmatic sources (Chapin and Lindley, 1986), which is a conclusion reinforced by results of this study. Adularia is present as part of the assemblage produced by alteration of plagioclase in all samples and is characteristically euhedral when examined by SEM analysis. The reaction by which plagioclase is converted to adularia during metasomatism is typically considered to be a simple alkali-exchange reaction:

$$NaAlSi_3O_8 + K^+ \rightleftharpoons KAlSi_3O_8 + Na^+$$

(i.e. Roddy et al., 1988; Glazner, 1988). This reaction assumes an albite endmember composition for plagioclase which is not valid for plagioclase from the Hells Mesa Tuff based on electron microprobe analyses, although it appears reasonable for plagioclase from the upper Lemitar as it is extremely Ca-poor (Table 2). Assuming little to no Ca content in the plagioclase, the K:Na ratio for an alkali-exchange reaction during metasomatism should approximate 1:1. Geochemical results in this study show a 1:1 exchange between K and Na for both units (Figure 11), which suggests an alkali-exchange reaction. However, this does not explain the occurrence of other phases, such as clay minerals, in the alteration assemblage; authigenic clay minerals would not form during this simple alkali-exchange reaction. Rather, data from this study suggest a dissolution-precipitation reaction as the most likely mechanism for formation of the alteration assemblage based on the abundance of clay minerals in the assemblage as well as the presence of dissolution textures within plagioclase phenocrysts (Figure 8). The dissolution of plagioclase in the presence of a K-rich fluid could account for the formation

of a variety of phases in the alteration assemblage including adularia, clay minerals and calcite. A dissolution-precipitation reaction for K-metasomatism in the Socorro area is therefore favored over an alkali-exchange reaction.

The dramatic increase in the K_2O content of metasomatized rocks has typically been attributed to adularia formation upon alteration. The use of separated samples is particularly beneficial in evaluating this concept, for when the samples are arranged in order of increasing amount of adularia in the assemblage, based upon ratios obtained by XRD analysis, several trends relating mineralogy to chemistry are evident. As predicted, an increase in the adularia content of the upper Lemitar and Hells Mesa ignimbrites corresponds to a general increase in whole rock K_2O content (Figure 20a and b).

The increase in Rb content of both the upper Lemitar and Hells Mesa ignimbrites can also be explained by an increase in the abundance of adularia within the alteration assemblage. Figure 20c and d shows that with an increasing amount of adularia, Rb concentration also increases. The increase in Rb is likely due to substitution for K in the crystal lattice of adularia (Deer, Howie and Zussman, 1966). Thus an increase in K_2O content (or adularia abundance) generally coincides with an increase in Rb concentration. Whole rock Hells Mesa Tuff samples show a 2 fold increase in Rb content while separated samples from this unit show a striking 10 fold increase when compared to unaltered material. The relative Rb increase of the Hells Mesa Tuff separated samples is more dramatic than the Rb increase in whole rock samples suggesting that minerals in the alteration assemblage, particularly adularia, strongly influence the concentration of Rb. The upper Lemitar Tuff does not show this effect because KM-148, which is the 'fresh'

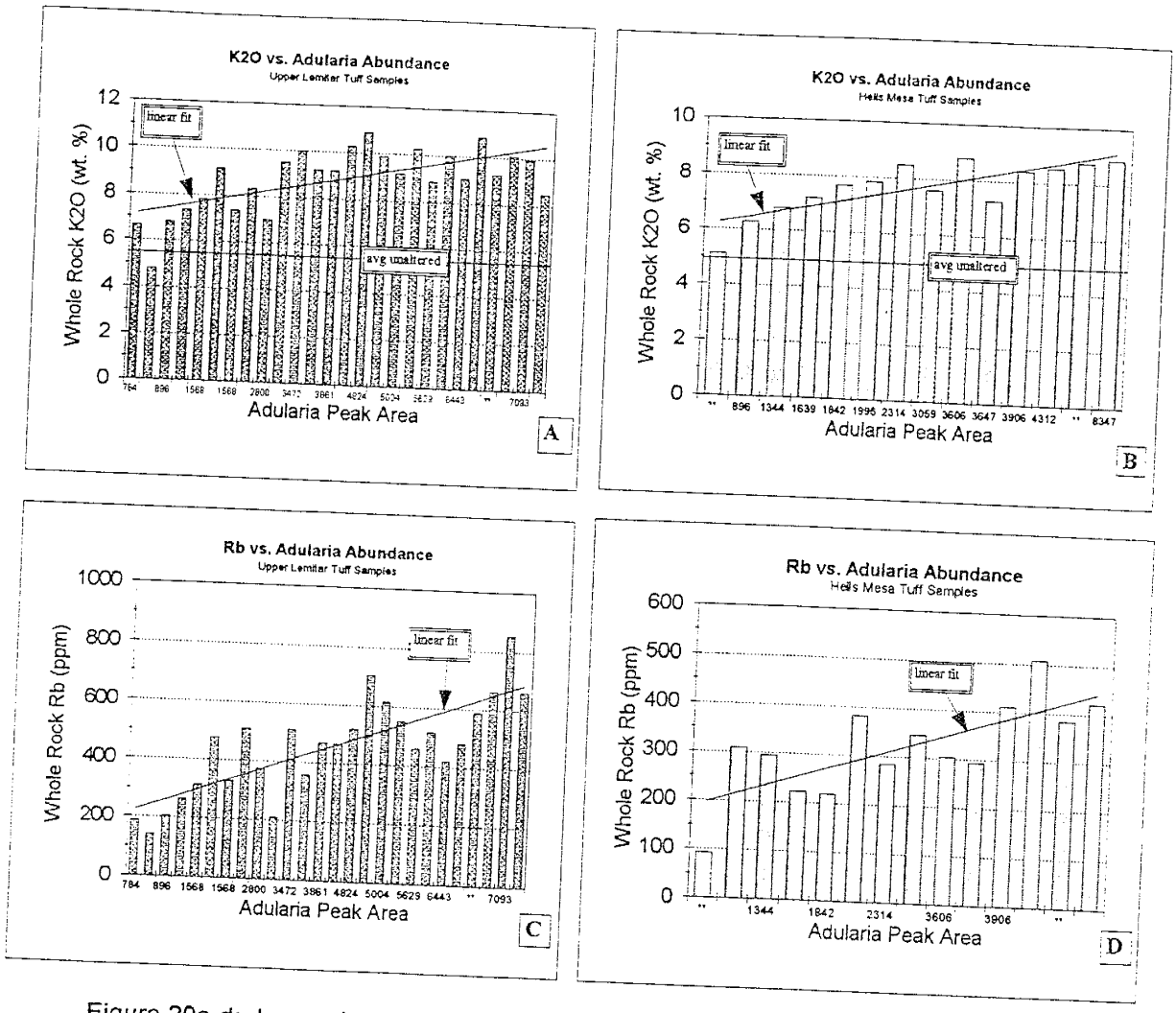

Figure 20a-d: Increasing adularia peak area (adularia content) of the separated samples vs. whole rock K2O (A&B) and Rb (C&D) content for the upper Lemitar and Hells Mesa Tuffs. * * indicates samples where peak area was estimated based on similar XRD patterns

sample used to construct the enrichment / depletion diagram for the separated samples, is actually slightly altered. Although established that KM-148 is only slightly altered, it appears that even this small amount of K-metasomatic alteration dramatically increased the Rb content of the separated samples.

Plagioclase

In thin section, plagioclase from fresh samples appears to be unaltered and shows no significant signs of replacement by clay or calcite due to weathering. Replacement of plagioclase during K-metasomatism is evident from XRD, SEM and electron microprobe analyses made during this study, and can be examined in detail because many samples were found to still contain measurable amounts of plagioclase as a result of incomplete alteration during K-metasomatism. The decrease in Na_2O and Sr in both whole rock and separated samples is attributable to the chemical breakdown of plagioclase. Figure 21a and b shows depletion of Na_2O in whole rock samples from the metasomatized area when arranged in order of increasing adularia abundance. The line at approximately 4 wt. % Na_2O represents the average Na_2O value for fresh equivalent or unmetasomatized rocks, thus showing the overall depletion of Na_2O in the Hells Mesa and upper Lemitar Tuffs.

Furthermore, Na_2O depletion in the separated samples is evident, and elucidates the process by which Na_2O depletion takes place during alteration (Figure 21c and d). Na_2O content within the separated samples is shown to decrease with the amount of residual plagioclase contained within a sample. The conclusion that much of the Na_2O was lost due to plagioclase dissolution is exemplified by the comparison of the relative

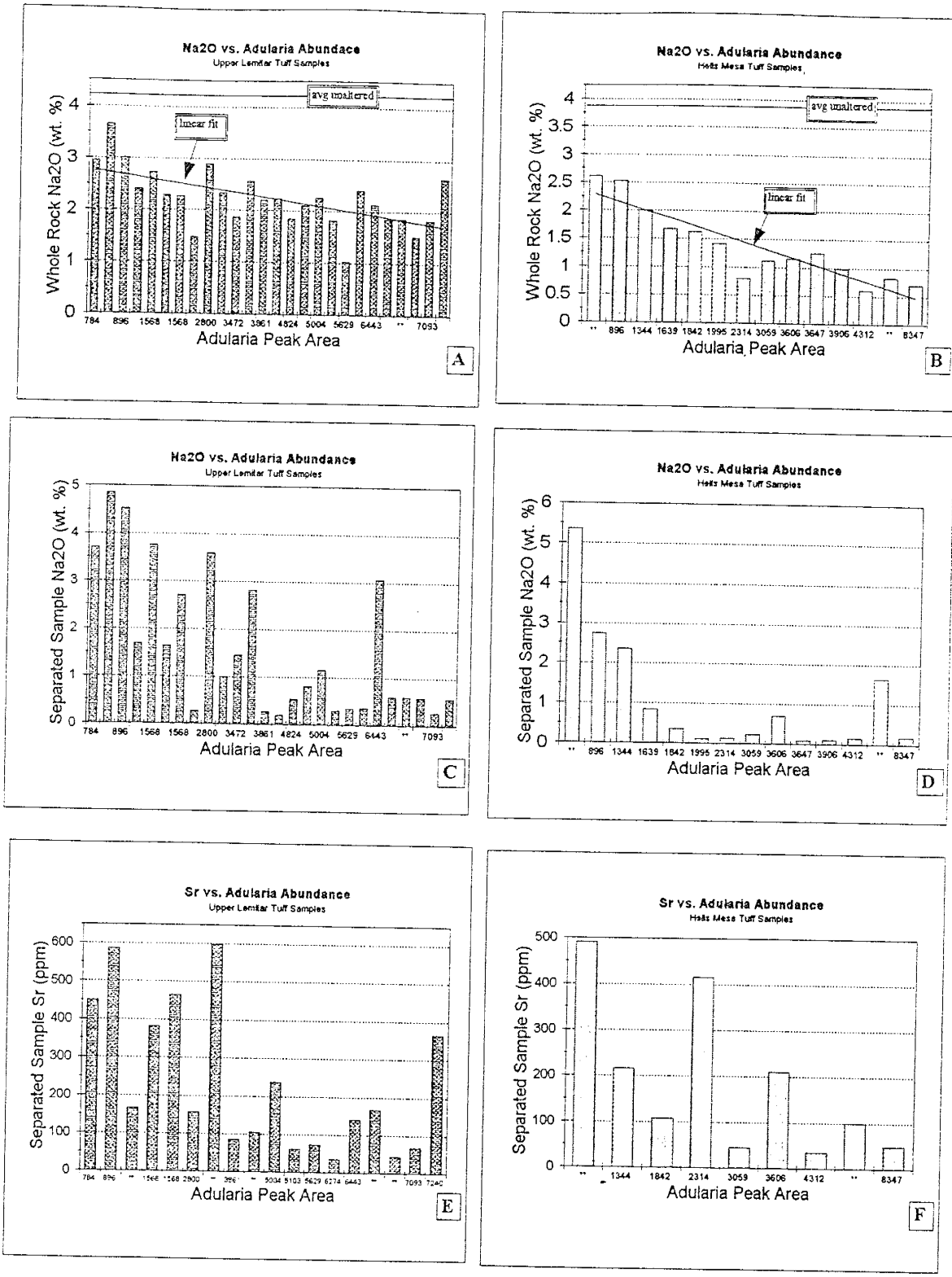

Figure 21a-f: Increasing adularia peak area (adularia abundance) within separated samples vs. whole rock Na2O (A&B), Na2O in separated samples (C&D), Sr in separated samples (E&F) for the upper Lemitar and Hells Mesa Tuffs. * * indicates samples where peak area was estimated based on similar XRD patterns.

Na_2O depletions in the altered whole rock and separated samples. The Na_2O content of the separated samples decreases by approximately 2 times whereas the relative decrease in altered whole rock is much less as a result of dilution due to the presence of other Na_2O bearing phases within the rock which are less easily altered compared to plagioclase. The Sr content of both whole rock and separated samples follows Na_2O depletion due to Sr compatibility in plagioclase. Hence, upon removal of plagioclase from the rock, Sr becomes depleted as indicated by decreasing Sr content with increasing adularia content (Figure 21e and f).

Discrete Smectite

Discrete smectite is the least abundant clay mineral in the K-anomaly, occurring as the dominant clay mineral in only a few samples, all of which show rather complete degrees of alteration; plagioclase is absent and altered crystals are abundant. Because previous studies of K-metasomatism did not recognize discrete smectite in the alteration assemblage, the origin of this phase has not been addressed prior to this study. SEM data for this study is somewhat ambiguous as to the stability of smectite, however it is interpreted to be authigenic because smectite is never found in primary, unaltered volcanic rocks.

Several lines of evidence suggest that discrete smectite is a product of K-metasomatism rather than being hydrothermally produced. First, is the temperature constraint placed on smectite formation and stability. Smectite was found by Boles and Franks (1979) to disappear, or become converted to a more illitic composition, at

temperatures >70°C. Fluid inclusion analyses from the Luis Lopez district suggest this alteration event formed between 150-375°C (Norman et al., 1983), which is fairly typical of most epithermal systems (Guilbert and Park, 1986), thus eliminating a hydrothermal source for smectite. Furthermore, smectite has been observed to have formed in alkaline, saline environments (i.e. de Pablo-Galan, 1990; Jones and Weir, 1983; Hay and Guldman, 1987), suggesting that smectite within the alteration assemblage may have been produced directly by K-metasomatic alteration.

Although smectite formation in alkaline environments has been proposed, it is generally believed that discrete smectite cannot form where the concentration of K is particularly high (Deer, Howie, and Zussman, 1966). It therefore seems likely that smectite formed during a stage of K-metasomatism when K concentration was relatively low. Assuming the fluid initially had a relatively low cation/H^+ activity ratio, precipitation of smectite from plagioclase dissolution may occur (Duffin et al., 1989; Harrison and Tempel, 1993). As the fluid increased in K^+/H^+ ratio, due to progressive evaporation of the lake brine and increased K input from the weathering of a K-rich source rock, the formation of smectite would cease. An increase in the K concentration of the fluid would result in precipitation of either mixed layer illite-smectite or adularia, depending on the K^+/H^+ ratio (Meyer and Hemley, 1967). Discrete smectite is noted to be particularly Mg-rich based on electron microprobe results (Figure 9). Mg content of plagioclase from the upper Lemitar and Hells Mesa Tuffs is very low (Table 2) suggesting Mg was brought in by the fluid. Dunbar et al. (1994) observe significant MgO depletion in overlying basaltic andesite deposits, which may be a possible source of Mg for smectite formation.

Illite and Mixed-Layer Illite/Smectite (I/S)

Mixed-layer I/S is one of the most common clay minerals present within the Socorro K-metasomatized area, whereas discrete illite is extremely rare in the alteration assemblage. SEM and electron microprobe data indicate the stability of mixed-layer I/S clay, however a definitive explanation for its presence within the alteration assemblage is difficult to ascertain. Based on data from this study and conclusions drawn by other researchers, however, it is possible to make some observations related to the origin of this mineral phase.

The breakdown of K-feldspar is frequently called upon as a mechanism for the formation of illite and/or mixed-layer I/S in diagenetic settings (i.e. Boles and Franks, 1979; Altaner, 1986; Wintsch and Kvale, 1994). SEM and electron microprobe data in this study, however, show euhedral adularia in direct contact with mixed-layer I/S, thus eliminating the possibility that the breakdown of adularia resulted in mixed-layer I/S formation. In the Socorro K-anomaly, mixed-layer I/S is most likely formed as a result of 'smectite cannibalization' by the reaction:

$$\text{Smectite} + K^{+} \rightarrow \text{Illite} + Si^{4+}$$

(Boles and Franks, 1979), which may also explain fine-grained quartz within the alteration assemblage due to the release of silica.

A fluid-mediated reaction such as illitization is likely governed by three processes: dissolution, solute mass transfer, and precipitation or crystallization (Eberl and Srodon, 1988). In a fluid dominated system, dissolution of primary smectite is typically not the

rate-limiting step during illitization. The fine-grained nature of the primary smectite and the sheet-like morphology of the grains significantly increase the rate of dissolution, which is further enhanced by extensive cationic substitution within the smectite (May et al., 1986; Whitney, 1990). K-metasomatism in the Socorro area was presumably fluid-dominated with an abundance of ions as indicated by the extensive addition of K throughout the anomaly. The high K concentration in the fluid would cause smectite to become illitized by K fixation between the smectite layers (Jones and Weir, 1983; Awwiller, 1993). The temperature required for transformation of smectite to mixed-layer I/S is about 100°C (Aoyagi, and Kazama, 1980), although illitization has been reported at lower temperatures (Srodon and Eberl, 1984; Jones and Weir, 1983). These estimated temperatures are similar to the temperatures at which K-metasomatism is thought to occur in the Socorro area (Chapin and Lindley, 1986; Dunbar et al., 1996).

An alternative explanation for the formation of mixed-layer I/S in the alteration assemblage is coprecipitation with adularia during K-metasomatism. SEM and electron microprobe data show mixed-layer I/S to be a stable, integral part of the mineral assemblage formed during metasomatic alteration, thus allowing for the possibility that mixed-layer I/S, and perhaps discrete smectite, coprecipitated with adularia. Unfortunately, convincing evidence for coprecipitation is difficult to obtain. However, it remains a distinct possibility based on SEM and electron microprobe data collected during this study.

Kaolinite

Kaolinite is an extremely common clay mineral component in the alteration assemblage of samples collected within the K-anomaly. SEM photographs clearly demonstrate the euhedral morphology of kaolinite, indicating an authigenic origin; however the mechanism through which kaolinite formed within the separated samples is somewhat difficult to ascertain.

Within the Socorro K-anomaly, areas of hydrothermal alteration tend to coincide with the presence of kaolinite in the alteration assemblage, suggesting a hydrothermal source for kaolinite within the assemblage. For example, Hells Mesa Tuff samples KM-112 through KM-116 were collected near the Luis Lopez manganese district and contain a considerable amount of kaolinite in the mineral assemblage (Table 1). The presence of barite in the separated sample of KM-115, as well as elevated Ba content in several others, further suggests these samples have experienced some amount of hydrothermal overprinting. Kaolinite is often recognized in many types of hydrothermal alteration such as argillic and advanced argillic due to wall-rock interaction. In these regimes, kaolinite formation is restricted to lower temperatures (<200°C), indicating its formation during the late stages of hydrothermal activity (Guilbert and Park, 1986). Hydrothermal kaolinite typically exhibits a characteristic texture of relatively small flakes that are tightly packed which tend to occur as single sheets, sheaves, or thin packets rather than expansive books (Keller, 1976), which is similar to the morphology of kaolinite observed by SEM analysis in this study.

Furthermore, kaolinite formation during diagenesis occurs under dilute, acidic

conditions while basic and concentrated solutions result in kaolinite instability (Dunoyer de Segonzac, 1970). Conditions for K-metasomatism in the Socorro area are believed to have been alkaline and highly concentrated, as indicated by the large amount of K added to the surrounding rock, (Chapin and Lindley, 1986), again implying kaolinite was formed as a product of hydrothermal events superimposed on the Socorro K-anomaly.

Calcite

When present in the alteration assemblage, calcite is rarely observed in large quantities. XRD of all 41 separated samples only detected calcite in a handful of samples. Calcite may form in response to the Ca released during plagioclase dissolution, which has been noted in many diagenetic settings (i.e. Harrison and Tempel, 1993; Boles and Franks, 1979). Because plagioclase from the Hells Mesa Tuff is significantly more Ca-rich than plagioclase from the upper Lemitar Tuff (Table 2), it would seem probable that calcite would occur more frequently in Hells Mesa Tuff samples upon plagioclase dissolution. There appears to be no such correlation, however.

Chemical Enrichments and Depletions

K-metasomatic alteration resulted in the enrichment of some elements and the depletion of others, causing significant deviation from the primary chemistry of the upper Lemitar and Hells Mesa ignimbrites. Notably, samples from this study are significantly enriched in K_2O, Rb, As, Ba, Pb, Sb, and Cs and depleted in Na_2O, CaO, and Sr as indicated by Figures 10 and 15. The lack of significant deviation for the major elements

TiO_2 and Al_2O_3 indicates no significant weight loss or gain within the units, thus suggesting the other elements represent real changes. As discussed earlier, the K_2O and Na_2O enrichment/depletion appear to be chemically coupled and related mainly to dissolution of Na-bearing phases, such as plagioclase. The depletion of MgO is noted by Dunbar et al. (1994) in silicic ignimbrites, but in this study only the Hells Mesa ignimbrite shows some depletion, possibly indicating variable behavior of this element during alteration. The enrichment or depletion of many of these elements has been recognized by Chapin and Lindley (1986) and Dunbar et al. (1994).

Several of the elements that are enriched in the area, however, are unlikely to have been affected by K-metasomatic alteration and may therefore reflect some amount of hydrothermal input. The elements most likely to represent input from a source other that K-metasomatism include As, Sb, Ba, and Pb as indicated by a relatively good correlation between high concentrations of these elements with proximity to hydrothermally affected regions. Low levels of As and possibly Ba and Sb enrichment appear to be related to K-metasomatism, however, high levels are clearly attributable to hydrothermal alteration.

Elements such as K_2O, Rb and possibly Ba, As, and Sb appear to be controlled primarily by the stability of the alteration assemblage produced upon plagioclase dissolution. In contrast, Na_2O and Sr are depleted as a result of plagioclase instability and are removed from the system upon alteration. The observation that the chemical changes associated with alteration reflect the alteration mineral assemblage is supported by the greater relative increase in the enrichment / depletion factor calculated for the separated samples compared to whole rock samples.

Rare Earth Elements

The depletion of REE in the upper Lemitar Tuff and enrichment in the Hells Mesa Tuff observed in this study are unique, for most studies of K-metasomatic alteration report little to no variation in REE distribution in rhyolitic rocks as a result of alteration (i.e. Glazner, 1988; Roddy et al., 1988; Hollocher et al., 1994). The striking enrichment and depletion of REE within the ignimbrites implies that redistribution or movement of these elements can indeed occur during alteration. Some researchers believe that movement of fluids during diagenesis has the ability to change element distributions and ratios (i.e. Alderton, 1980; Condie et al., 1995), however others believe diagenetic and low-grade metamorphic effects on REE are minimal (i.e. Chaudhuri and Cullers, 1979; Elderfield and Sholkovitz, 1987; Sholkovitz, 1988), especially when the fluid temperature is <230°C (Michard, 1989). In the Socorro anomaly, the whole rock REE enrichment or depletion trends are not particularly strong, for many of the REE values of altered samples fall into a range defined by fresh samples. The separated sample trends reflect those seen in whole rock samples, but are distinctly more pronounced suggesting that variations in REE may be a function of alteration mineralogy produced by the metasomatic process as proposed by Dunbar et al. (1994).

Alderton (1980) concludes that REE gains and losses are primarily controlled by: 1. REE concentrations of the reacting minerals; 2. relative stability of the mineral phases with respect to the fluid; 3. the availability of sites within the secondary assemblage to accommodate released REE; 4. the REE concentration of the incoming fluid; and 5. the ability of the fluid phase to transport REE out of the system. Several of these factors,

especially the first two, are fairly well constrained for the Socorro area. For instance, the REE concentrations of plagioclase from the upper Lemitar and Hells Mesa Tuffs, the most reactive mineral during K-metasomatic alteration, have been analyzed (KM-148 and KJH-26). SEM and electron microprobe data indicate the relative stability of minerals contained within the alteration assemblage, including clay minerals, and it is hypothesized that the clay minerals produced during K-metasomatism in the Socorro area may provide the necessary sites for REE accommodation. Unfortunately, the REE concentration of the incoming fluid and the ability of the fluid to transport REE is unknown for the Socorro area, although inferences may still be possible as discussed in the following section.

Rare Earth Element Enrichment / Depletion

A possible mechanism by which REE may have been depleted in the upper Lemitar Tuff and enriched in the Hells Mesa Tuff is through re-equilibration between the mineral assemblage and the altering fluid. Because plagioclase is the primary mineral phase affected by K-metasomatism, its initial REE content, with respect to the fluid REE content, may control whether enrichment or depletion would occur upon alteration. Variation in plagioclase REE composition does exist, although it is generally considered to have a low REE content. As indicated by Figure 22, upper Lemitar Tuff plagioclase is significantly more REE-rich than Hells Mesa Tuff plagioclase. Notably, upper Lemitar Tuff plagioclase is approximately 1.2 to 3.0 times greater in light REE (La, Ce, and Nd), and 6.6 to 11 times greater in middle and heavy REE (Sm to Lu, excluding Eu) content compared to Hells Mesa Tuff plagioclase. From Figure 17, it appears that the separated

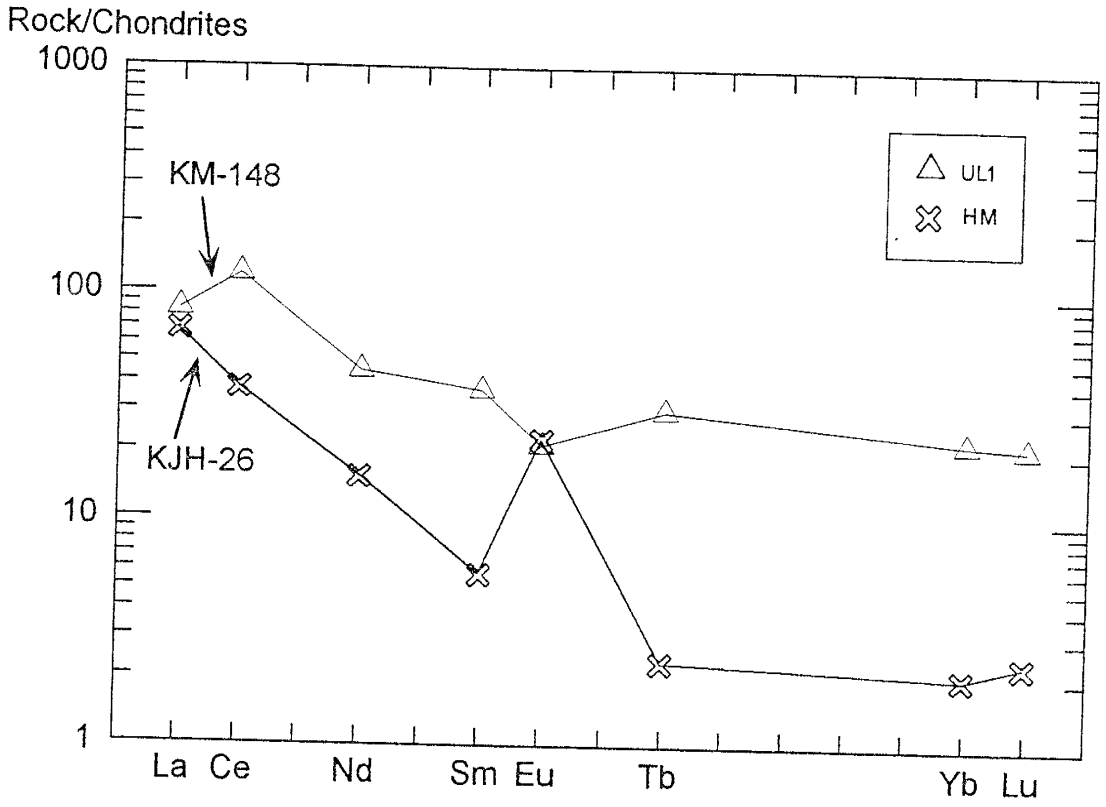

Figure 22: REE spider diagram for upper Lemitar plagioclase (KM-148) and Hells Mesa plagioclase (KJH-26). Note relatively large difference in heavy REE content between the upper Lemitar and Hells Mesa plagioclase.

samples converge toward a similar REE content upon alteration, suggesting a fluid REE content roughly intermediate to the REE content of upper Lemitar and Hells Mesa Tuff plagioclase. Because the difference between the light REE content of plagioclase from the two units is relatively minor, a fluid of an intermediate composition would not likely cause a significant change in the light REE content upon re-equilibration. The substantial deviation between the middle and heavy REE content of plagioclase from the two units, however, may explain why enrichment or depletion of these REE is particularly dramatic while the light REE appear to show variable concentrations.

Unfortunately, because the chemistry of the altering fluid is not known, the chemical potential to redistribute REE is also unknown. Initial results from this study, however, appear to indicate that re-equilibration between the fluid and alteration mineral assemblage may be a viable mechanism to explain the REE contents of the separated samples.

Incorporation of REE

An important consideration when evaluating enrichment or depletion of REE within an alteration mineral assemblage is identifying which minerals can incorporate REE into their crystal lattice. In the Socorro K-metasomatized area, the main alteration reaction is the chemical dissolution of plagioclase resulting in formation of adularia and various clay minerals. Generally, the reaction of plagioclase to K-feldspar (adularia) results in little change in REE content (Alderton, 1980; Condie et al., 1995). Clay minerals, however, can show quite significant variation in REE content, which is typically a function of the clay mineralogy, the REE content of the source, weathering conditions,

and exchange reactions during transportation or deposition (Cullers et al., 1975).

Preliminary data from this study suggests that clay minerals may play a significant role in incorporating REE, and may provide the mechanism for REE redistribution during K-metasomatism. Variations in clay REE content are typically a function of clay mineralogy. In general, the REE content of illite is greater than kaolinite, which is greater than smectite (Caggianelli et al., 1992), although the differences are relatively minor. As a result, the clay minerals within the separated samples are grouped together in order to obtain a maximum number of data points when comparing REE contents. The trends of REE depletion in the upper Lemitar Tuff and enrichment in the Hells Mesa Tuff may be related to the clay content in the separated samples (Figures 23 and 24). However, the light REE display trends similar to those found for heavy REE, which does not appear to coincide with other diagrams of enrichment or depletion (compare Figures 23 and 24 to Figures 10 and 15). This may be a function of the lack of data points and the fact that a few points appear to control the linear regression. The lack of data points, especially for the Hells Mesa Tuff separated samples, makes evaluation of where REE are located within the alteration assemblage somewhat speculative, although preliminary data suggests incorporation of REE in the clay minerals.

Stable Isotopes

Stable isotope data on both whole rock and separated samples from the upper Lemitar and Hells Mesa Tuffs clearly indicate enrichment of ^{18}O within the metasomatized area, but are difficult to interpret without better temperature constraints. Several factors

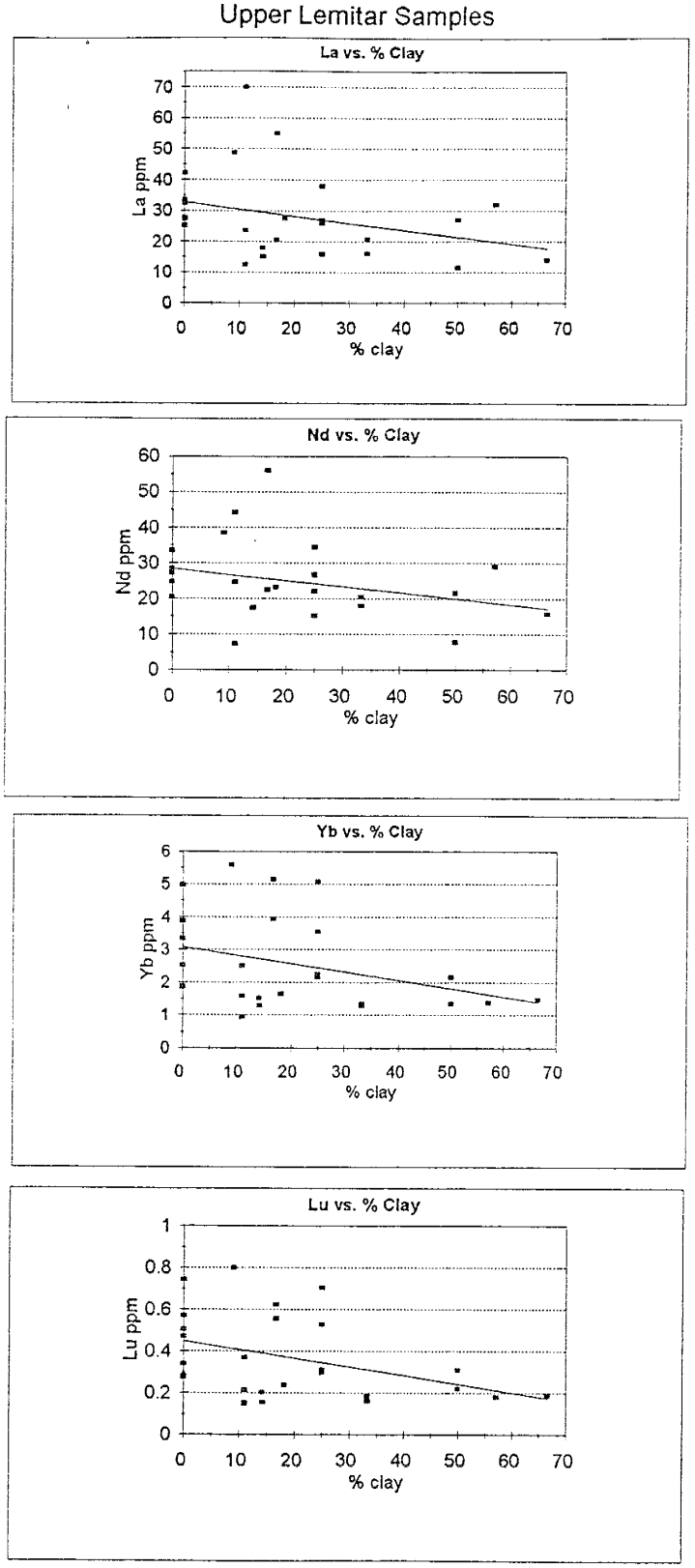

Figure 23: Percent clay vs. REE content of upper Lemitar separated samples.

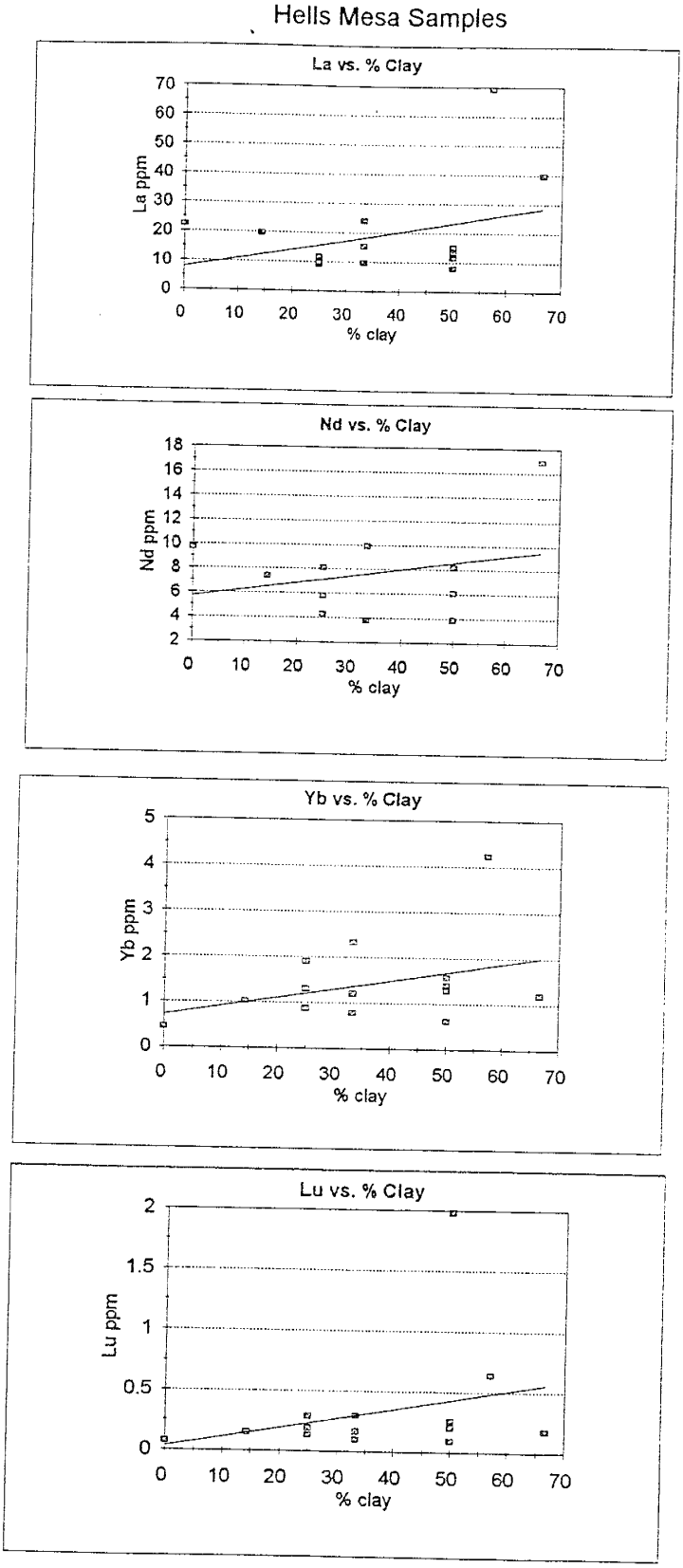

Figure 24: Percent clay vs. REE content of Hells Mesa separated samples

suggest that $\delta^{18}O$ values from rocks in the Socorro K-anomaly represent equilibration with meteoric waters at temperatures of 30-80°C, although it should be mentioned that these values also support equilibration with high temperature, magmatic water (Chapin and Lindley, 1986). Secondary fluid inclusions within quartz phenocrysts from the Hells Mesa Tuff produce homogenization temperatures ranging from 90-170°C, with a sizable number of samples reflecting a T_h of 120°C (Eggleston, unpub data). Eggleston also notes that several inclusions measured at a temperature of ~90°C have a much higher salinity than other inclusions within the area, hypothesizing that these inclusions are most likely related to potassic alteration. In addition, apatite fission-track analysis indicates that samples collected from the upper Lemitar and Hells Mesa ignimbrites have been exposed to temperatures on the order of 170-200°C and suggests a rapid cooling event during the middle-Miocene (Dunbar et al., 1996). Compared to other areas of K-metasomatism, the temperatures of alteration obtained for the Socorro area are similar (i.e. Glazner, 1988; Girard, 1988; Roddy et al., 1988). However, additional direct measurement of temperature in the Socorro area is needed before accurate conclusions can be drawn for the stable isotope data.

Summary

K-metasomatism near Socorro, New Mexico has affected the geochemical, mineralogical, and isotopic composition of Cenozoic rocks including two silicic ignimbrites, the upper Lemitar and Hells Mesa, which were investigated in this study. K-metasomatism strongly affected Na-rich minerals, particularly plagioclase, while K-rich minerals such as sanidine are basically unaffected during alteration. The preferential sampling of plagioclase in this study allows for the direct determination of the minerals present in the altered plagioclase phenocrysts. Using XRD and semi-quantitative clay mineral analysis, the alteration assemblage was found to consist of various amounts of adularia (a low-temperature K-feldspar), quartz, mixed-layer I/S, kaolinite, discrete smectite and illite, and occasional calcite and barite. Some residual plagioclase also remains in the assemblage as a result of incomplete dissolution during K-metasomatism. Kaolinite and mixed-layer I/S occur most frequently, and often in the greatest abundance, of all the clay minerals present within the altered plagioclase. Discrete montmorillonite and illite occur infrequently in the alteration assemblage. SEM and electron microprobe data from this study suggest the alteration assemblage formed through a dissolution-precipitation reaction as indicated by the presence of dissolution embayments within plagioclase phenocrysts and mixed-layer clay in the assemblage.

It is probable that mixed layer illite-montmorillonite, discrete smectite and illite were formed during K-metasomatism as a result of changes in the fluid chemistry. Smectite likely formed during stages of metasomatism when the fluid was relatively dilute and had a low (cation)/(H^+) ratio. As the fluid became progressively more concentrated in

K^+, it is likely that 'smectite cannibalization' occurred resulting in illitization and the formation of mixed-layer clays. Kaolinite is most likely the result of hydrothermal overprinting as indicated by a good correlation between areas of known hydrothermal activity and large abundances of kaolinite in the alteration assemblage. Kaolinite formation is also promoted by acidic conditions suggesting it is not likely to have formed under the alkaline conditions imposed during K-metasomatic alteration, thus further supporting a hydrothermal origin for this mineral. Calcite, which is extremely rare in the alteration assemblage, is fine-grained and likely formed as a result of plagioclase dissolution. Barite is present in the assemblage due to localized hydrothermal events in the Socorro area.

The chemical composition of altered rocks, analyzed by XRF and INAA, show an overall enrichment of K_2O, Rb, Ba, As, Sb, Cs, and Pb along with marked depletion of Na_2O, CaO, and Sr when compared to unmetasomatized rocks from outside of the potassium anomaly. Enrichment of K_2O and Rb in whole rock samples is correlated with the abundance of adularia in the separated, altered plagioclase samples suggesting the presence of adularia in the alteration assemblage controls the K_2O and Rb content of the ignimbrite units. Element mapping for K on the electron microprobe also indicates adularia as the dominant K-rich phase produced during alteration. The enrichment of Rb during K-metasomatism is due to substitution for K in the crystal lattice of adularia. A good correlation is also shown for Na_2O and Sr content with increasing adularia content in the separated samples, indicating that the decrease in Na_2O and Sr within whole rock and separated samples is due to the destruction of plagioclase during the alteration process. In

general, the silicic ignimbrites investigated have a wide variety of chemical concentrations present, suggesting that K-metasomatism is somewhat inhomogeneous.

Enrichment of Ba, As, Sb, Cs, and Pb in the two ignimbrites is likely a result of input from a hydrothermal source, for many of the samples possessing particularly high levels of these elements were collected in the vicinity of known areas of hydrothermal overprinting. Low levels of As and possibly Ba and Sb enrichment, however appear to be related to K-metasomatism. Several elements such as SiO_2, TiO_2, Fe_2O_3, Nb, Y, and Zr show neither enrichment or depletion upon K-metasomatism, but clearly demonstrate the chemically zoned nature of the upper Lemitar ignimbrite due to progressive tapping of the magma chamber.

In addition to the enrichment or depletion of elements already mentioned, the redistribution of REE, rare earth elements, has also occurred in the Socorro K-metasomatized area. Depletion of REE in the upper Lemitar Tuff and enrichment in the Hells Mesa Tuff is unique in that most studies of K-metasomatism report no significant change in REE content upon alteration (i.e. Glazner, 1988; Roddy et al., 1988). The depletion and enrichment of REE in the Socorro anomaly may have resulted from a fluid REE composition intermediate to the REE content of upper Lemitar Tuff and Hells Mesa Tuff plagioclase. The observation that REE enrichment and depletion is more dramatic in the separated samples compared to whole rock samples further suggests that the initial composition of plagioclase may have been responsible for the resultant change in REE content. Also, upper Lemitar Tuff plagioclase contains significantly more middle and heavy REE compared to Hells Mesa Tuff plagioclase, which is consistent with the greater

enrichment/depletion of these REE compared to the light REE within the separated samples. Preliminary results suggest REE may be incorporated into the clay minerals of the alteration assemblage, although additional data is required before a definitive conclusion can be made.

Stable isotope data clearly indicates enrichment of $\delta^{18}O$ within the K-metasomatic area, however a conclusive explanation for this enrichment is elusive due to poor temperature constraint for the Socorro anomaly. Temperature ranges thought to be representative of K-metasomatism suggest low-temperature (~100-170°C) equilibration with meteoric waters as the most likely mechanism for K-metasomatism, however high-temperature (>250°C) equilibration with magmatic waters cannot be ruled out based strictly on $\delta^{18}O$ values obtained. Separated sample $\delta^{18}O$ values are comparable to whole rock values, suggesting the alteration assemblage does not exclusively control the enrichment or depletion of ^{18}O within the K-anomaly.

Conclusions

K-metasomatism of silicic ignimbrites near Socorro, New Mexico caused the dissolution of Na- and Ca-rich minerals, in particular plagioclase, and the precipitation of K-rich adularia along with a variety of clay minerals and quartz. Geologic evidence, such as the large aerial extent of the metasomatized area along with the presence of thick playa deposits, suggests a lacustrine system containing a low-temperature, alkaline-saline, meteoric derived fluids. Long-term leaching of K-rich source rocks followed by evaporation and concentration of basinal fluids resulted in a K-enriched brine solution. However, the variable K content of the fluid over time can explain the presence and stability of K-poor minerals such as discrete smectite within the alteration assemblage. Instabilities in evaporation-induced density stratification beneath saline lakes may have been the driving mechanism for movement and interaction of the K-rich brines with the rock underlying the playa system (Leising et al., 1995). Upon interaction between the host rocks and the fluid, K was removed from the fluid and added to the rock through the formation of authigenic adularia and mixed-layer I/S. The strong depletion of Na in host rocks during metasomatism should have resulted in a Na-enriched fluid, however the absence of secondary, Na-rich phases both in and adjacent to the K-anomaly continues to be problematic. Further complicating interpretation of the mechanism responsible for K-metasomatism in the Socorro area is the lack of distinct, K-depleted source rocks. The long term leaching of elements from surrounding rocks may explain the lack of a noticeably depleted source area for elements enriched during K-metasomatic alteration.

During K-metasomatism, elements such as K, Na, Ca, Mg, Rb and Sr are typically

mobile on a regional scale (i.e. Glazner, 1988; Roddy et al., 1988; Hollocher, 1994), however the mobilization of REE during alteration in the Socorro area also suggests element redistribution on a localized scale through attempted chemical equilibration between the altering fluid and the host rock. Formation and stability of the alteration assemblage produced through K-metasomatism, in particular clay minerals, may provide available sites for REE incorporation. The chemical nature of the metasomatic fluid with respect to the initial starting composition of the phases undergoing alteration is apparently sufficient to cause REE mobilization on a localized scale.

Additional evidence for an alkaline, saline system may be found within the secondary mineral assemblage produced through K-metasomatism. Alkaline, saline lakes are sometimes characterized by concentric zones of authigenic minerals thereby reflecting a lateral hydrogeochemical gradient within the lake basin. Zonation of authigenic minerals, particularly an increase in the amount of adularia basinward, in the Socorro K-anomaly may be present as indicated by a correlation between K_2O content and adularia abundance. However, the zonation of authigenic minerals within the Socorro area could be complicated by the chemical signature of localized, hydrothermal events superimposed on the K-metasomatized region. The presence of superimposed, hydrothermal activity should also be evaluated in other studies of K-metasomatism in the Western United States. Recognition of mineral zonation within areas of K-metasomatism could provide evidence for a lacustrine depositional environment as the mechanism for K enrichment.

Suggestions for Future Research

(1.) The distribution of kaolinite within the K-anomaly has been determined by this study, however the mechanism through which this mineral is produced is still speculative. Thin section microscopy of unaltered tuff samples generally indicates that plagioclase has not undergone significant alteration through weathering or diagenesis, however at least one unaltered sample shows slight plagioclase replacement by either clay or calcite. If plagioclase has been partially replaced by kaolinite prior to K-metasomatism, this may account for the presence of kaolinite within the alteration assemblage. A few thin sections of unaltered samples impregnated with blue epoxy should be sufficient to determine whether the plucked plagioclase grains in unaltered samples are due to alteration through weathering or as a result of the thin section making process. SEM or electron microprobe analysis of fresh plagioclase from a few unaltered samples could also better establish the effects of weathering and diagenesis prior to K-metasomatism.

(2.) A recent $^{40}Ar/^{39}Ar$ geochronology study of K-metasomatism in the northern Grand Range, Nevada found that sanidine can become adularized during alteration (Brooks and Snee, 1996). Data from this study suggest sanidine is basically unaffected by K-metasomatism, although sanidine was not closely investigated. Investigation of sanidine adularization within the Socorro area through electron microprobe analysis may provide additional insight regarding the intensity of metasomatism.

(3.) The hydrogeology of the area affected by K-metasomatism near Socorro is largely unknown. A thorough hydrogeological model of the Socorro K-metasomatized area could provide useful information to evaluate the mechanism through which metasomatism occurred.

(4.) Better temperature constraint for K-metasomatism could possibly eliminate one of the two possibilities indicated by oxygen isotope data. Thermometric analysis of secondary fluid inclusions in quartz phenocrysts in conjunction with fission-track data may provide important data regarding the temperature at which K-metasomatism occurred.

(5.) The source of K is still unknown. In addition, the Na-enriched fluid produced through the dissolution of plagioclase should have deposited Na-rich phases either in or around the Socorro K-anomaly. However, no evidence for Na deposition in regions adjacent to the K-anomaly has been located.

References Cited

Agron, N. and Bentor, Y.K., 1981, The volcanic massif of Biq'at Hayareah (Sinai-Negev): A case of potassium metasomatism: Journal of Geology, v. 89, p. 479-495.

Alderton, D.H.M., Pearce, J.A., Potts, P.J., 1980, Rare earth element mobility during granite alteration: Evidence from southwest England: Earth and Planetary Science Letters, v. 49, p. 149-165.

Altaner, S.P., 1986, Comparison of rates of smectite illitization with rates of K-feldspar dissolution: Clays and Clay Minerals, v. 5, p. 608-611.

Aoyagi, K. and Kazama, T., 1980, Transformational changes of clay minerals, zeolites, and silica minerals during diagenesis: Sedimentology, v. 27, p. 179-188.

Austin, G.S. and Leininger, R.K., 1976, Effects of heat-treating mixed-layer illite-smectite as related to quantitative clay mineral determinations: Journal of Sedimentary Petrology, v. 46, p. 206-215.

Awwiller, D.N., 1993, Illite/smectite formation and potassium mass transfer during burial diagenesis of mudrocks: a study from the Texas gulf coast Paleocene-Eocene: Journal of Sedimentary Petrology, v. 63, p. 501-512.

Bates, R.L. and Jackson, J.A., 1984, Dictionary of geologic terms (2nd edition): Doubleday publishers, 571 p.

Boles, J.R. and Franks, S.G., 1979, Clay diagenesis in Wilcox Sandstones of Southwest Texas: Implications of Smectite diagenesis on sandstone cementation: Journal of Sedimentary Petrology, v. 49, p. 55-70.

Briggs, R.M., Gifford, M.G., Moyle, A.R., Taylor, S.R., Norman, M.D., Houghton, B.F., Wilson, C.J.N., 1993, Geochemical zoning and eruptive mixing in ignimbrites from Mangakino Volcano, Taupo Volcanic Zone, New Zealand: Journal of Volcanology and Geothermal Research, v. 56, p. 175-203.

Brooks, W.E., 1986, Distribution on anomalously high K_2O volcanic rocks in Arizona: Metasomatism at the Picacho Peak detachment fault: Geology, v. 14, p. 339-342.

Brooks, W.E. and Snee, L.W., 1996, Timing and effect of detachment-related potassium metasomatism on $^{40}Ar/^{39}Ar$ ages from the Windous Butte Formation, Grant Range, Nevada: U.S. Geological Survey Bulletin 2154, p. 1-25.

Caggianelli, A., Fiore, S., Mongelli, G., Salvemini, A., 1992, REE distribution in the clay fraction of pelites from the southern Apennines, Italy: Chemical Geology, v. 99, p. 253-263.

Chamberlin, R.M., 1980, Cenozoic stratigraphy and structure of the Socorro Peak volcanic center, central New Mexico [Ph.D. thesis]: Colorado School of Mines, 495 p.

Chapin, C.E., 1983, Selected tectonic elements of the Socorro region: New Mexico Geological Society Guidebook, 34th Field Conference, Socorro Region II, p. 97.

Chapin, C.E., Chamberlin, R.M., Osburn, G.R., White, D.L., Sanford, A.R., 1978, Exploration framework of the Socorro geothermal area, New Mexico, *in* Chapin, C.E. and Elston, W.E., eds., Field guide to selected cauldrons and mining districts of the Datil-Mogollon volcanic field, New Mexico: New Mexico Geological Society Special Publication 7, p. 115-129.

Chapin, C.E. and Lindley, J.I., 1986, Potassium metasomatism of igneous and sedimentary rocks in detachment terranes and other sedimentary basins: Economic implications: Arizona Geological Society Digest, v. 16, p. 118-126.

Chaudhaui, S. and Cullers, R.L., 1979, The distribution of REE in deeply buried Gulf Coast sediments: Chemical Geology, v. 24, p. 327-338.

Clayton, R.N. and Mayeda, T.K., 1963, The use of bromine pentafluoride in the extraction of oxygen from oxides and silicates for isotopic analysis. Geochimica et Cosmochimica Acta, v. 27, p. 43-52.

Colville, A.A. and Ribbe, P.H., 1968, The crystal structure of and adularia and a refinement of the structure of orthoclase: American Mineralogist, v. 53, p. 25-37.

Condie, K.C., Dengate, J., Cullers, R.L., 1995, Behavior of rare earth elements in a paleoweathering profile on granodiorite in the Front Range, Colorado, USA: Geochimica et Cosmochimica Acta, v. 59, p. 279-294.

Craig, H., 1961b, Standard for reporting concentrations of deuterium and oxygen-18 in natural waters: Science, v. 133, p. 1833-1834.

Cullers, R.L., Chaudhuri, S., Arnold, B., Lee, M., Wolf, C.W., Jr., 1975, Rare earth distributions in clay minerals and in the clay-sized fraction of the Lower Permian Havensville and Eskridge shales of Kansas and Oklahoma: Geochimica et Cosmochimica Acta, v. 39, p. 1691-1703.

D'Andrea, J.F., 1981, The geochemistry of the Socorro K_2O anomaly, New Mexico [M.S. Thesis]: Tallahassee, Florida State University, 243 p.

D'Andrea-Dinkelman, J.F., Lindley, J.I., Chapin, C.E., Osburn, G.R., 1983, The Socorro K_2O anomaly: A fossil geothermal system in the Rio Grande rift: New Mexico Geological Society Guidebook, p. 76-77.

Davis, G.A., Lister, G.S., Reynolds, S.J., 1986, Structural evolution of the Whipple and South Mountains shear zones, Southwestern United States: Geology, v. 14, p. 7-10.

Deal, E.G., 1973, Geology of the northern part of the San Mateo mountains, Socorro County, New Mexico: A study of a rhyolite ash-flow tuff cauldron and the role of laminar flow in ash-flow tuffs [Ph.D. thesis]: Albuquerque, University of New Mexico, 134 p.

Deer, W.A., Howie, R.A., and Zussman, J., 1992, An introduction to the rock forming minerals (2nd edition): London, Longman Group Limited, 528 p.

Duffin, M.E., Lee, M., Klein, G.D., Hay, R.L., 1989, Potassic diagenesis of Cambrian sandstones and Precambrian granitic basement in UPH-3 deep hole, Upper Mississippi Valley, U.S.A: Journal of Sedimentary Petrology, v. 59, p. 848-861.

Dunbar, N.W., Chapin, C.E., Ennis, D.J., Campbell, A.R., 1994, Trace element and mineralogical alteration associated with moderate and advanced degrees of K-metasomatism in a rift basin at Socorro, New Mexico: New Mexico Geological Society Guidebook 45th field conference, p. 225-231.

Dunbar, N.W., Kelley, S., Miggins, D., 1996, Chronology and thermal history of potassium metasomatism in the Socorro, NM area: Evidence from $^{40}Ar/^{39}Ar$ dating and fission track analysis: New Mexico Geological Society Proceeding Volume [abstract], p. 23.

Dunoyer de Segonzac, G., 1970, The transformation of clay minerals during diagenesis and low-grade metamorphism: A review: Sedimentology, v. 15, p. 281-346.

Duval, J.S., 1990, Modern aerial gamma-ray spectrometry and regional potassium map of the conterminous United States: Journal of Geochemical Exploration v. 39, p. 249-253.

Eberl, D. D. and Srodon, J., 1988, Ostwald ripening and interparticle-diffraction effects for illite crystals: American Mineralogist, v. 73, p. 1335-1345.

Eggleston, T.L., Norman, D.I., Chapin, C.E., Savin, S., 1983, Geology, alteration, and genesis of the Luis Lopez manganese district, New Mexico: New Mexico Geological Society Guidebook 34th field conference, p. 241-246.

Elderfield, H. and Sholkovitz, E.R., 1987, REE in the pore waters of reducing marine sediments. Earth and Planetary Science Letters, v. 82, p. 280-288.

Ferguson, C.A., 1985, Geology of the east-central San Mateo mountains, Socorro County, NM [M.S. Thesis]: Socorro, New Mexico Institute of Mining and Technology, 118 p.

Girard, J., Aronson, J.L., Savin, S.M., 1988, Separation, K/Ar dating and $^{18}O/^{16}O$ ratio measurements of diagenetic K-feldspar overgrowths: An example from the Lower Cretaceous arkoses of the Angola Margin: Geochimica et Cosmochimica Acta, v. 52, p. 2207-2214.

Glazner, A.F., 1988, Stratigraphy, structure, and potassic alteration of Miocene volcanic rocks in the Sleeping Beauty area, Central Mojave Desert, California: Geological Society of America Bulletin, v. 100, p. 424-435.

Goldstein, J.I., Newbury, D.E., Echlin, P., Hoy, D.C., Fiori, C. and Lifshin, E., 1981, Scanning electron microscopy and x-ray microanalysis: New York, Plenum Press, 673 p.

Guilbert, J.M. and Park, C.F., 1986, The geology of ore deposits: New York, W.H. Freeman and Company, 985 p.

Harrison, W.J. and Tempel, R.N., 1993, Diagenetic pathways in sedimentary basins, *in* Horbury, A.D. and Robinson, A.G., eds., Diagensis and Basin Development, Vol. AAPG Studies in Geology #36: American Association of Petroleum Geologists, Tulsa, Oklahoma, p. 69-86.

Hay, R.L. and Guldman, S.G., 1987, Diagenetic alteration of silicic ash in Searles Lake, California: Clays and Clay Minerals, v. 35, p. 449-457.

Hildreth, W., 1979, The Bishop Tuff: Evidence for the origin of compositional zonation in silicic magma chambers: Geological Society of America Special Paper 180, p. 43-75.

Hoefs, J., 1973, Stable isotope geochemistry: New York, Springer-Verlag, 140 p.

Hollocher, K., Spencer, J., Ruiz, J., 1994, Composition changes in an ash-flow cooling unit during K-metasomatism, West-Central Arizona: Economic Geology, v. 89, p. 877-888.

Jacobs, J.W., Korotev, R.L., Blanchard, D.P., and Haskins, L.A., 1977, A well-tested procedure for instrumental neutron activation analysis of silicate rocks and minerals: Geochimica et Cosmochimica Acta, v. 40, p. 93-114.

Jones, B.F. and Weir, A.H., 1983, Clay minerals of Lake Abert, an alkaline saline lake: Clays and Clay Minerals, v. 31, p. 161-172.

Keller, W.D., 1976, Scan electron micrographs of kaolins collected from diverse environments of origin - I: Clays and Clay Minerals, v. 24, p. 107-113.

Korotev, R. and Lindstrom, D.J., 1985, Interferences from fission of U-235 in INAA in rocks: Transactions of the American Nuclear Society, v. 49, p. 177-178.

Krewedl, D.A., 1974, Geology of the central Magdalena Mountains, Socorro county, New Mexico [Ph.D. thesis]: Tucson, University of Arizona, (New Mexico Bureau of Mines and Mineral Resources Open-File Report 44), 128 p.

Lasky, S.G., 1932, The ore deposits of Socorro County, New Mexico: New Mexico Bureau of Mines and Mineral Resources Bulletin 8, 139 p.

Lee, M.R. and Parsons, I., 1995, Microtextural controls of weathering of perthitic alkali feldspars: Geochimica et Cosmochimica Acta, v. 59, p. 4465-4488.

Leising, J.F., Tyler, S.W., Miller, W.W., 1995, Convection of saline brines in enclosed lacustrine basins: A mechanism for potassium metasomatism: Geological Society of America Bulletin, v. 107, p. 1157-1163.

Lindley, J.I., 1985, Potassium metasomatism of Cenozoic rocks near Socorro, New Mexico [Ph.D. Thesis]: Chapel Hill, University of North Carolina, 563 p.

Lindley, J.I., 1979, Chemical changes associated with the propylitic alteration of two ash-flow tuffs, Datil-Mogollon volcanic field, New Mexico [M.S. Thesis]: Chapel Hill, Univ. of North Carolina, 197 p.

May, H.M., Kinniburgh, D.G., Helmke, P.A., Jackson, M.L., 1986, Aqueous dissolution, solubilities and thermodynamic stabilities of common aluminosilicate clay minerals: Kaolinite and smectites: Geochimica et Cosmochimica Acta, v. 50, p. 1667-1677.

McBirney, A.R., 1993, Igneous petrology (2nd edition): Boston, Jones and Bartlett, 508 p.

McIntosh, W.C., Sutter, J.F., Chapin, C.E., Kedzie, L.L., 1990, High-precision $^{40}Ar/^{39}Ar$ sanidine geochronology of ignimbrites in the Mogollon-Datil volcanic field, southwestern New Mexico: Bulletin of Volcanology, v. 52, p. 584-601.

Meyer, C. and Hemley, J.J., 1967, Wall rock alteration, *in* Barnes, H.L., ed., Geochemistry of hydrothermal ore deposits (2nd edition): New York, Holt, Rinehart and Winston, Inc., p. 166-235.

Michard, A., 1988, Rare earth elements systematics of hydrothermal fluids: Geochimica Cosmochimica Acta, v. 53, p. 745-750.

Moore, D.M. and Reynolds, R.C., Jr., 1989, X-ray diffraction and the identification and analysis of clay minerals: New York, Oxford University Press, 332 p.

Muecke, G.K., 1980, Neutron activation analysis in the geosciences: Halifax, Mineralogical Association of Canada, 279 p.

Nockolds, S.R., Knox, R.W.O'B., Chinner, G.A., 1978, Petrology: London, United Kingdom, Cambridge University Press, 435 p.

Norman, D.I., Bazrafshan, K., Eggleston, T.L., 1983, Mineralization of the Luis Lopez epithermal manganese deposits in light of fluid inclusion and geologic studies: New Mexico Geological Society Guidebook 34th field conference, p. 247-251.

Norrish, K. and Chappell, B.W., 1977, X-ray fluorescence spectrometry; *in* Physical Methods in Determinative Mineralogy: Academic Press.

North, R.M., 1983, Histroy and geology of the precious metal occurrences in Socorro County, New Mexico: New Mexico Geological Society Guidebook, 34th Field Conference, Socorro Region II, p. 261-268.

O'Neil, J.R., 1979, Stable isotope geochemistry of rocks and minerals, *in* Jarer, E. and Humziker, J.C, eds., Lectures in Isotope Geology: Berlin, Springer-Verlag, p. 235-263.

Osburn, G.R., 1978, Geology of the eastern Magdalena Mountains, Water Canyon to Pound Ranch, Socorro County, New Mexico [M.S. Thesis]: Socorro, New Mexico Institute of Mining and Technology, 150 p.

Osburn, G.R and Chapin, C.E., 1983a, Nomenclature for Cenozoic rocks of northeast Mogollon-Slope volcanic field, New Mexico: New Mexico Bureau of Mines and Mineral Resources Stratigraphic Chart 1.

Osburn, G.R. and Chapin, C.E., 1983b, Ash-flow tuffs and cauldrons in the northeast Mogollon-Datil volcanic field: A summary, *in* Chapin, C.E. and Callender, J.F., eds., Socorro Region II: Guidebook for the 34th annual field conference, New Mexico Geological Society, p. 197-204.

Pablo-Galan, L., 1990, Diagenesis of Oligocene-Miocene vitric tuffs to montmorillonite and K-feldspar deposits, Durango, Mexico: Clays and Clay Minerals, v. 38, p. 426-436.

Reed, S.J.B., 1993, Electron microprobe analysis (2nd Edition): Cambridge University Press, New York, 326 p.

Rehrig, W.A, Shafiquallah, M., Damon, P.E., 1980, Geochronology, geology and listric normal faulting of the Vulture Mountains, Mohave County, Arizona: Arizona Geological Society Digest, v. 12, p. 89-111.

Roddy, M.S., Reynolds, S.J., Smith, B.M., Ruiz, J., 1988, K-metasomatism and detachment-related mineralization, Harcuvar Mountains, Arizona: Geological Society of Arizona Bulletin, v. 100, p. 1627-1639.

Roy, S., 1981, Manganese deposits: New York, Academic Press, 458 p.

Shafiquallah, M., Lynch, D. J., Damon, P. E., and Peirce, H.W., 1976, Geology, geochronology and geochemistry of the Picacho Peak area, Pinal County, Arizona: Arizona Geological Society Digest, v. 10, p. 305-324.

Sholkovitz, E.R., 1988, REE in sediments of the north Atlantic Ocean, Amazon delta, and east China Sea: Reinterpretation of terrigenous input patterns to the oceans. American Journal of Science, v. 288, p. 236-281.

Srodon, J. and Eberl, D.D., 1984, Illite, *in* Mineralogical Society of America Reviews in Mineralogy, v. 13, p. 495-544.

Stix, J., Goff, F., Gorton, M.P., Heiken, G., Garcia, S.R., 1988, Restoration of compositional zonation in the Bandelier silicic magma chamber between two caldera-forming eruptions: Geochemistry and origin of the Cerro Toledo rhyolite, Jemez Mountains, New Mexico: Journal of Geophysical Research, v. 93, no. 86, p. 6129-6147.

Taylor, H.P., 1968, The oxygen isotope geochemistry of igneous rocks: Contributions to Mineralogy and Petrology, v. 19, p. 1-71.

Turner, C.E. and Fishman, N.S., 1991, Jurassic lake T'oo'dichi': A large alkaline, saline lake, Morrison Formation, Eastern Colorado Plateau: Geological Society of America Bulletin, v. 103, p. 538-558.

Walker, C. W and Renault, J.R., 1972, Determinative table of $2\theta_{Cu}$ and $2\theta_{Fe}$ for minerals of Southwestern United States: New Mexico Bureau of Mines and Mineral Resources Circular 127.

Welton, J.E., ed., 1984, SEM Petrology Atlas: The American Association of Petroleum Geologists, Tulsa, Oklahoma, 237 p.

Whitney, G., 1990, Role of water in the smectite-to-illite reaction: Clays and Clay Minerals, v. 38, p. 343-350.

Willard, M.E., 1973, Geology of the Luis Lopez manganese district, New Mexico: New Mexico Bureau of Mines and Mineral Resources Open-File Report 186, 81 p.

Winchester, J.A. and Floyd, P.A., 1977, Geochemical discrimination of different magma series and their differentiation products using immobile elements: Chemical Geology, v. 20, p. 325-343.

Wintsch, R.P. and Kvale, C.M., 1994, Differential mobility of elements in burial diagenesis of siliciclastic rocks: Journal of Sedimentary Research A64, p. 349-361.

APPENDIX I

Analytical Methods

X-Ray Diffraction Analysis

X-ray diffraction analysis allows for the determination of the mineral assemblage present within a sample. During x-ray diffraction (XRD) analysis, a beam of x-rays is produced and directed toward a sample. The x-rays interacting with the sample will diffract due to the differences in crystal lattice dimensions and create a characteristic interference pattern. The geometry of the pattern is a function of the repeat distances (lattice dimensions) of the periodic array of atoms in the crystal. The intensities of the diffracted beam give information about the atomic arrangement and unit-cell dimensions (Bates and Jackson, 1984).

Semi-Quantitative Clay Analysis

In order to better examine the clay mineral content of the separated samples, oriented clay slides were prepared for XRD by immersing the samples in distilled water in a beaker, then allowing the coarse material to settle to the bottom of the beaker (material was left to settle for 10 minutes). A residual <2 micron-size fraction (clay fraction) is left at the top of the suspension. A 2 ml pipette was then touched to the surface of the suspension and the drawn material was placed on a petrographic slide and allowed to dry at room temperature. Approximately 3 ml of material was used per petrographic slide. Samples that would not suspend properly (i.e. were flocculating) were centrifuged then resuspended until flocculation ceased. No chemicals, such as NH_4OH or sodium

hexametaphosphate, were used to control the flocculation as this can sometimes cause ion-exchange reactions thus altering the original clay mineral composition. Flocculation was not able to be controlled in all cases and therefore some of the separated samples do not have a semi-quantitative description of the clay present.

Three scans for each sample were then run on the Rigaku x-ray diffractometer described previously. The initial run was an airdried, oriented scan from a 2θ angle of 2-35° to determine all the material present in the <2 micron-size fraction. All slides were then placed in an ethylene glycol chamber. Glycolation causes expansion of smectite and interstratified smectite layers within mixed-layer clay minerals and thus causes shifts in the reflection positions of the oriented clay samples, which aids in the task of identification (Austin and Leininger, 1976). Glycolated sides were the second run on the x-ray diffractometer and were scanned from a 2θ angle of 2-15°. After glycolation, the slides were heated at 375-380°C for 30 minutes in a Blue M lab-Heat Muffle furnace then scanned with the diffractometer between 8-9.8° 2θ immediately after removal from the furnace in order to scan over the first order illite peak (10-Å peak) while the slide remained hot. The scan between 2θ 2-15° was used to demarcate background scatter on the diffractograms. Enhancement of the 10-Å illite peak between 2θ 8-9.8° due to heating is attributed to the collapse of interstratified smectite layers between the mixed layer clays (Austin and Leininger, 1976).

Semi-quantitative XRD analysis was then performed on each clay-containing sample using equations developed by G.S. Austin (verbal and written communication, 1992; Table A) which determine the relative abundances of the major clay mineral groups

Formulas for Semi-Quantitative Clay Mineral Analysis

$$Illite = \frac{I_{1G}}{T} x10$$

$$Smectite = \frac{S_{1G}/4}{T} x10$$

$$Mixed\text{-}layer(illite/smectite) = \frac{I_{1H} - (I_{1G} + S_{1G}/4)}{T} x10$$

$$Kaolinite = \frac{K_1}{T} x10$$

$$T = Total = I_{1H} + K_1$$

Table A: Equations for semi-quantitative XRD analysis of clay minerals. Peak heights are measured from airdried, glycolated (G), or heated (H) runs. Subscript number refers to the peak order measured. For example, I_{1H} is the height of the first order illite peak on the heated run. Equations produce clay mineral abundances to parts in ten.

and quantifies them to parts in 10 based on the heights of the 001 peaks above background.

Scanning Electron Microscopy

Scanning electron microscopy (SEM) utilizes a finely focused beam of electrons which are repeatedly moved across the sample to be examined. The reflected and emitted electron intensity is measured and displayed and the image is built up sequentially (Bates and Jackson, 1984). To further the identification of minerals using SEM, energy dispersive x-ray spectra was collected, which provided qualitative data on the mineral assemblage. SEM is particularly useful for two reasons. First, high resolution images of bulk objects can be obtained even at very high magnification, and second, SEM provides a three-dimensional appearance of the specimen. SEM analyses in this study were performed on carbon-coated thin sections using a Hitachi S450 with a beam current of 15-20 kV at the University of New Mexico.

Electron Microprobe Analysis

During electron microprobe analysis, electron bombardment generates X-rays in the sample to be analyzed. The characteristic wavelength and intensity of the emitted X-rays allows the measurement of element concentrations within the sample. The generated electron beam is finely focussed allowing for a very small selected area to be analyzed (Reed, 1993). Quantitative analysis of the intensity of the X-rays from the specimen are compared with those a standard of known composition. In microprobe analysis, the X-ray

spectrum is detected with either a wavelength- or energy-dispersive spectrometer (Reed, 1993).

X-Ray Fluorescence Analysis

In X-ray fluorescence (XRF), characteristic secondary x-rays are generated from a sample upon exposure to a beam of primary x-rays. The secondary x-rays are characteristic of a particular element and have unique wavelengths. The intensity of x-rays emitted by a sample is proportional to the elemental abundance.

XRF analysis was used to determine the concentration of trace elements and major elements in whole rock samples from the silicic ignimbrite sheets. For trace element determination, approximately 7 g of <200 mesh powder was pressed into pellets using 10 tons of pressure and boric acid as the backing or matrix material. Trace element analyses were performed at the New Mexico Institute of Mining and Technology X-Ray Fluorescence Facility in Socorro, New Mexico.

Fused disks were used for determining major element concentrations and were formed via two methods: using approximately 1 g of powder material and 9 g of lithium tetraborate as a flux material followed by heating for 15 minutes in a muffle furnace prior to detection (for samples KM-31 through KM-61) and using .5 g of powder material and approximately 2.70 g of Sigma 901 as a flux material for the remaining samples. Samples KM-31 through KM-61 were analyzed at the University of New Mexico. The remaining samples were analyzed for major elements at the New Mexico Institute of Mining and Technology X-Ray Fluorescence Facility.

Neutron Activation Analysis

For Instrumental Neutron Activation Analysis (INAA), the samples are first irradiated, thus converting some stable isotopes to radioactive nuclides. These radioactive nuclides decay with some emitting gamma particles of a characteristic energy. The number and intensity of gamma particles is directly proportional to the quantity of the parent element in the sample (Muecke, 1980). The sensitivity of determination for a particular element depends on the number of its atoms that must be present in the sample to provide enough detectable and identifiable decays of the daughter isotope (Muecke, 1980). INAA was used to determine the concentrations of a number of trace and rare earth elements (Jacobs et al., 1977), particularly Sc, Cr, Co, Zn, As, Br, Rb, Sb, Cs, Ba, La, Ce, Cd, Sm, Eu, Tb, Yb, Lu, Hf, Ta, W, Th, and U as well as two major elements Na and Fe.

Approximately 75 to 100 mg of material from all 41 separated samples and whole rock samples KM-31 through KM-61 were packed into fused, ultrapure silica tubes and irradiated at the University of Missouri Research Reactor Facility for approximately 40 hours at a flux of 2.5×10^{13} N· cm^{-2}· s^{-1} (P.R. Kyle, personal comm., 1996). Samples were counted for 2 to 3 hours each at 7 days and 40 days after irradiation using 2 high-purity germanium detectors and the data was reduced using a Nuclear 6620 system and TEABAGS data reduction program (Korotev and Lindstrom, 1985). Standards used were AL-1, AL-2, D2-1, G2-2, BCR-1, BCR-2, FA-1 and FA-2. Analyses for all separated samples and whole rock samples KM-31 through KM-61 were performed at the New

Mexico Institute of Mining and Technology. The remaining whole rock INAA analyses were performed at X-Ray Assay Laboratories (XRAL) using the NA-IMPROVED method. Detection limits for the NA-IMPROVED method are as follows:

Element	Detection Limit(ppm)
As	2.0
Sb	0.2
Cs	1.0
La	0.5
Ce	3.0
Nd	5.0
Sm	0.1
Eu	0.2
Yb	0.2
Lu	0.05

Stable Isotope Geochemistry

Stable isotope geochemistry is concerned with variations in the isotopic ratios of several elements, of which oxygen is the most important for this study. In order to correctly interpret the variation seen in stable isotope data, it is important to have knowledge of the magnitude and temperature dependence of isotopic fractionation factors between the minerals present and the corresponding fluid. The use of fractionation factors has been discussed at length by many authors including Hoefs (1973) and O'Neil (1979). It is important to stress that at a given temperature, different minerals fractionate oxygen isotopes relative to the external reservoir by varying amounts. The degree of fractionation is also a function of the type of bonding present in the mineral(s) of interest. For instance, the Si-O-Si bond is a very strong bond that will tend to retain heavy oxygen (^{18}O) more easily than other bonds.

Oxygen isotopic data are reported as $\delta^{18}O$ values in per mil versus SMOW (Standard Mean Ocean Water) according to the equation

$$\delta^{18}O = \left(\frac{(^{18}O/^{16}O)_{sample}}{(^{18}O/^{16}O)_{SMOW}} - 1\right) x 10^3$$

(Craig, 1961b; Clayton and Mayeda, 1963). $\delta^{18}O$ values for this study were determined at the Stable Isotope Geochemistry Lab at New Mexico Institute of Mining and Technology.

Estimation of Adularia Abundance

One goal of XRD analysis was to estimate the relative proportions of mineral phases in separated samples, particularly adularia abundance. The adularia content of the separated samples was determined using the following technique. To obtain a relative mineralogical abundance for each constituent in an XRD pattern, the peak areas of the ~23.5° peak and the ~22.5° peak are measured, which for this study was produced via JADE pattern-processing software. An Average Area Factor was then obtained by averaging the area ratios of the ~23.5° peak (adularia + plagioclase peak) and the ~22.5° peak (adularia only peak) for each XRD scan that does not contain plagioclase within the sample set. For samples containing plagioclase in the assemblage, the value obtained for the ~22.5° peak is then multiplied by the Average Area Factor, resulting in the relative abundance of adularia present in the sample. The relative amount of plagioclase present in the sample is obtained by subtracting the calculated amount of adularia from the peak area of the ~23.5° peak (adularia + plagioclase peak). If plagioclase is not present within the

separated sample, measuring the peak area of the ~23.5° provides an estimate of the relative abundance of adularia. For each sample examined, the same volume of separated plagioclase material was used, thus allowing for comparison of the peak areas.

Table B provides areas under the peak that were used to estimate the abundance of adularia within the separated samples. An Average Area Factor of 4.48 was calculated for this study. An example calculation of adularia abundance is demonstrated below:

Sample: KM-41

(Area of ~22.5° 2θ peak) x (Average Area Factor) = Area of Adularia
(775) x (4.48) = 3472

(Area of ~23.5° 2θ peak) - (Area of Adularia) = Area of Plagioclase
(4005) - (3472) = 533

The separated samples were then ordered from least to greatest based on the calculated or measured area of adularia, thus arranging the separated samples in order of increasing adularia content.

In addition to estimates of adularia abundance, clay mineral abundances were also evaluated. For clay minerals, the area of the ~19.8° 2θ peak, which represents all the clay present in the sample, was used to approximate abundance. It should be noted that this method cannot provide an absolute abundance of the mineral constituents present within a sample due to the non-quantitative nature of XRD. However, this method does appear to provide a reasonable first approximation to the relative proportions of phases present within the separated samples. The amount of adularia present within a sample is considered to represent the amount of alteration the sample has undergone. Thus, if the

Area of Plagioclase and Adularia Peaks from Separated Samples

Sample Number	Area of ~22.5° 2θ	Area of ~23.5° 2θ	Ratio of 23.5 / 22.5	Plagioclase Area	Adularia Area
KM-36	550	2542	4.62	N/A	2542
KM-41	775	4005	NC	533	3472
KM-46	175	4252	NC	3468	784
KM-51	500	3415	6.83	N/A	3415
KM-54	362	1995	5.51	N/A	1995
KM-55	993	4824	4.858	N/A	4824
KM-56	1952	6634	3.398	N/A	6634
KM-58	859	3906	4.547	N/A	3906
KM-59	723	3647	5.044	N/A	3647
KM-60	366	2805	NC	1165	1639
KM-61	200	2002	NC	1106	896
KM-86	2031	6443	3.172	N/A	6443
KM-90	1443	7240	5.017	N/A	7240
KM-91	1117	5861	NC	856	5004
KM-94	1017	5103	5.017	N/A	5103
KM-95	1817	6274	3.453	N/A	6274
KM-96	2306	4312	1.869	N/A	4312
KM-102	1326	8347	6.295	N/A	8347
KM-107	350	3554	NC	1986	3554
KM-111	200	5361	NC	4465	896
KM-112	1292	3059	2.367	N/A	3059
KM-113	417	1842	4.417	N/A	1842
KM-114	649	3606	5.556	N/A	3606
KM-115	1573	2314	1.471	N/A	2314
KM-116	300	2437	NC	1093	1344
KM-127	902	4636	5.139	N/A	4636
KM-128	2012	3861	1.918	N/A	3861

Sample Number	Area of ~22.5° 2θ	Area of ~23.5° 2θ	Ratio of 23.5 / 22.5	Plagioclase Area	Adularia Area
KM-129	625	4844	NC	2044	2800
KM-131	350	4116	NC	2548	1568
KM-144	1383	7093	5.129	N/A	7093
KM-148	175	5113	NC	4329	784
KM-149	350	6716	NC	5148	1568
KM-150	3	32	NC	19	13
KM-153	9	64	NC	24	40
KM-154	1958	5629	2.875	N/A	5629
KM-155	2	11	5.5	N/A	11
KM-156	12	72	6	N/A	72
KM-157	1	31	NC	27	4
KM-158	1	78	NC	74	4
KM-159	11	75.3	6.845	N/A	75.3
KM-160	11	58.3	5.3	N/A	58.3

Table B: Area under XRD peaks as determined by JADE peak-processing software. NC = ratio not calculated due to presence of plagioclase; N/A = not applicable due to absence of plagioclase.

samples are arranged in order of increasing amount adularia, it may be possible to discern any trend seen in the geochemical analyses.

APPENDIX II

Mineralogy and Mineral Morphology

X-Ray Diffraction and Scanning Electron Microscopy

The alteration mineral assemblage of the separated samples, as determined using XRD and semi-quantitative clay mineral analysis, consists of some combination of adularia, quartz, kaolinite, smectite, illite, mixed-layer I/S, remnant plagioclase and occasionally calcite and barite. Although little mineralogical variation has been reported by previous workers (i.e. Chapin and Lindley, 1986), a wide range of mineralogical variation is observed in the present study. It is unlikely, however, that all the variation seen in the separated samples is due solely to K-metasomatism, for documented hydrothermal events are known to be superimposed over the K anomaly. Previous workers report the formation of hematite during alteration (Chapin and Lindley, 1986), which is something not recognized here primarily because XRD was performed on separated plagioclase rather than whole rock samples in this study. Lindley (1985) notes that the presence of hematite is due to oxidation of magnetite during K-metasomatism, which results in the characteristic reddening associated with this alteration.

Mineral phases were identified using standard techniques, and approximate relative abundances of the various phases were estimated using full-width, half-maximum measurements of peak size. XRD does not allow an exact determination of the ratio of mineral phases without using a wide range of standards, yet the relative importance of different mineral phases, within a group of samples that are mineralogically similar, can be approximately estimated based on XRD relative peak height. Table 1 contains the relative

percentage of minerals found in the alteration assemblage for each separated sample, along with the type(s) of clay present. Scanning electron microscopy (SEM) was used to look at six ignimbrite samples in an attempt to assess paragenetic relationships between the mineral constituents in the alteration assemblage. Samples examined through SEM are designated in Table 1.

Remnant Plagioclase

Some of the separated samples contain remnant plagioclase, likely due to the incomplete dissolution of plagioclase during the alteration process and not as a direct result of the potassic alteration. The presence of plagioclase was determined with comparison to sample KJH-26, from the Hells Mesa Tuff, which was collected outside of the K-metasomatized area. Plagioclase was separated from this sample in order to provide an XRD pattern for unaltered plagioclase, so that this could be distinguished from alteration minerals. Upon examination, a distinctive peak at a 2θ angle of approximately 21.8°-21.9° (35% relative intensity) is noted, as is a shift in the feldspar peak at approximately 23.4° for adularia to about 23.6° for plagioclase. Together, these two features were used to characterize the presence of remnant plagioclase within the samples collected from the metasomatized area. The plagioclase examined in this study consistently resembles albite in XRD analysis.

In SEM analysis, the instability of plagioclase is clearly demonstrated. KM-46, for example, shows the dissolution of plagioclase to form the alteration assemblage of remnant plagioclase + adularia + quartz (Figure 2). From KM-111, plagioclase is

distinctly unstable and tends to display a sawtooth pattern of dissolution (Figure A).

Adularia (K-feldspar)

Adularia is the most common alteration product formed in the K-metasomatized area; it is present, in varying amounts, in all 42 of the separated samples (Table 1). Chapin and Lindley (1986) state that this secondary K-feldspar is approximately $Or_{95\text{-}100}$, is monoclinic, and has a structure very similar to that of orthoclase. On XRD patterns, a characteristic orthoclase peak at ~22.5° 2θ is noted and is used as an immediate indicator as to the presence of adularia within the separated samples. Occasionally, however, this peak is not present on the XRD scan due to the weak intensity (19% relative intensity) associated with this peak (Colville and Ribbe, 1968). When the ~22.5° 2θ adularia peak is not present, it becomes necessary to examine either the adularia peak at ~23.6° 2θ (72% relative intensity) or the first-order, 100% relative intensity peak at 26.94° 2θ (Colville and Ribbe, 1968). The first-order adularia peak is, however, commonly masked by plagioclase and quartz peaks that occur near this 2θ angle. Associated with adularia in the alteration assemblage is the presence of fine-grained quartz, which appears to be ubiquitous in all the samples collected for this study. Quartz has two characteristic peaks on an XRD pattern; one at ~20.8° 2θ and another at ~26.6° 2θ. Oftentimes, the 26.6° quartz peak overlaps with plagioclase and adularia peaks, which also occur near this 2θ angle.

SEM analysis consistently displays the euhedral nature of adularia within the alteration mineral assemblage, however, the crystal morphology of adularia can be

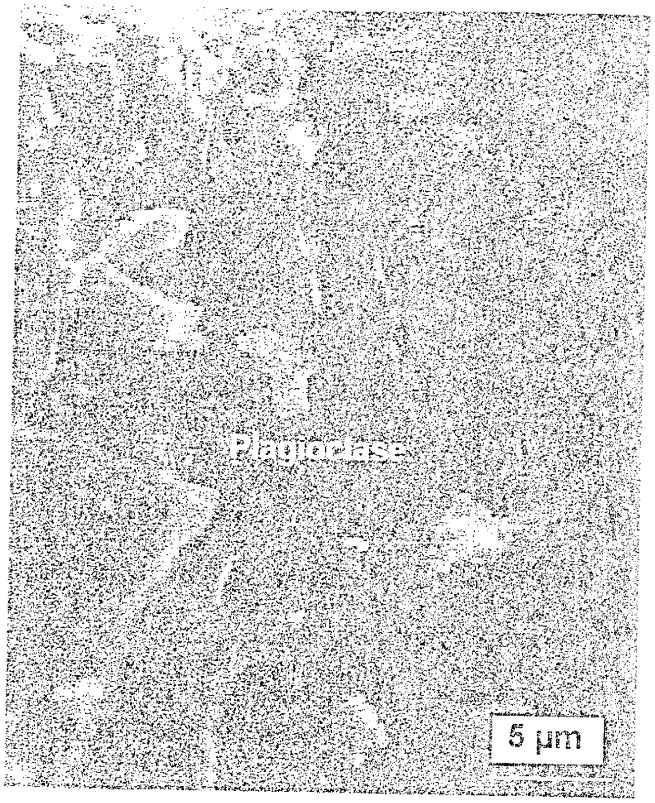

Figure A: SEM photo of plagioclase.

somewhat variable. In this study, several morphologies of adularia were found including a monoclinic tabular form and a rhombohedral form, which are the most common types observed (Figures B, C, and D). These morphologies are similar those found in previous studies (Lindley, 1985). Two other morphologies of adularia are recognized, however, including a pseudohexagonal prismatic form, and a tabular diamond-shaped form (Figure 3). Although the crystal morphology of adularia can differ, adularia is found to be perfectly euhedral in almost every sample examined by SEM analysis.

Sanidine

It is believed that sanidine and other K-rich phases remain relatively stable during K-metasomatism (Chapin and Lindley, 1986). This hypothesis is generally supported by the SEM photo in Figure E. This figure is a close up examination of the sanidine crystal, which appears to show clay minerals present in a small, ~5 to 10 μm wide seam. The occurrence of the clay minerals within the sanidine crystal is likely due to Ca- and Na-rich exsolution lamellae within the sanidine undergoing dissolution during metasomatic alteration, hence the relatively limited occurrence within the sanidine grain (Lee and Parsons, 1995). Except for dissolution of the exsolution lamellae, the remainder of the sanidine crystal appears to be unaffected by K-metasomatic alteration.

Kaolinite

Along with adularia and quartz, the alteration mineral assemblage contains various amounts and types of clay minerals. The presence of kaolinite within the alteration

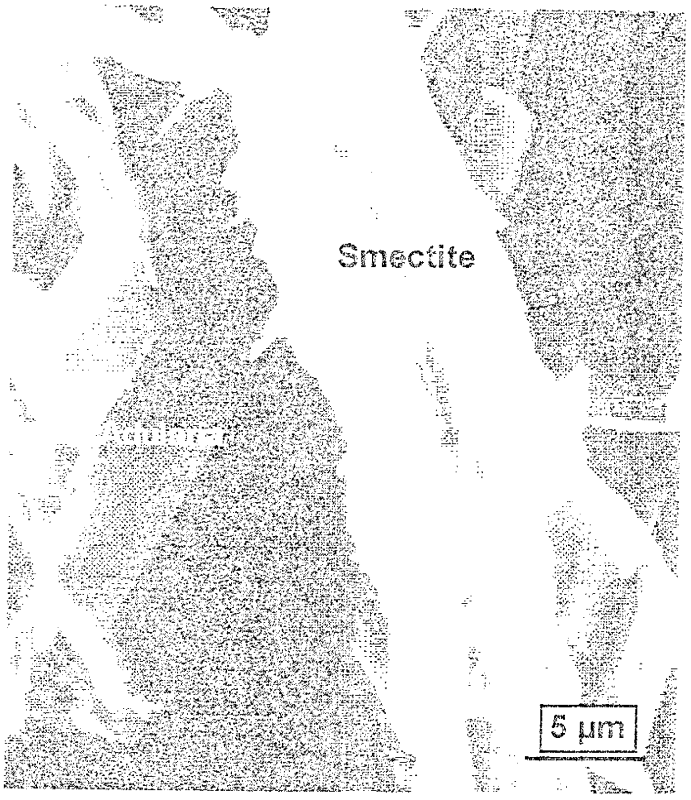

Figure B: Monoclinic, tabular morphology of adularia with smectite.

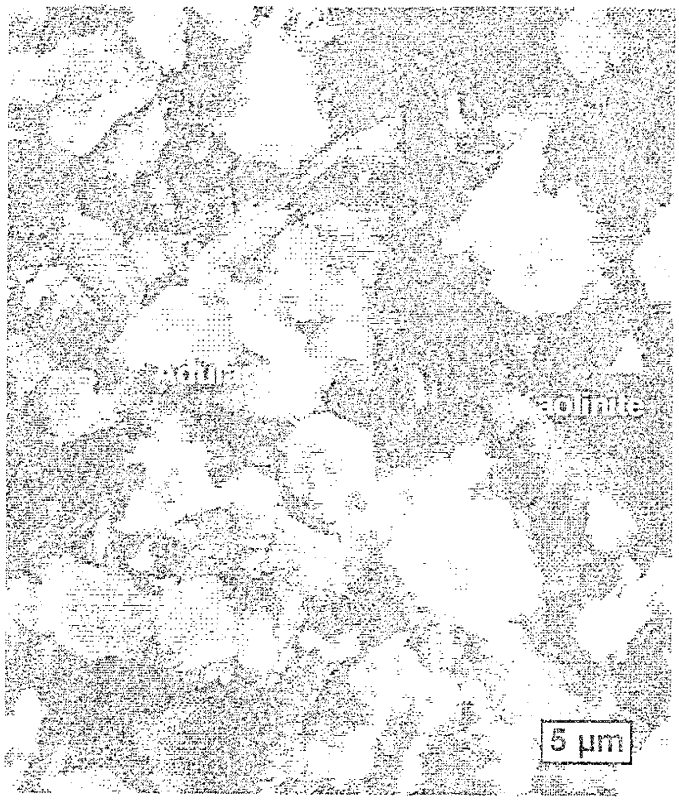

Figure C: SEM photo of rhombohedral adularia with kaolinite books.

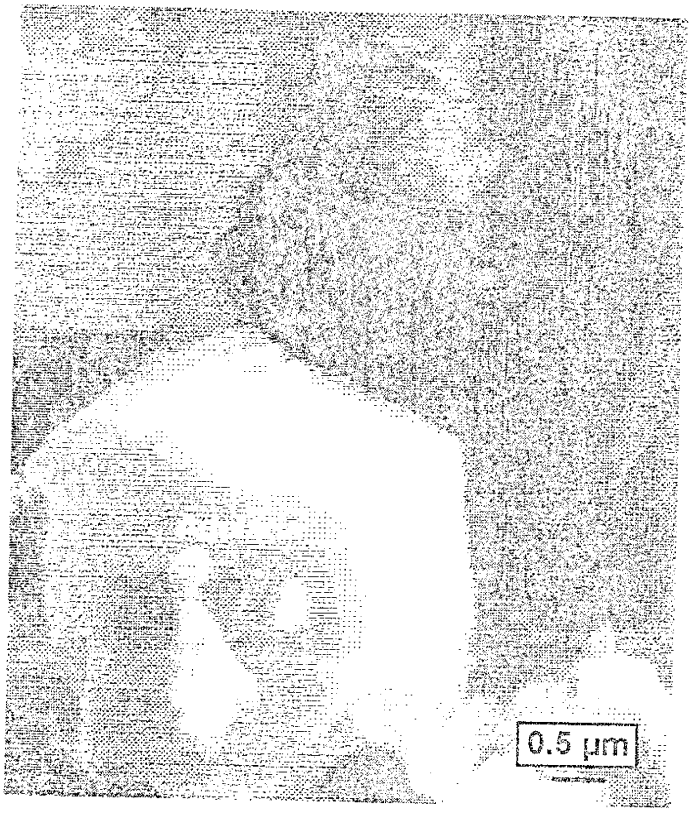

Figure D: SEM photo of rhombohedral adularia.

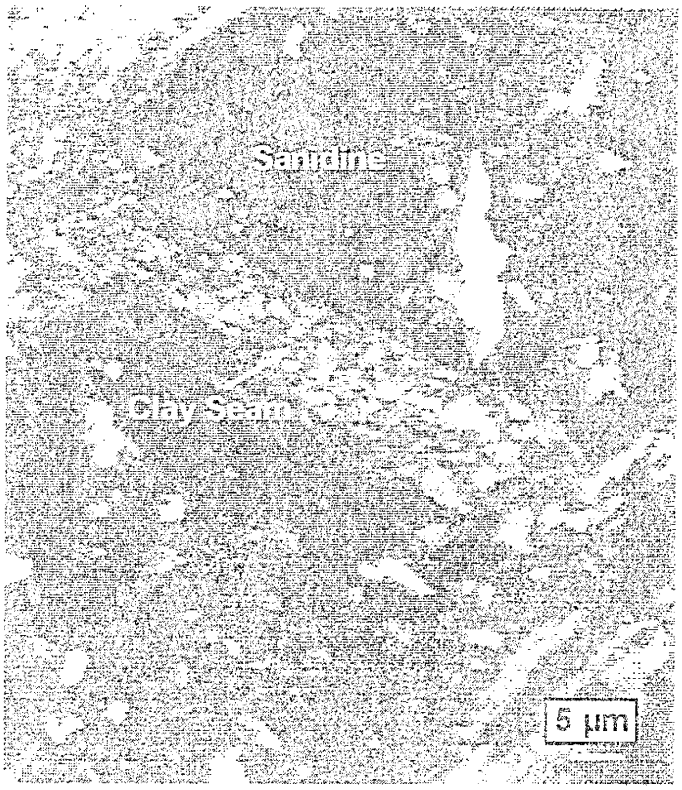

Figure E: Sanidine crystal with ~5 micrometer wide clay seam.

assemblage of the Hells Mesa Tuff was noted by Lindley (1985), who states that kaolinite appears to be replacing phenocrystic plagioclase. Also, according to Lindley (1985), kaolinite does not appear to be a weathering product because it lacks a well-developed, crystallized structure and it is absent from the fine-grained groundmass. Although kaolinite was recognized by Lindley (1985), the distribution and potential importance of this mineral as an alteration phase was not assessed.

The presence of kaolinite is most noticeable using XRD where a distinctive first-order, 100% relative intensity peak at 12.4° 2θ is noted (Walker and Renault, 1972). Based on XRD results from this study, kaolinite is extremely common within the alteration assemblage of the separated samples and it typically represents a major constituent of the total amount of clay in the sample (Table 1). Kaolinite is abundant throughout the K-metasomatized area, but appears to be particularly prominent near areas of hydrothermal activity (i.e. samples KM-112 through KM-116 collected near the Luis Lopez Manganese District).

Kaolinite typically has a unique and characteristic morphology when viewed by SEM analysis. Figure C shows the morphology of kaolinite to be composed of euhedral books in direct association with adularia. Kaolinite etchings can also be seen in the adularia possibly implying adularia formation prior to kaolinite.

Mixed Layer Illite-Smectite

Equally as common as kaolinite in the alteration assemblage is the presence of mixed-layer I/S (Table 1). Chapin and Lindley (1986) also recognize the presence of

mixed-layer I/S within the Socorro K-metasomatized area. Mixed-layer I/S is most noticeable in the results produced by semi-quantitative clay analysis; rarely is XRD of bulk samples sufficient to determine the extent to which mixed-layer clays occur in the assemblage. Due to the nature of mixed-layer clays, there is not a characteristic 2θ angle at which mixed-layer I/S occurs. Rather, mixed-layer clays typically occupy a 2θ angle between 5-10° as a broad, unresolved rise on an XRD pattern. As a result, it becomes necessary to implement semi-quantitative clay mineral analysis in order to evaluate the extent to which mixed-layer I/S occurs in the alteration assemblage.

Discrete Smectite

Based on semi-quantitative clay analysis, the presence of discrete smectite is fairly uncommon within the metasomatized area with only 6 of the 42 separated samples containing any significant amount of smectite (Table 1). Sample KM-51 shows a distinctive first-order, 100% relative intensity smectite peak at a 2θ angle of roughly 5.90° (Figure 6), which is something that is unrecognized in previous studies (i.e. Chapin and Lindley, 1986). A 2θ angle of ~5.90° for smectite is, however, by no means characteristic, for discrete smectite is frequently observed at 2θ angles ranging from 5.7 - 7.4 ° 2θ (Walker and Renault, 1972). This wide range of 2θ angles for smectite is a result of the ability of smectite to expand or swell in the presence of water; i.e., as humidity increases, the d-spacing of smectite also increases (Moore and Reynolds, 1989). The change in d-spacing of smectite is also related to cation exchange capacity, a phenomena in which cations may be exchanged when the clay minerals holding them come into contact with a

solution rich in other cations. The ability of smectite to engage in cation exchange results in variability of the d-spacing which, in turn, results in variation in the 2θ angle at which smectite can occur on an XRD scan (Moore and Reynolds, 1989). Smectite, in SEM, is typically found to coat euhedral adularia crystals as either long or short strands as seen in Figures B and F.

Discrete Illite

Similar to the infrequent occurrence of discrete smectite, discrete illite is also rarely encountered in the alteration assemblage. However, when present, a first-order, 100 % relative intensity peak at 8.8° 2θ on XRD scans is characteristic (Walker and Renault, 1972). Unlike discrete smectite, pure illite occurs regularly at 8.8° 2θ on XRD scans due to its nonexpanding nature. It should be noted that the term 'pure illite' is a slight misnomer, for Moore and Reynolds (1989) state that 'pure illite' may actually contain up to 5% of an interstratified component (most commonly smectite). However, because this small amount of interstratified material is difficult to detect by conventional X-ray methods, it is commonly ignored, thus allowing use of the term 'pure illite.'

A significant amount of illite was detected in KM-96 and was therefore investigated by SEM in order to evaluate the morphological characteristics as well as the paragenetic relationship of this mineral. Figure G, SEM photo of KM-96, shows what is interpreted to be an altered plagioclase crystal adjacent to an unaltered sanidine crystal. Examination of the minerals contained inside the relict plagioclase grain appears to show adularia undergoing dissolution to form discrete illite + I/S mixed-layers. Illite is

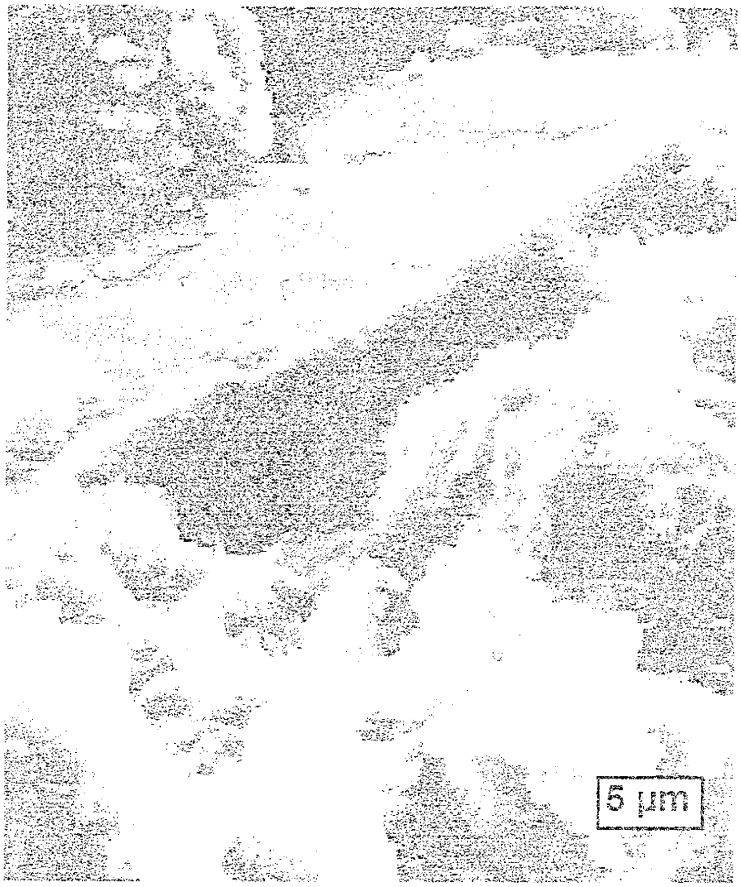

Figure F: SEM photo of adularia + smectite.

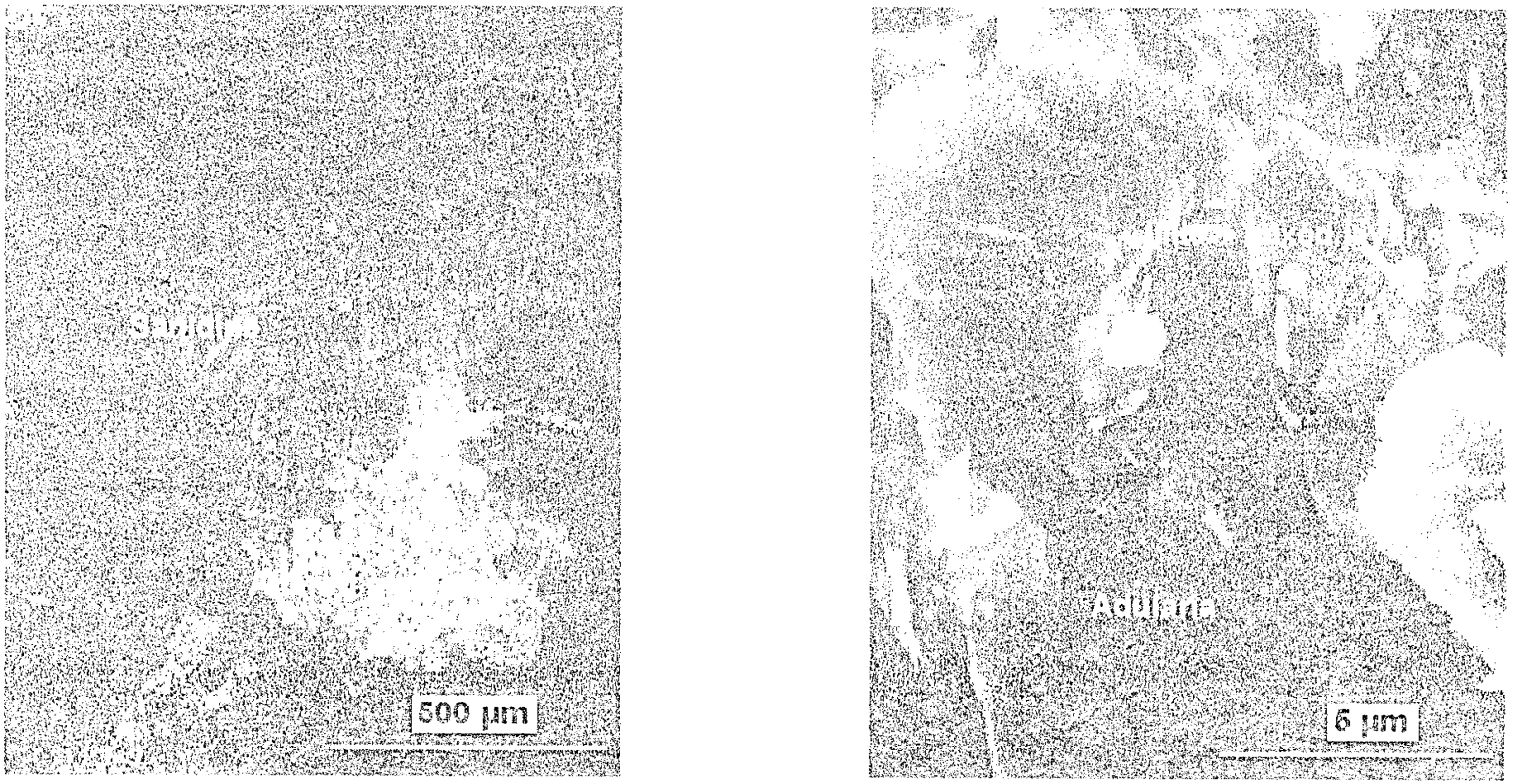

Figure G: SEM photos of KM-96. Photo at left shows a sanidine crystal adjacent to an altered plagioclase phenocryst. Photo at right is a close up of the altered plagioclase and shows the assemblage adularia + illite + mixed-layer I/S.

distinguished from adularia based on relative grain size, morphology, and EDX; K-feldspar typically displays a greater K:Al ratio than illite (Welton, 1984). This is the only sample examined by SEM that appears to show adularia in an unstable state.

Calcite and Barite

The presence of calcite and barite within the alteration mineral assemblage has previously not been recognized. Several samples collected for this study, however, clearly demonstrate calcite in the mineral assemblage of the separated samples. For instance, KM-60 shows a distinctive calcite peak at ~29.4° 2θ on an XRD pattern (See Figure H). The peak at ~29.4° is the 100% relative intensity peak for calcite and, hence, the most prominent peak (Walker and Renault, 1972). Calcite can also be seen in several thin sections, even though XRD did not detect the presence of calcite in those samples (i.e. KM-46). Because XRD did not reliably detect the presence of calcite within the alteration assemblage, the extent to which calcite occurs in the metasomatized area is unknown. Calcite was found during electron microprobe analyses to be extremely fine-grained (see section on element mapping by electron microprobe analysis). It appears that when calcite is present, it is present in exceedingly small amounts and is thus virtually undetectable in XRD analyses.

In addition to calcite, barite is also found within the alteration assemblage of a few samples, notably KM-115 (See Figure I). Barite is most noticeable at a 2θ angle of ~22.8°, though this peak is only 57 % relative intensity. A stronger, more intense barite peak occurs at ~25.9° (100 % relative intensity), but is less diagnostic due to interference

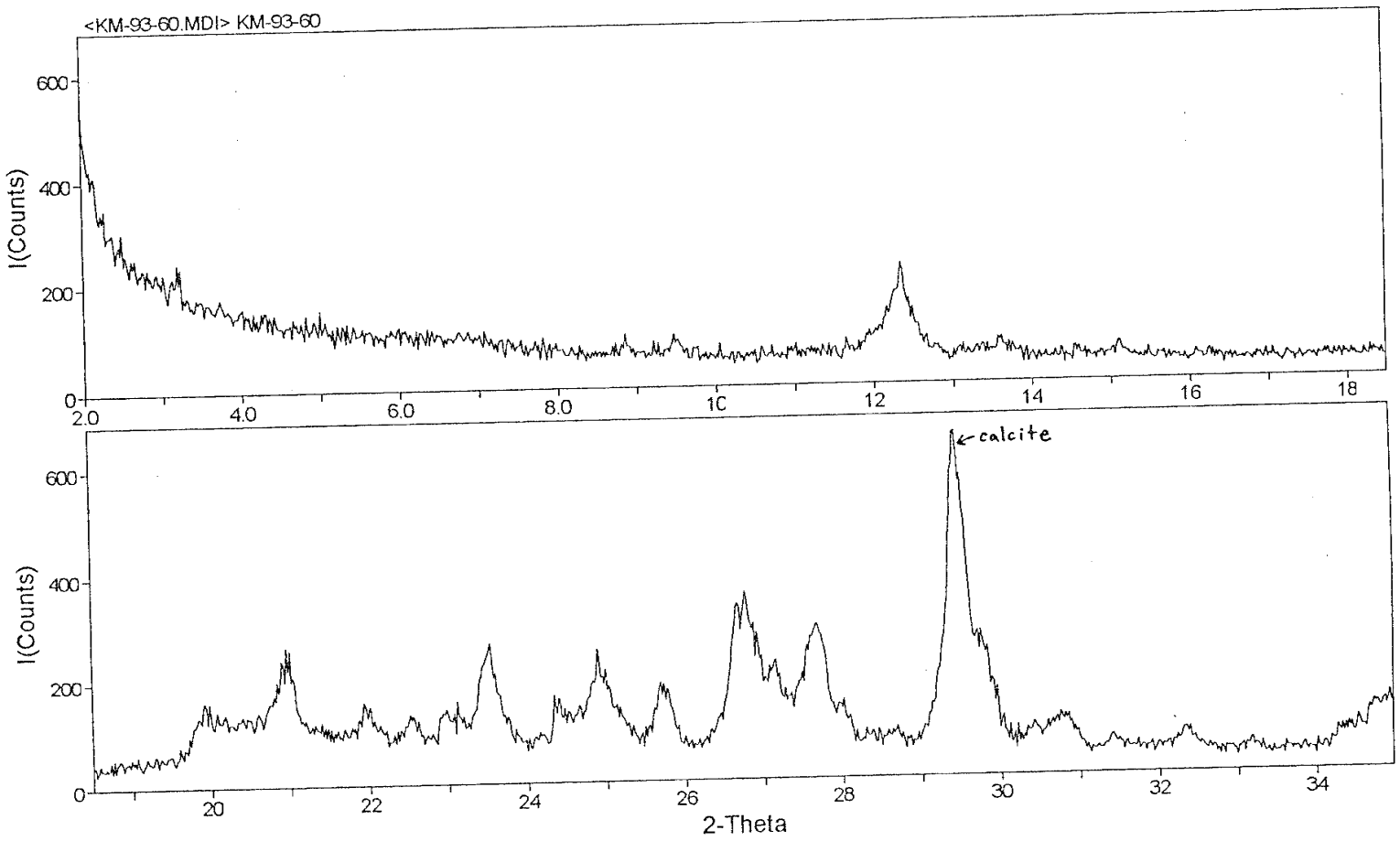

Figure H: XRD pattern for sample KM-60. Note large calcite peak at ~29.5° 2-Theta.

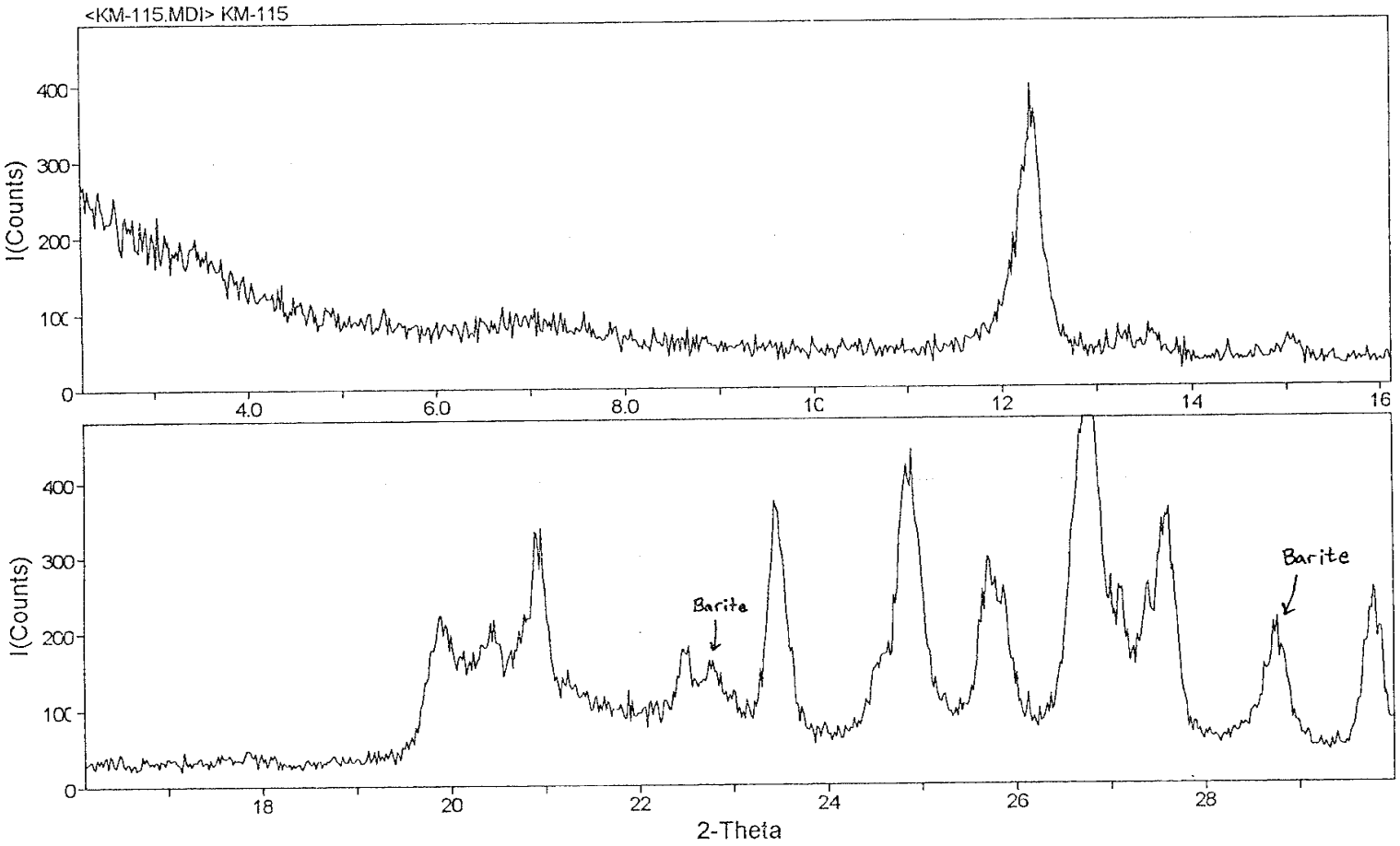

Figure 1: XRD pattern for sample KM-115. Note barite peaks at ~22.8° and ~ 28.8° 2-Theta.

from adularia, which occurs at 25.6° 2θ (Walker and Renault, 1972; Colville and Ribbe, 1968). The extent to which barite occurs in the alteration assemblage is uncertain, however, it appears to be most prevalent in samples collected near localized areas of hydrothermal activity.

Lateral Variation in Mineralogy Across a Potential Boundary for K-Metasomatism

Hells Mesa ignimbrite clasts were collected from the Popotosa Formation near Red Canyon in the northern Chupadera Mountains across an area thought to be a potential boundary of K-metasomatism (Figure J; R. Chamberlin personal comm., 1995). The ridge from which the samples were collected has two visually distinct regions: the northern portion consists of very well indurated Popotosa with strongly K-metasomatized Hells Mesa Tuff clasts contained within, while the southern portion is poorly indurated Popotosa and contains Hells Mesa Tuff clasts that exhibit slight to no effects of K-metasomatism. The transition from the northern portion to the southern portion of the ridge is defined by a relatively sharp break in slope (Figure K), likely as a result of the differing degrees of induration.

With respect to the mineralogy of the Hells Mesa Tuff clasts, a noticeable change is recognized between samples collected from the well indurated Popotosa and samples collected from the poorly indurated Popotosa. Separated samples from Hells Mesa Tuff clasts north of the proposed boundary, in the well indurated portion of the Popotosa, were found by XRD analysis to be absent of plagioclase. In contrast, KM-116, a Hells Mesa Tuff clast sample collected from the poorly indurated portion of the ridge, contains a

Hells Mesa Tuff Clast Sampling Across Possible K-Metasomatized Boundary, north of Red Canyon, Chupadera Mountains, Socorro County, NM.

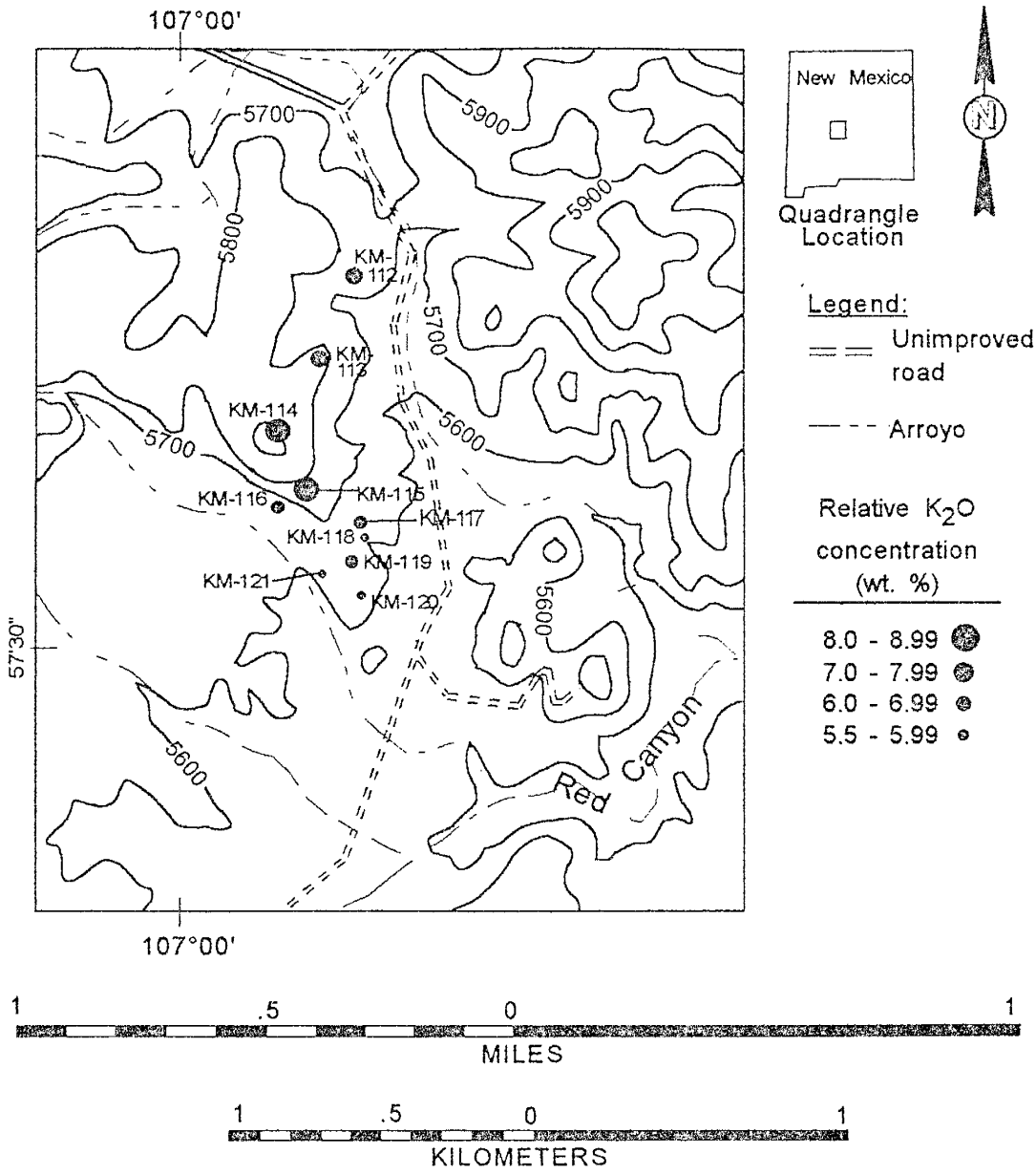

Figure J: Generalized map area north of Red Canyon, Chupadera Mountains. Hells Mesa Tuff clast samples sampled from the Popotosa Formation across a proposed lateral K-metasomatism boundary.

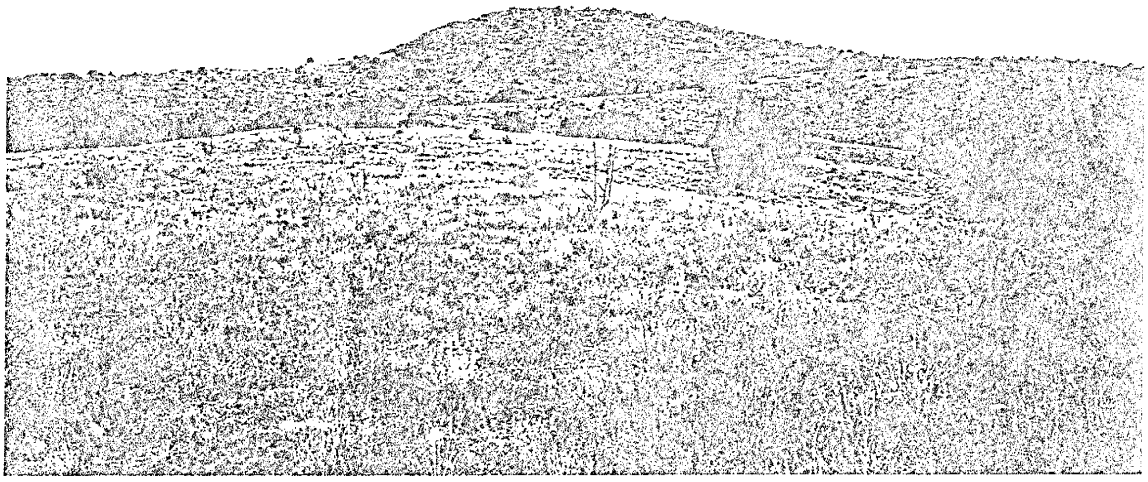

Figure K: Ridge comprised of the Popotosa Formation near Box Canyon, looking northwest. Note sharp break in slope between well indurated and poorly indurated Popotosa.

significant amount of plagioclase in the alteration assemblage (Table 1). Sample KM-116 is the only Hells Mesa Tuff clast sample from the poorly indurated Popotosa that was able to be drilled for altered plagioclase. Separated, altered plagioclase for the other samples collected from the poorly indurated Popotosa, KM-117 through KM-121, was unable to be collected due to the minor amount of metasomatic alteration that has occurred to these samples. Plagioclase from these samples appears relatively fresh and unaltered and whole rock XRD detected relatively abundant plagioclase in these samples.

The clay mineralogy of the separated Hells Mesa Tuff samples was found to consist of large abundances of kaolinite, 25 to 50% of the total alteration assemblage of the separated samples, regardless of whether the sample was collected north or south of the proposed boundary (Table 1). No other minerals were found to vary in abundance across the boundary separating the two regions of the Popotosa Formation, except for the occasional occurrence of barite in the assemblage (notably KM-114 and KM-115). A discussion on the geochemistry associated with this proposed K-metasomatic boundary can be found in Appendix IV, Part I.

APPENDIX III

Electron Microprobe Analysis

Quantitative Chemical Analyses

In addition to element mapping, the electron microprobe allows the quantitative measurement of the chemical composition of minerals present within the alteration assemblage. Quantitative analyses of both upper Lemitar and Hells Mesa Tuff plagioclase were performed, however, due to the sparsity of plagioclase within KM-51, the upper Lemitar Tuff sample examined, only one plagioclase measurement was made. Data points for Hells Mesa Tuff plagioclase are more abundant due to the amount of plagioclase located in the sample. The quantitative measurements of plagioclase for the two units are given in Table C.

In addition to plagioclase, thirteen chemical analyses of adularia were made on the electron microprobe, which can be found in Table D. Some of the quantitative measurements were made within the back-scattered electron microprobe images of KM-54 and KM-51, the locations of which are shown in Figures L and M. Several additional adularia measurements, however, were performed elsewhere in the altered grain and are therefore not shown.

Analyses of calcite, mixed layer illite-montmorillonite and discrete montmorillonite were also made all with limited success. The analyses made on these minerals are only moderately representative due to the low oxide totals obtained, but do provide a cursory look at the composition. Low oxide totals are due to calibration of the electron microprobe for only the elements listed; i.e. had the probe been calibrated for other oxides

Quantitative Chemistry of Plagioclase

Hells Mesa Tuff Plagioclase:

Sample	Na_2O	MgO	Al_2O_3	SiO_2	K_2O	CaO	FeO	Total
KM54-1	8.4	0.021	22.36	63.28	0.93	4.36	0.207	99.6
KM54-2	8.5	0.015	22.44	63.08	0.95	4.39	0.204	99.6
KM54-3	8.4	nd	22.34	62.37	0.91	4.45	0.219	98.7
KM54-4	8.33	nd	22.22	62.81	0.98	4.35	0.239	98.9
KM54-5	8.45	0.015	22.27	62.77	1.07	4.3	0.232	99.1
KM54-6	8.73	0.009	22.28	62.65	0.96	4.37	0.26	99.3

Upper Lemitar Tuff Plagioclase:

KM51-9	9.64	0.135	19.53	67.96	0.077	0.622	0.092	98.06

Table C: Quantitative analysis of Hells Mesa and upper Lemitar Tuff plagioclase. Wt. % errors as follows: ±0.07 Na_2O, ±0.01 MgO, ±0.11 Al_2O_3, ±0.39 SiO_2, ±0.01 K_2O, ±0.02 CaO, ±0.03 FeO.

Quantitative Analyses of Adularia

Sample	Na_2O	MgO	Al_2O_3	SiO_2	K_2O	CaO	FeO	Total
KM54-7	0.144	0.023	18.27	66.33	14.39	0.02	nd	99.2
KM54-8	0.136	0.022	17.99	64.42	18.82	0.026	0.033	99.45
KM54-9	0.097	0.022	17.69	63.73	16.47	0.036	0.084	98.12
KM54-10	0.04	nd	17.63	65.85	16.88	0.051	0.048	100.5
KM54-11	0.045	0.025	18.13	65.09	16.81	0.023	0.048	100.17
KM54-12	0.022	nd	17.17	64.42	16.31	0.027	nd	97.94
KM51-1	0.015	nd	17.79	66.55	16.82	nd	0.05	101.2
KM51-2	0.02	nd	18.5	65.62	16.94	nd	0.074	101.15
KM51-8	0.302	nd	17.48	65.76	16	0.058	0.039	99.64
KM51-11	0.014	nd	17.54	65.16	17.8	0.057	0.06	99.63
KM51-12	0.018	0.009	18.11	67.92	16.38	0.084	0.062	102.6
KM51-13	nd	0.023	18.13	68.93	16.89	0.046	0.048	104.07
KM51-14	0.022	nd	17.06	65.11	16.68	0.051	0.03	98.95

Table D: Chemical analyses of adularia within the alteration assemblage. nd=not detected. Wt. % errors as follows: ±0.01 Na_2O, ±0.01 MgO, ±0.10 Al_2O_3, ±0.37 SiO_2, ±0.095 K_2O, ±0.01 CaO, ±0.02 FeO.

Backscattered Image of KM-51: Clay and Adularia Analyses Points

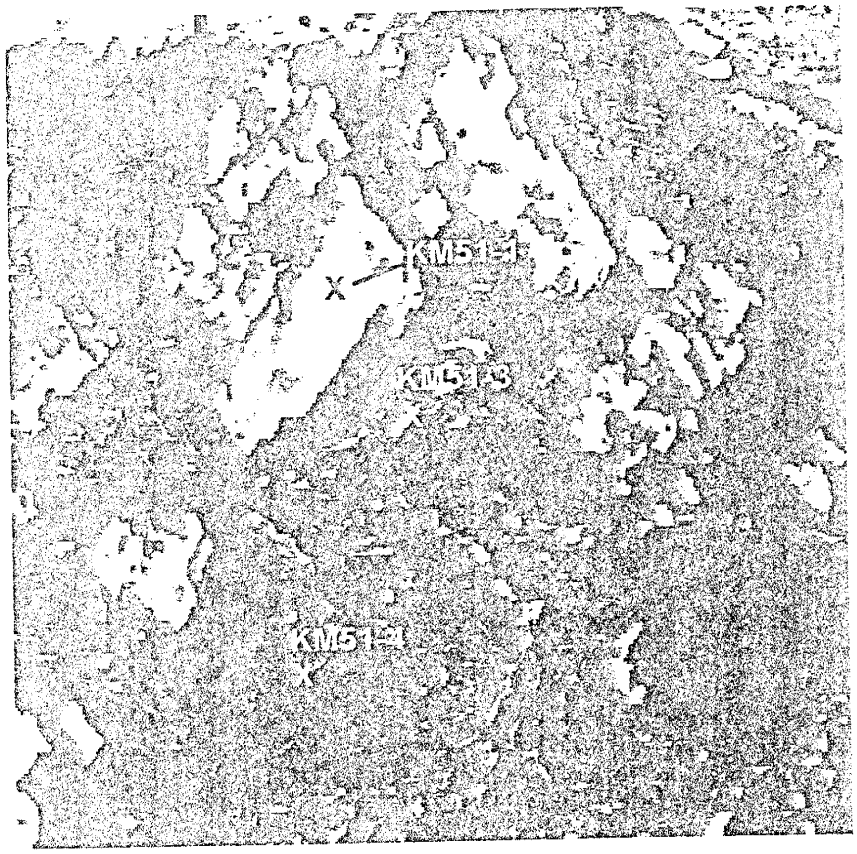

Figure L: Electron microprobe back-scattered image. Locations shown are for quantitative analyses made on adularia and smectite. Numbers correspond to analyses given in Tables D and G .

Backscattered Image of KM-54:
Adularia Analyses Points

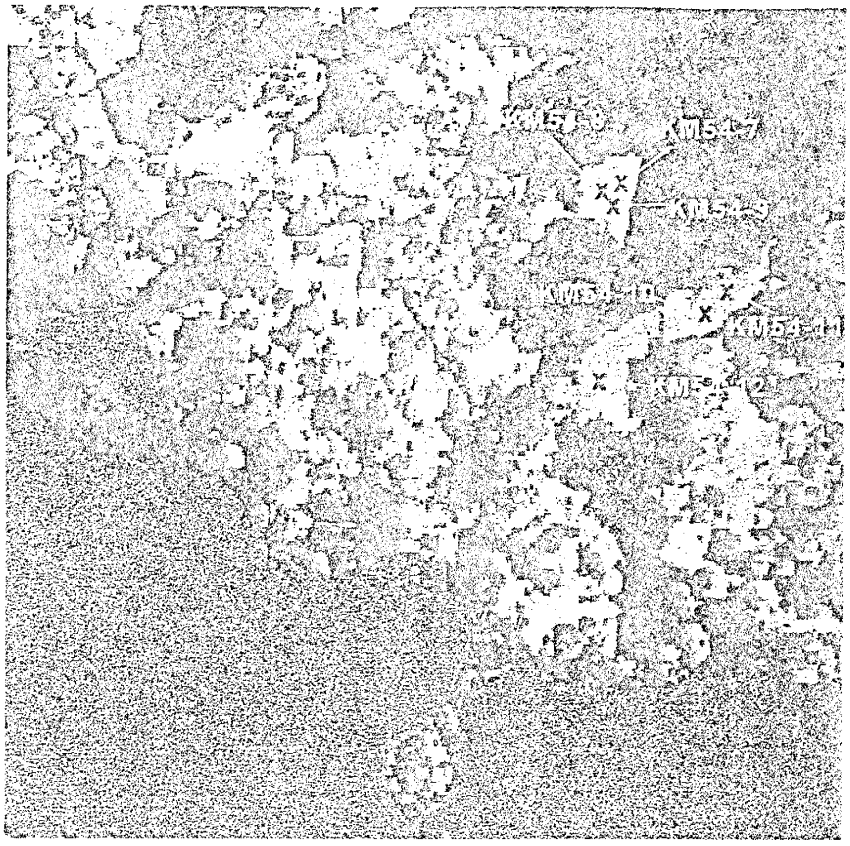

Figure M: Electron microprobe back-scattered image of KM-54 showing locations of quantitative analyses. Numbers correspond to Table D.

such as TiO_2 and MnO, the totals would likely be much better. The presence of water within the clay minerals may have further affected the totals obtained through microprobe analysis. Tables E, F, and G provide the chemical analyses made for each mineral. Figures L and N show the locations of measurements made for mixed-layer I/S, calcite, and discrete smectite within the back-scattered images obtained for KM-51 and KM-54. Several discrete smectite analyses were made in other portions of the altered grain for KM-51 and are therefore not shown on Figure L.

Quantitative Analyses of Mixed-Layer I/S, Calcite and Discrete Smectite

Mixed-layer clay from KM-54:

Sample	Na_2O	MgO	Al_2O_3	SiO_2	K_2O	CaO	FeO	Total
KM54-13	0.15	1.08	30.31	42.6	6.09	0.585	0.317	81.125
KM54-14	0.14	1.22	33.18	48.47	6.32	0.612	0.364	90.3
KM54-15	0.14	1.22	31.74	48.16	6.38	0.615	0.363	88.62

Table E: Quantitative analyses by electron microprobe analysis. Wt. % errors as follows: ±0.01 Na_2O, ±0.02 MgO, ±0.14 Al_2O_3, ±0.28 SiO_2, ±0.06 K_2O, ±0.02 CaO, ±0.03 FeO.

Calcite from KM-54:

Sample	Na_2O	MgO	Al_2O_3	SiO_2	K_2O	CaO	FeO	Total
KM54-16	nd	0.121	0.074	nd	0.376	56.04	0.059	56.66
KM54-17	0.057	0.104	2.77	7.35	1.65	46.49	0.073	58.44
KM54-18	nd	0.142	5.92	7.66	0.69	42.8	0.107	57.33
KM54-19	0.025	0.194	0.693	1.51	0.744	52.71	0.025	55.9

Table F: Quantitative analyses of calcite. nd=not detected. Wt. % errors as follows: ±0.014 Na_2O, ±0.01 MgO, ±0.04 Al_2O_3, ±0.07 SiO_2, ±0.03 K_2O, ±0.17 CaO, ±0.03 FeO.

Montmorillonite from KM-51:

Sample	Na_2O	MgO	Al_2O_3	SiO_2	K_2O	CaO	FeO	Total
KM51-3	0.076	3.43	17.43	43.15	0.419	1.23	0.976	66.72
KM51-4	0.084	3.46	14.06	40.71	0.319	0.633	0.748	60.01
KM51-5	0.123	5.24	21.83	60.7	0.304	1.04	0.917	90.15
KM51-6	0.177	5.35	20.83	60.35	0.476	0.781	1.012	88.97
KM51-7	0.168	4.079	17.37	46.67	0.523	1.57	0.824	71.21

Table G: Quantitative analyses of montmorillonite. nd=not detected. Wt. % errors as follows: ±0.013 Na_2O, ±0.04 MgO, ±0.12 Al_2O_3, ±0.35 SiO_2, ±0.02 K_2O, ±0.03 CaO, ±0.04 FeO.

Backscattered Image of KM-54:
Calcite and Clay Analyses Points

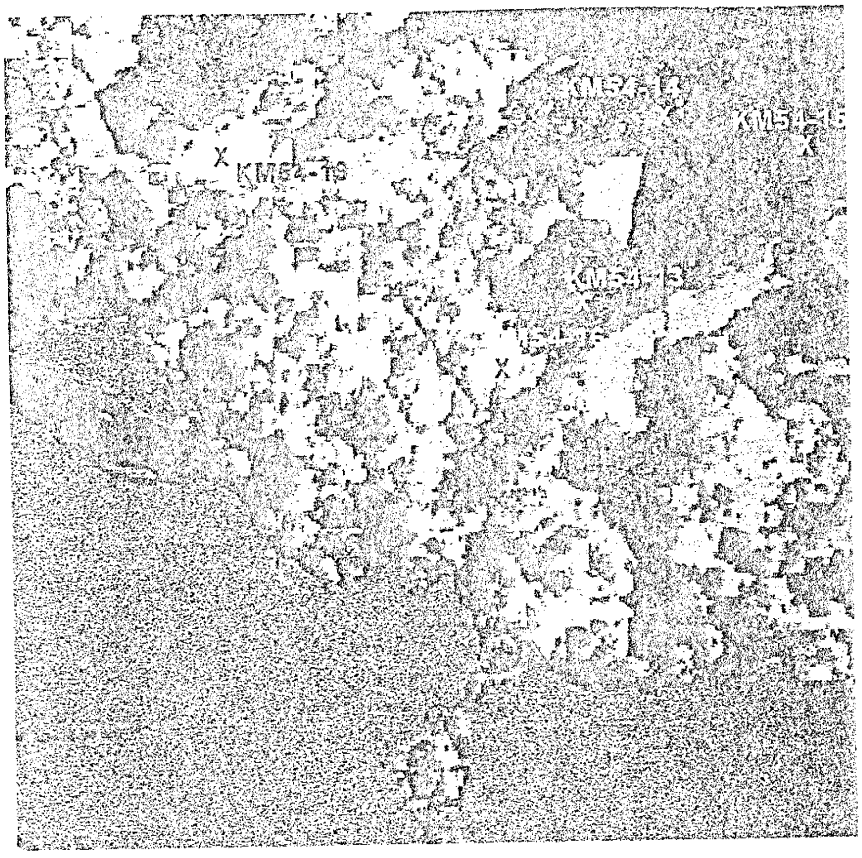

Figure N: Back-scattered electron microprobe image of sample KM-54. Shown are locations of quantitative analyses made on calcite and mixed-layer clay. Numbers correspond to Tables E and F.

APPENDIX IV - PART I

Geochemistry

In order to assess whether a particular element is enriched or depleted within the K-metasomatized area, comparison is made to several unaltered samples from both the Hells Mesa and the upper Lemitar Tuffs (Appendix VI). The geochemical data for these samples was obtained from the literature. Only geochemical data which the author of the reference material determined to be unaltered was used as a comparison for this study.

Whole Rock Upper Lemitar and Hells Mesa Tuff Samples

Major Elements

Upper Lemitar Tuff sample KM-148, which was collected within the metasomatized area, appears to only show slight degrees of alteration. Several lines of evidence are used to arrive at this conclusion. First, in hand sample, this upper Lemitar Tuff sample appears relatively fresh compared to the other samples collected for this study. When plotted on a CaO-K_2O-Na_2O ternary diagram (Figure 12), KM-148 plots very near whole rock, unaltered upper Lemitar Tuff samples and falls into the "fresh ash-flow tuff" field established by D'Andrea-Dinkelman (1983) based on data compiled by D'Andrea (1981) and Lindley (1979). In addition, a program called DELTAS was used to calculate the hypothetical igneous precursor composition prior to K-metasomatic alteration (See Appendix V for details on DELTAS). The DELTAS program produced a precursor composition very similar to the composition seen today (Table H).

Sample	SiO_2	TiO_2	Al_2O_3	Fe_2O_3	FeO	MgO	CaO	MnO	Na_2O	K_2O
KM-148	72.8	0.44	14.2	2.33	NA	0.52	1.12	0.05	3.69	4.84
KM-148*	72.2	0.33	15.02	1.42	0.95	0.15	2.02	0.07	3.65	4.18

Table H: KM-148* indicates hypothetical igneous precursor composition calculated by DELTAS program. Addition of Fe_2O_3 and FeO for KM-148* comes very close to the Fe_2O_3 concentration of KM-148. Note similar concentrations of Na_2O and K_2O. NA= not analyzed.

The similarity between the measured composition and the calculated composition implies only a slight degree of K alteration. Based on these lines of evidence in addition to those mentioned previously, it appears reasonable to use KM-148 as a comparison for chemical values obtained for the other upper Lemitar Tuff separated samples.

K_2O/Na_2O ratios within the Hells Mesa Tuff range from 1.81 - 53.0, while K_2O/CaO ratios are similarly high and range between 4.01 - 145.75. It is curious to note that sample KM-155 appears to be contributing significantly to the upper limit of both of these ratios; KM-155 contains extremely low Na_2O and CaO concentrations (0.11 wt. % and 0.04 wt. %, respectively). When this sample is removed from the rest of the Hells Mesa Tuff sample population, the K_2O/Na_2O ratio range drops dramatically to between 1.81 - 14.20, while the K_2O/CaO ratio then falls between 4.01 - 87.40. These values appear much more reasonable and thus suggest the possibility that KM-155 has been affected by some process other than K-metasomatism, such as hydrothermal overprinting.

Stratigraphic Chemical Results for the Upper Lemitar Tuff

Major Elements

The upper Lemitar ignimbrite was sampled stratigraphically in South Canyon, Magdalena Mountains (Figure O). Samples KM-86, -90, -91, -92, -93, -94, and -95 were collected from this area and were found to have significant differences in whole rock, major element geochemistry with respect to stratigraphic position. The stratigraphically highest samples, KM-92 and KM-93, which are poorly welded upper Lemitar Tuff samples, are the most enriched in K_2O content and the most depleted in Na_2O (12.21 and 10.35 wt. % K_2O; 1.26 and 1.59 wt. % Na_2O, respectively). The stratigraphically lowest samples, KM-86, KM-90 and KM-91, have relatively low K_2O contents compared to KM-92 and KM-93, yet are still significantly enriched in K_2O when compared to unaltered upper Lemitar Tuff samples; K_2O contents for KM-86, KM-90 and KM-91 are 9.06, 8.50 to 9.20 wt. % respectively. A graph of K_2O vs Na_2O (Figure P) shows a progressive increase in the K_2O content from the stratigraphically lowest to the stratigraphically highest samples, which coincides with a decrease in Na_2O content.

Most major elements, Al_2O_3, Fe_2O_3, CaO, MgO, MnO, and P_2O_5, show no apparent trends with stratigraphic height. The major elements SiO_2 and TiO_2 do, however, show some evidence for compositional zonation within the stratigraphic section of the upper Lemitar Tuff as discussed in subsequent sections (Figure P).

Upper Lemitar Sample Locations in South Canyon, Magdalena Mountains, Socorro County, NM.

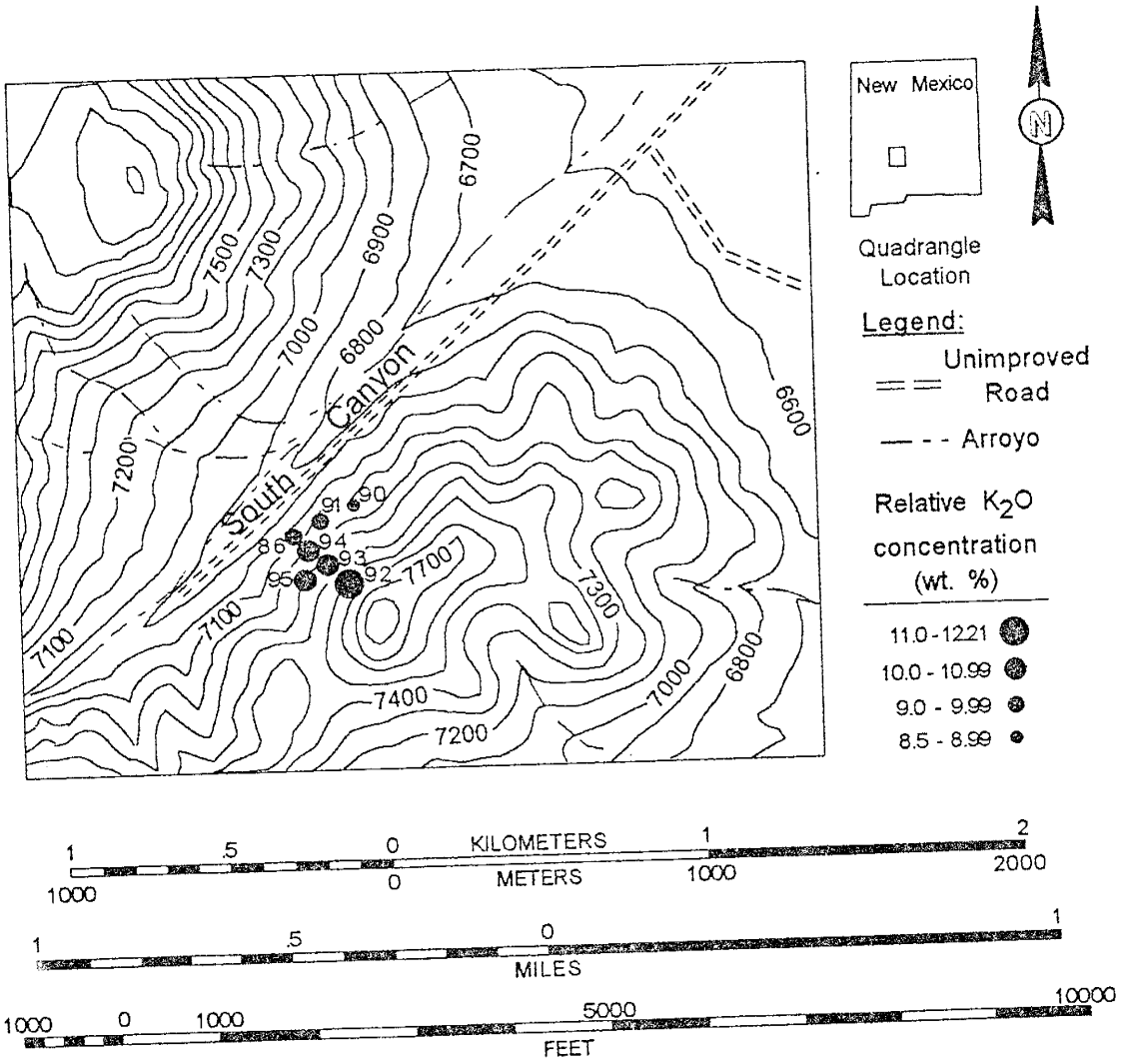

Figure O: Generalized map area of South Canyon, Magdalena Mountains. Stratigraphic sampling of the upper Lemitar Tuff.

Stratigraphic Variations in the Upper Lemitar Tuff, South Canyon

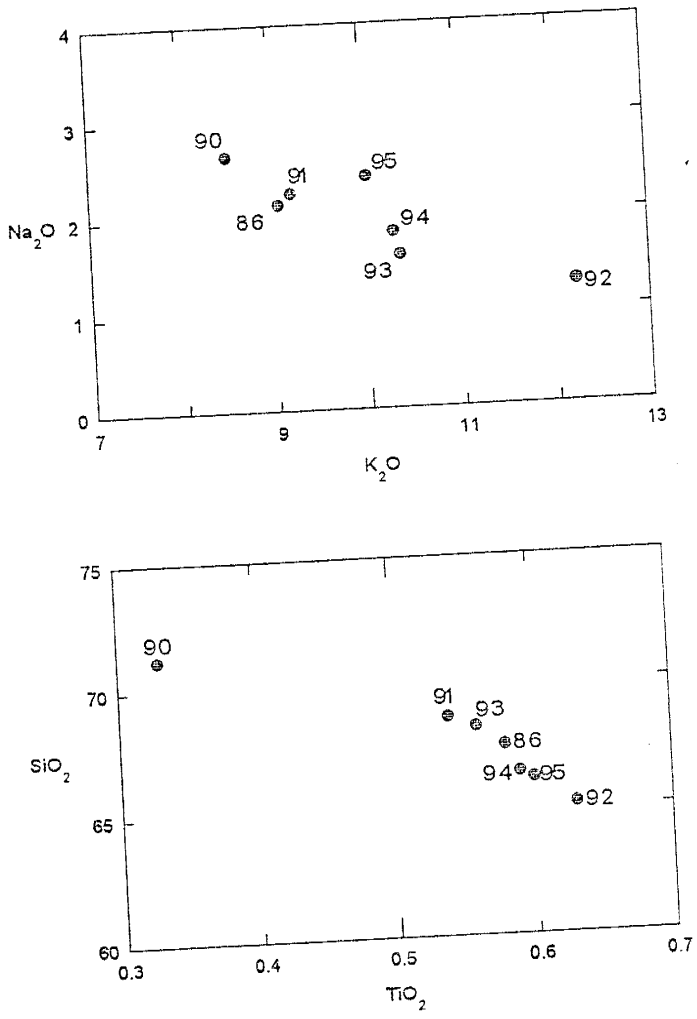

Figure P: Major element chemistry from the upper Lemitar stratigraphic section in South Canyon. Numbers next to data points represents sample number.

Trace Elements

In addition to differences in major element content with stratigraphic variation, minor and trace elements also show significant variation. In accordance with high K_2O contents and low Na_2O contents, KM-92 and KM-93 have elevated Rb and depleted Sr contents; KM-92 has 535 ppm Rb and 83 ppm Sr, KM-93 has 486 ppm Rb and 127 ppm Sr. In general, the Rb content of whole rock samples tends to increase with stratigraphic height while Sr decreases, although KM-90 does not fit this generalization due to an unusual Sr concentration in this sample (Figure Q). The elements Rb and Sr are the only minor elements that appear to show any changes in stratigraphic height as a result of K-metasomatic alteration.

Although little variation is found in trace elements as a result of K-metasomatism, the elements Zr and Nb appear to show compositional differences within the stratigraphic section of the upper Lemitar Tuff, suggesting some degree of zonation within the unit (Figure Q). Compositional zonation of the upper Lemitar Tuff, based on the trace elements Zr and Nb in conjunction with major elements such as SiO_2, is discussed in subsequent sections. Other trace elements, including REE were not found to vary systematically with changes in stratigraphic position whether it be due to metasomatic alteration or composition zonation.

Discussion on Stratigraphic Variation

Several conclusions can be drawn based on geochemical and mineralogical data obtained from samples collected stratigraphically in this region. Within the South Canyon

section, the stratigraphically highest samples, KM-92 and KM-93, are the most enriched in K_2O with respect to other South Canyon samples and to those collected throughout the K-anomaly. These two samples are poorly welded compared to other upper Lemitar Tuff samples, suggesting that the porosity and permeability of these samples is significantly higher, which would account for the high degree of K_2O enrichment within these samples. Permeability is regarded to be a controlling factor for vertical alteration within the Socorro K-anomaly (Chapin and Lindley, 1986).

In addition to a correlation between degree of welding and degree of metasomatism, stratigraphic sampling of the upper Lemitar Tuff also shows systematic variation in chemical composition. The upper Lemitar Tuff clearly shows an increase in K_2O and decrease in Na_2O content with increasing stratigraphic height within the South Canyon area (Figures O and P). Mineralogical data also demonstrates a decrease in plagioclase abundance with increasing stratigraphic height, again suggesting a correlation between stratigraphic position and degree of alteration. Furthermore, the trace elements Rb and Sr also demonstrate the relatively greater alteration of samples in the uppermost portion of the upper Lemitar Tuff compared to stratigraphically lower samples (Figure Q).

Based on geochemical and mineralogical data collected from the stratigraphic section of upper Lemitar Tuff, the general direction of fluid movement can be inferred. The uppermost samples appear to have experienced the most thorough degree of alteration while stratigraphically lower samples experienced only slight to moderate degrees of metasomatism, suggesting the downward movement of metasomatic fluid. Although two upper Lemitar Tuff samples from South Canyon (KM-92 and KM-93) are

Stratigraphic Variation in the Upper Lemitar Tuff, South Canyon

Whole rock chemistry -- Major and Trace Elements

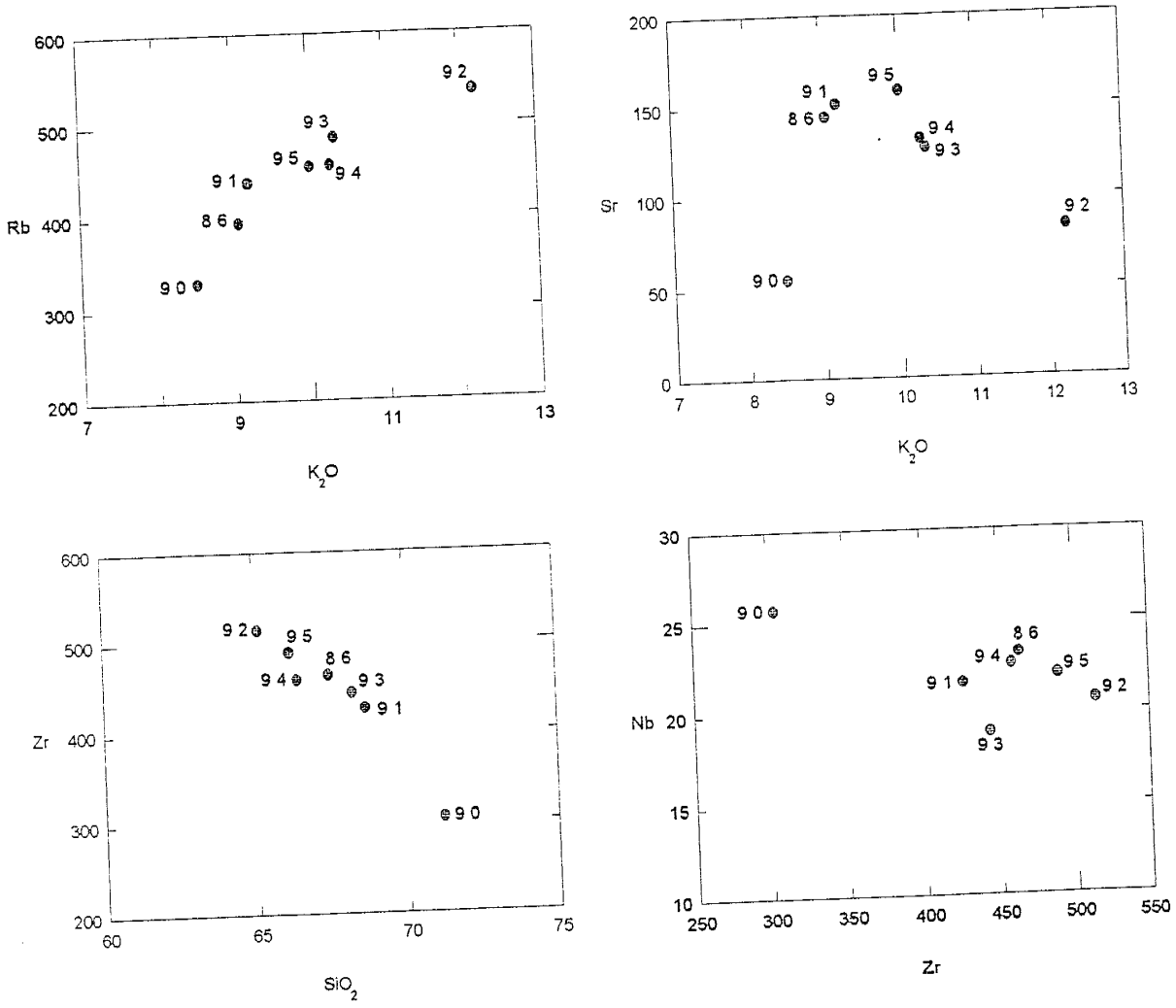

Figure Q: Major and trace element chemistry of upper Lemitar samples from the stratigraphic section in South Canyon. Numbers next to data points represent sample numbers. See Figure O for generalized map of sample locations.

poorly welded and are notably higher in porosity and permeability, lateral movement of metasomatic fluids caused by permeability differences within the upper Lemitar Tuff is not supported. The remainder of upper Lemitar Tuff samples collected from South Canyon (samples KM-86, -91, -90, -94, -95) possess similar hydrologic conductivities, yet still show evidence for an increase in K_2O and decrease in Na_2O content with stratigraphic height. This conclusion provides support for the theory that metasomatism in the Socorro area was caused by the downward percolation of alkaline, saline brines as proposed by Chapin and Lindley (1986).

Lateral Variation Across a Potential K-Metasomatic Boundary

Major and Trace Elements

As discussed in the mineralogy appendix (Appendix II), the abundance of plagioclase in the alteration assemblage of Hells Mesa Tuff clasts is found to increase southward along a lateral traverse near Red Canyon in the northern Chupadera Mountains. In addition to mineralogy differences, the Hells Mesa Tuff clasts collected across the break in slope show trends in major element chemistry, thus providing additional support for the hypothesis that this area may represent a boundary of K-metasomatism. Figures J and R generally show increasing K_2O content and decreasing Na_2O and CaO content from south to north across the induration boundary. The K_2O content of Hells Mesa Tuff clasts from the poorly indurated portion of the Popotosa averages 6.08 wt. %, while K_2O averages 8.14 wt. % from Hells Mesa Tuff clasts collected from the well indurated, northern

Lateral variation in the Hells Mesa Tuff across suspected K-metasomatic boundary, Red Canyon -- Whole rock chemistry

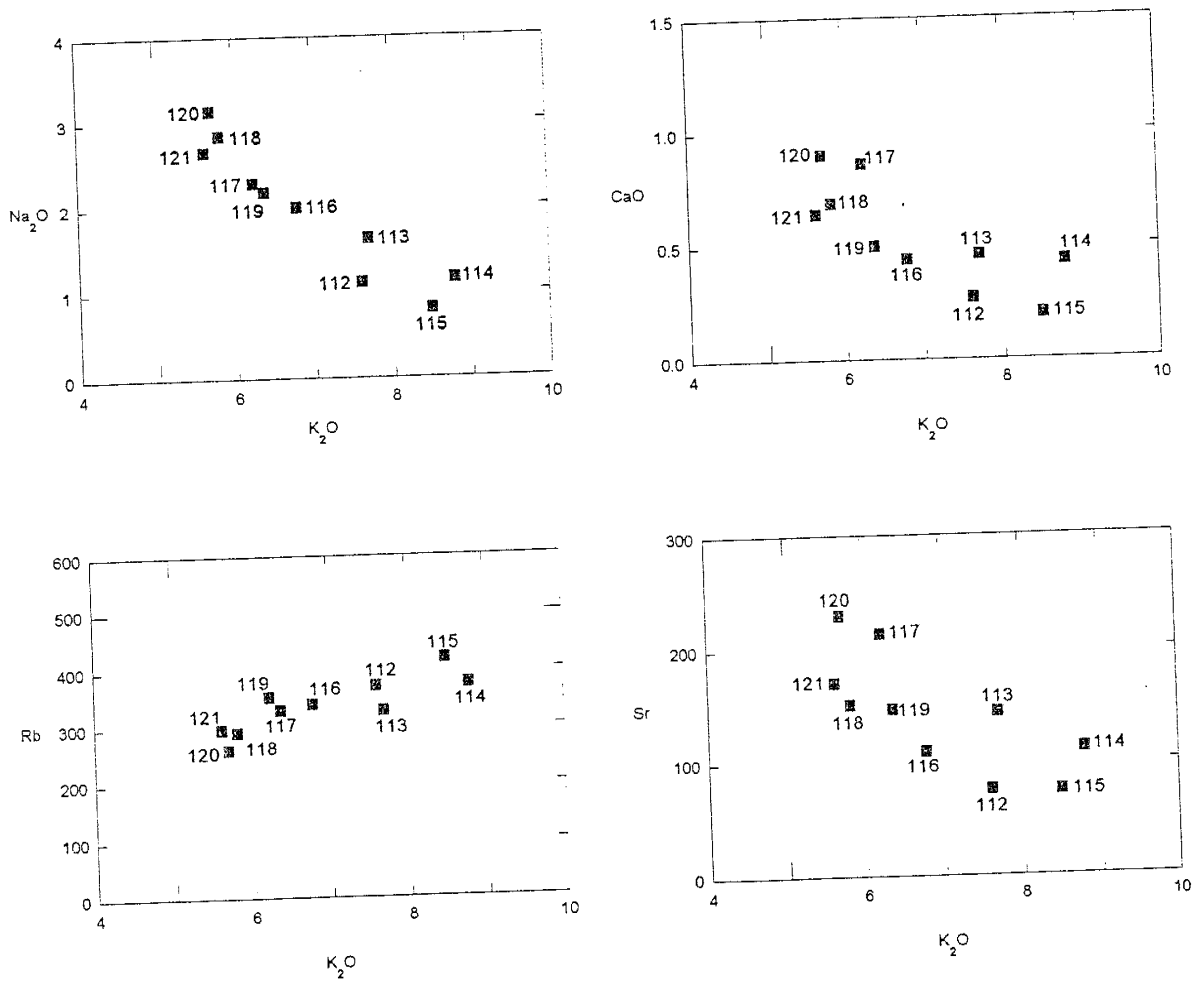

Figure R: Major and trace element chemistry in Hells Mesa Tuff samples collected across a potential K-metasomatism boundary near Red Canyon. Numbers next to data points represent sample numbers. See Figure J for generalized map of sample locations.

portion of the ridge. Na_2O content of the clasts decreases from 2.52 wt. % in the southern portion to 1.18 wt. % in the northern part along with a decrease in CaO content from 0.67 wt. % to 0.34 wt. %. Interestingly, the most K-rich samples, KM-114 and KM-115, are located near the topographically highest portion of the ridge on the northern side of the boundary, possibly indicating that the degree of K-metasomatism is related to the degree of induration of the Popotosa Formation.

Two trace elements, Rb and Sr, show similar trends to K_2O and Na_2O across the potential boundary for K-metasomatic alteration. With increasing K_2O content in whole rock Hells Mesa Tuff clasts from south to north across the boundary, Rb is also found to increase; Rb in the northern portion averages 373.5 ppm and a slightly lower 312 ppm in the southern section (Figure R). Similarly, with decreasing Na_2O content from south to north across the boundary, Sr is noticeably decreased in concentration, likely due to plagioclase dissolution (Figure R). Sr concentrations were found to average 101 ppm north of the potential boundary and 170.5 ppm south of the boundary. Various other minor, trace, and REE were not found to show systematic variations in Hells Mesa Tuff clasts collected laterally across the potential K-metasomatic boundary.

Discussion on Lateral Variation

Hells Mesa Tuff clasts collected within the Popotosa Formation north of Red Canyon in the Chupadera Mountains clearly show gradation in K_2O, Na_2O, Rb, Sr and mineralogy across the proposed boundary for K-metasomatism. K_2O and Rb are clearly elevated in concentration in the northern portion with a systematic decline in these

elements to the south across the boundary. Na_2O and Sr vary inversely to K_2O and Rb in this particular section, again providing evidence for a K-metasomatic boundary. Clearly, metasomatism had a significant influence on the degree of induration of the Popotosa due to a higher K_2O and lower Na_2O content in the well-indurated Popotosa, while poorly-indurated Popotosa reflects a more unaltered chemical composition. The sharp break in slope as one traverses from north to south across the ridge of Popotosa, caused by the difference in degree of induration, further supports this area as a boundary for K-metasomatic alteration. Lateral variation in K-metasomatic alteration is, however, difficult to explain. The presence of faulting along the boundary, assuming faulting predated metasomatism, could have focused metasomatic fluids thus allowing for the preferential flow of metasomatic fluids to the north. The presence of jasper within the fault, which is typically associated with K-metasomatic alteration in other areas (Glazner, 1988), likely indicates faulting prior to the metasomatic event.

APPENDIX IV - PART II

Geochemical Analytical Results

Whole Rock Upper Lemitar and Hells Mesa Samples

Average analytical error, determined by duplicate and triplicate analyses, for the elements in the subsequent tables are:

Element	Error (Wt. %)
SiO_2	±0.16
TiO_2	± 0.01
Al_2O_3	± 0.03
Fe_2O_3	± 0.01
MnO	±0.004
MgO	±0.04
CaO	±0.01
Na_2O	±0.04
K_2O	±0.03
P_2O_5	± 0.01

Element	Error(ppm)
V	±4.0
Cr	±12.0
Ni	±1.0
Cu	±1.0
Zn	±1.0
Ga	±0.3
As	±0.7
Rb	±0.8
Sr	±0.7
Y	±1.0
Zr	±8.0
Nb	±0.1
Mo	±0.1
Ba	±10.0
Pb	±0.2
Th	±1.0
U	±0.5

Element	Error(ppm)
Sc	±0.04
FeO	±0.02
Co	±0.13
Br	±0.07
Sb	±0.1
Cs	±1.4
La	±1.8
Ce	±1.4
Nd	±0.7
Sm	±0.07
Eu	±0.14
Tb	±0.02
Yb	±0.07
Lu	±0.01
Hf	±0.12
Ta	±0.04
W	±0.5

In the following data tables, oxides are given in wt. %, all trace elements are measured in parts per million (ppm), na=not analyzed, nd=not detected, and nr=not recorded. Unaltered chemistry for upper Lemitar and Hells Mesa samples 78-6-48, 78-6-61, 78-6-62 and 78-7-75 were obtained from D'Andrea (1981), 78-6-63 and 19-D from Lindley (1985), and 84-5-4 from Ferguson (1985). Values for the samples LEMITAR, HELLS MESA, and 84-10-28 are from N.W. Dunbar (pers. comm., 1995).

	Upper Lemitar -- Fresh Whole Rock						Altered	
SAMPLE	LEMITAR	78-6-48	78-6-61	78-6-62	78-6-63	84-5-4	KM-31	KM-36
SiO2	71.34	65.98	69.07	67.60	68.67	73.60	77.38	74.79
TiO2	0.50	0.49	0.40	0.56	0.42	0.27	0.19	0.20
Al2O3	nr	16.23	15.55	16.36	15.38	14.08	11.81	13.04
Fe2O3	2.52	1.93	1.74	2.40	1.95	1.42	1.13	1.69
MnO	0.05	0.03	0.07	0.07	0.06	0.02	0.05	0.06
MgO	0.06	0.37	0.40	0.53	0.55	0.11	0.17	0.34
CaO	nr	1.17	1.09	1.66	1.31	0.55	0.17	0.31
Na2O	3.93	4.25	4.51	4.75	4.30	3.58	1.59	1.48
K2O	4.80	5.58	5.58	5.38	5.11	5.54	7.81	8.32
P2O5	0.14	0.12	0.07	0.02	0.12	0.04	0.03	0.03
LOI	nr	nr	nr	nr	0.00	0.64	0.02	0.04
Total	nr	nr	nr	nr	nr	nr	100.35	100.30
V	nr	nr	nr	nr	nr	nr	na	na
Cr	nr	nr	nr	nr	nr	nr	171	62
Ni	nr	nr	nr	nr	nr	nr	na	na
Cu	4.9	nr	nr	nr	nr	nr	na	na
Zn	75	nr	nr	nr	nr	nr	40	55
Ga	nr	nr	nr	nr	nr	nr	na	na
As	1	nr	nr	nr	nr	nr	49	22
Rb	157	124	74	77	93	nr	318	296
Sr	248	247	nr	nr	nr	nr	105	111
Y	80	41	78	60	80	nr	18	14
Zr	363	350	352	483	325	nr	175	149
Nb	27	18	29	14	29	nr	23	25
Mo	nr	nr	nr	nr	nr	nr	na	na
Ba	1245	nr	nr	nr	1299	nr	478	2348
Pb	31	nr	nr	nr	nr	nr	17	33
Th	22	14	50	14	nr	nr	24	27
U	4	9	20	6	0	nr	3	5
Sc	4.5	nr	nr	nr	nr	nr	2.5	5.4
FeO	nr	nr	nr	nr	nr	nr	1.2	2.8
Co	nr	nr	nr	nr	nr	nr	1.8	29.6
Br	0	nr	nr	nr	nr	nr	nd	0.3
Sb	0.1	nr	nr	nr	nr	nr	5.2	0.9
Cs	1.8	nr	nr	nr	nr	nr	3.2	5.9
La	70.2	nr	nr	nr	nr	nr	34.7	69.3
Ce	136	nr	nr	nr	nr	nr	78	140
Nd	61	nr	nr	nr	nr	nr	32.2	57.1
Sm	12.4	nr	nr	nr	nr	nr	8.4	12.0
Eu	1.9	nr	nr	nr	nr	nr	0.5	2.3
Tb	1.9	nr	nr	nr	nr	nr	1.5	1.6
Yb	7.0	nr	nr	nr	nr	nr	5.5	5.6
Lu	0.97	nr	nr	nr	nr	nr	0.8	0.7
Hf	10.9	nr	nr	nr	nr	nr	6.4	12.7
Ta	2.2	nr	nr	nr	nr	nr	2.0	1.9
W	nr	nr	nr	nr	nr	nr	2.7	87.6

	Upper Lemitar -- Altered Whole Rock							
SAMPLE	KM-41	KM-46	KM-51	KM-55	KM-56	KM-86	KM-90	KM-91
SiO2	67.25	70.60	62.48	65.77	66.03	67.49	71.21	68.67
TiO2	0.57	0.43	0.63	0.56	0.56	0.58	0.33	0.54
Al2O3	15.47	13.37	17.36	15.99	15.68	15.43	14.67	14.94
Fe2O3	2.94	2.04	3.11	3.23	2.90	2.83	1.51	2.81
MnO	0.04	0.04	0.03	0.07	0.10	0.06	0.03	0.03
MgO	0.40	0.55	1.07	0.42	0.48	0.39	0.12	0.30
CaO	0.42	1.32	0.83	0.40	0.37	0.48	0.27	0.44
Na2O	1.87	2.95	2.34	1.85	1.86	2.14	2.65	2.25
K2O	10.00	6.64	9.50	10.93	10.87	9.06	8.50	9.20
P2O5	0.09	0.07	0.09	0.08	0.08	0.15	0.03	0.15
LOI	0.06	0.12	0.22	0.02	0.03	1.01	0.48	0.43
Total	99.11	98.13	97.66	99.32	98.96	99.62	99.80	99.76
V	na	na	na	na	na	31	11	36
Cr	685	39	41	387	85	9	12	21
Ni	na	na	na	na	na	<5	<5	<5
Cu	na	na	na	na	na	6.7	<5	9.1
Zn	29	32	81	74	84	56	25	34
Ga	na	na	na	na	na	19	18	20
As	3	3	5	77	91	9	34	9
Rb	401	255	384	376	376	394	329	438
Sr	68	146	142	93	91	144	55	151
Y	17	58	69	73	70	75	75	65
Zr	122	377	550	454	444	464	304	426
Nb	28	23	26	30	26	23	26	22
Mo	na	na	na	na	na	<3	<3	<3
Ba	435	1288	1582	1493	1474	2678	595	1786
Pb	21	19	23	66	64	21	21	20
Th	29	20	22	19	22	14	21	13
U	11	9	9	9	9	6	5	8
Sc	1.6	4.3	5.9	5.3	5.0	na	na	na
FeO	1.5	2.0	2.9	2.9	2.8	na	na	na
Co	40.8	36.6	4.7	6.1	3.7	na	na	na
Br	0.1	0.1	0.1	0.1	0.2	na	na	na
Sb	0.3	0.2	0.2	12.0	8.4	0.4	1.9	16.0
Cs	5.0	4.8	9.5	3.0	3.5	6.0	3.0	8.0
La	38.3	54.9	82.2	69.2	67.8	82.8	86.7	74.8
Ce	52	121	165	151	141	148	158	134
Nd	19	52.9	69.4	61.7	59.9	67	69	57
Sm	2.7	10.3	13.5	12.9	12.4	11.7	12.7	10.4
Eu	0.5	1.6	2.5	2.3	2.2	2.1	1.5	2.4
Tb	0.3	1.5	1.78	1.9	1.8	na	na	na
Yb	2.1	5.7	6.4	6.8	6.5	5.7	5.6	5.0
Lu	0.4	0.8	0.9	0.9	0.9	0.9	0.8	0.8
Hf	4.3	11.1	15.4	12.8	12.8	na	na	na
Ta	2.4	2.2	1.7	2.1	1.8	na	na	na
W	130	108	1.8	2.4	1.6	na	na	na

	Upper Lemitar – Altered Whole Rock							
SAMPLE	KM-92	KM-93	KM-94	KM-95	KM-106	KM-107	KM-108	KM-109
SiO2	65.15	68.26	66.43	66.18	64.97	69.18	71.36	67.11
TiO2	0.63	0.56	0.59	0.60	0.51	0.50	0.42	0.52
Al2O3	16.26	14.84	15.35	16.05	15.52	14.59	13.10	15.60
Fe2O3	2.20	2.86	2.88	2.98	2.19	2.41	2.14	2.54
MnO	0.02	0.04	0.04	0.02	0.05	0.04	0.07	0.04
MgO	0.42	0.22	0.33	0.30	0.85	0.39	0.37	0.42
CaO	0.37	0.44	0.43	0.43	1.77	0.51	0.74	0.34
Na2O	1.26	1.59	1.83	2.41	4.66	2.29	1.92	2.17
K2O	12.21	10.35	10.29	10.02	3.58	9.15	8.57	10.13
P2O5	0.17	0.15	0.15	0.15	0.11	0.14	0.11	0.12
LOI	0.76	0.78	0.93	0.52	4.76	0.51	0.81	0.55
Total	99.45	100.09	99.25	99.66	98.97	99.71	99.61	99.54
V	36	23	39	41	22	47	35	69
Cr	14	21	19	9	15	10	17	10
Ni	6.7	<5	<5	<5	<5	<5	5.3	5.7
Cu	<5	5.4	6.6	<5	<5	<5	<5	6.1
Zn	36	38	43	31	54	53	35	52
Ga	19	18	21	21	18	17	16	20
As	7	21	34	15	3	3	22	16
Rb	535	486	456	455	526	402	395	422
Sr	83	127	132	159	391	90	77	89
Y	67	61	68	66	59	68	62	69
Zr	514	443	459	489	455	419	337	429
Nb	21	19	23	22	20	23	23	25
Mo	<5	<3	<3	<3	3.1	<3	<3	<3
Ba	2186	1845	2584	1991	2247	1462	1110	1564
Pb	12	18	18	22	20	19	13	26
Th	15	13	15	15	15	16	15	20
U	6	5	5	6	5	5	5	6
Sc	na	na	na	na	na	na	na	na
FeO	na	na	na	na	na	na	na	na
Co	na	na	na	na	na	na	na	na
Br	na	na	na	na	na	na	na	na
Sb	2.1	5.4	1.7	10.0	1.10	0.20	<.2	<.2
Cs	5.0	4.0	5.0	4.0	88.0	5.0	3.0	2.0
La	78.6	77.2	69.4	74.6	90.2	68.2	60.3	77.2
Ce	146	137	126	138	153	128	112	142
Nd	59	63	54	54	61	50	48	62
Sm	10.3	10.2	9.7	10.0	10.0	9.6	9.1	10.6
Eu	2.4	1.9	2.6	1.9	1.6	2.0	1.7	2.1
Tb	na	na	na	na	na	na	na	na
Yb	4.9	4.7	5.3	4.8	4.2	5.0	5.7	5.7
Lu	0.8	0.7	0.76	0.76	0.63	0.80	0.84	0.83
Hf	na	na	na	na	na	na	na	na
Ta	na	na	na	na	na	na	na	na
W	na	na	na	na	na	na	na	na

	Upper Lemitar -- Altered Whole Rock							
SAMPLE	KM-110	KM-111	KM-122	KM-123	KM-124	KM-125	KM-126	KM-127
SiO2	66.86	68.91	68.47	74.67	68.13	71.34	66.86	65.96
TiO2	0.41	0.36	0.49	0.26	0.52	0.33	0.55	0.62
Al2O3	15.01	15.01	15.79	12.72	15.89	14.50	15.59	15.98
Fe2O3	1.80	2.44	2.32	1.50	2.56	1.71	2.76	3.18
MnO	0.05	0.05	0.04	0.04	0.04	0.03	0.05	0.06
MgO	0.69	0.41	0.22	0.07	0.22	0.11	0.48	0.37
CaO	1.30	1.20	0.27	0.22	0.39	0.29	0.60	0.42
Na2O	3.99	3.01	2.24	2.42	2.23	2.94	2.59	2.24
K2O	4.73	6.82	9.57	7.24	9.38	8.29	8.87	10.30
P2O5	0.07	0.12	0.08	0.03	0.10	0.04	0.14	0.17
LOI	5.08	1.36	0.59	0.47	0.56	0.42	1.27	0.56
Total	99.99	99.69	100.08	99.64	100.02	100.00	99.76	99.88
V	34	40	33	32	35	28	37	42
Cr	31	12	101	241	86	149	104	100
Ni	<5	<5	8.7	5.5	6.4	<5	6	9.5
Cu	<5	7.6	<5	<5	<5	<5	<5	6
Zn	18	40	32	33	48	24	53	47
Ga	7	17	18	17	20	17	21	20
As	5	3	26	27	37	78	15	10
Rb	241	305	379	285	367	319	364	453
Sr	67	234	128	48	177	47	168	133
Y	144	26	59	72	64	75	78	66
Zr	401	197	397	235	450	293	442	484
Nb	21	20	20	26	17	26	24	22
Mo	3.3	<3	6	13.2	6.1	8.7	5.9	6.2
Ba	1319	967	2298	633	2687	579	2285	2222
Pb	15	15	26	18	23	26	21	23
Th	17	17	19	17	15	21	16	14
U	6	5	7	6	6	7	7	5
Sc	na	na	na	na	na	na	na	na
FeO	na	na	na	na	na	na	na	na
Co	na	na	na	na	na	na	na	na
Br	na	na	na	na	na	na	na	na
Sb	1.10	<.2	10.0	10.0	8.3	5.9	1.2	0.4
Cs	77.0	8.0	6.0	4.0	4.0	3.0	5.0	3.0
La	114.0	50.1	122.0	70.1	121.0	93.1	83.2	69.3
Ce	201	83	209	134	205	165	152	127
Nd	78	28	80	58	79	70	58	53
Sm	12.9	4.4	13.7	11.5	13.7	13.4	11.1	9.7
Eu	1.9	1.2	2.7	0.7	3.0	1.5	2.8	2.3
Tb	na	na	na	na	na	na	na	na
Yb	5.3	2.7	5.1	5.7	5.0	6.2	6.6	4.8
Lu	0.79	0.41	0.78	0.79	0.72	0.93	0.95	0.73
Hf	na	na	na	na	na	na	na	na
Ta	na	na	na	na	na	na	na	na
W	na	na	na	na	na	na	na	na

	Upper Lemitar -- Altered Whole Rock							
SAMPLE	KM-128	KM-129	KM-130	KM-131	KM-138	KM-143	KM-144	KM-147
SiO2	68.66	72.57	70.04	72.61	63.83	64.10	69.06	72.90
TiO2	0.54	0.42	0.52	0.43	0.59	0.51	0.51	0.39
Al2O3	14.93	13.43	14.70	12.95	16.79	17.50	14.53	13.50
Fe2O3	2.81	2.21	2.67	2.32	3.08	2.36	2.68	2.05
MnO	0.06	0.06	0.07	0.06	0.08	0.03	0.05	0.06
MgO	0.38	0.32	0.35	0.36	0.67	0.30	0.49	0.41
CaO	0.61	0.58	0.85	0.44	0.57	0.36	0.40	0.73
Na2O	2.21	2.89	3.20	2.27	2.02	2.85	1.84	3.28
K2O	9.21	7.01	7.26	7.39	11.43	10.72	9.97	5.88
P2O5	0.14	0.09	0.14	0.10	0.20	0.10	0.14	0.09
LOI	0.86	0.55	0.63	1.04	0.90	0.74	0.60	0.87
Total	100.41	100.13	100.43	99.97	100.16	99.57	100.27	100.16
V	44	39	35	37	57	37	66	33
Cr	140	142	101	158	68	43	116	118
Ni	6.3	<5	7.5	7.8	<5	7.4	5.8	<5
Cu	<5	<5	<5	5.7	8.2	<5	9	5.9
Zn	46	42	51	43	54	46	44	47
Ga	19	19	20	18	21	23	19	19
As	9	18	13	18	24	19	19	8
Rb	384	278	282	313	504	402	378	226
Sr	127	122	181	96	118	146	76	121
Y	71	79	70	67	70	76	59	84
Zr	414	309	390	338	493	468	416	278
Nb	25	27	25	25	25	25	22	28
Mo	8	7.3	7.2	9.1	5	4.5	6.7	6.9
Ba	1718	989	1500	1055	1878	1981	1458	739
Pb	20	18	17	18	24	25	17	17
Th	15	17	17	15	19	20	16	18
U	4	6	5	6	6	7	6	5
Sc	na	na	na	na	na	na	na	na
FeO	na	na	na	na	na	na	na	na
Co	na	na	na	na	na	na	na	na
Br	na	na	na	na	na	na	na	na
Sb	130	<.2	0.5	0.4	130	<.2	<.2	<.2
Cs	4.0	2.0	3.0	4.0	2.0	4.0	3.0	3.0
La	66.2	59.8	64.7	61.2	72.9	105.0	65.2	57.5
Ce	117	117	124	111	129	188	118	112
Nd	55	51	49	48	57	70	52	49
Sm	10.0	10.1	9.7	9.0	10.2	11.8	9.2	10.1
Eu	1.8	1.3	1.6	1.1	2.3	2.6	1.5	1.5
Tb	na	na	na	na	na	na	na	na
Yb	5.6	6.2	5.7	5.2	5.1	4.8	4.5	6.8
Lu	0.82	0.94	0.83	0.75	0.73	0.74	0.73	1.03
Hf	na	na	na	na	na	na	na	na
Ta	na	na	na	na	na	na	na	na
W	na	na	na	na	na	na	na	na

	Upper Lemitar -- Altered Whole Rock								
SAMPLE	KM-148	KM-149	KM-150	KM-151	KM-154	KM-156	KM-157	KM-159	KM-160
SiO2	72.05	71.77	68.47	69.42	70.07	68.15	69.80	69.16	66.57
TiO2	0.44	0.43	0.53	0.50	0.52	0.55	0.49	0.54	0.57
Al2O3	14.00	14.21	15.29	14.75	14.21	15.35	14.61	14.60	15.43
Fe2O3	2.30	2.26	2.74	2.69	2.81	2.98	2.70	2.85	3.02
MnO	0.05	0.07	0.03	0.04	0.02	0.05	0.06	0.03	0.07
MgO	0.51	0.39	0.39	0.40	0.58	0.38	0.47	0.29	0.46
CaO	1.11	0.44	0.49	0.51	0.30	0.33	0.48	0.30	1.19
Na2O	3.65	2.73	2.57	2.72	1.03	2.11	2.41	1.53	1.87
K2O	4.79	7.82	9.22	8.15	8.90	9.89	7.33	10.10	9.26
P2O5	0.09	0.09	0.13	0.11	0.14	0.13	0.11	0.13	0.15
LOI	1.26	0.52	0.53	0.81	1.48	0.42	1.57	0.48	1.51
Total	100.25	100.73	100.39	100.10	100.06	100.34	100.03	100.01	100.10
V	31	32	40	39	38	40	34	47	42
Cr	98	101	97	90	115	108	120	167	112
Ni	<5	<5	5.3	<5	8.2	6	5	7	7
Cu	<5	<5	<5	<5	6.6	<5	<5	9	<5
Zn	49	38	44	41	40	45	57	59	67
Ga	20	20	21	21	23	21	21	17	19
As	3	19	3	26	3	44	11	3	42
Rb	168	309	136	320	386	490	342	452	397
Sr	206	114	56	113	65	127	106	111	184
Y	74	83	117	79	57	71	68	63	70
Zr	327	330	418	380	417	421	382	419	433
Nb	28	28	25	27	20	25	27	22	21
Mo	5.9	5.9	6.1	5.7	5.4	7	7	9	7
Ba	1093	1060	1458	1100	1605	1822	1278	2683	2728
Pb	19	20	60	25	13	25	22	25	18
Th	19	17	84	18	15	16	18	15	15
U	6	6	5	5	6	4	7	5	4
Sc	na	na	na	na	na	na	na	na	na
FeO	na	na	na	na	na	na	na	na	na
Co	na	na	na	na	na	na	na	na	na
Br	na	na	na	na	na	na	na	na	na
Sb	<.2	0.4	0.5	<.2	11.0	1.3	0.5	2.7	3.0
Cs	1.0	3.0	3.0	2.0	8.0	3.0	6.0	3.0	7.0
La	62.1	66.7	66.9	60.2	65.8	70.0	59.8	62.6	71.2
Ce	118	121	124	114	121	128	111	116	131
Nd	51	51	51	47	49	55	50	50	52
Sm	9.9	10.5	9.6	10.0	8.9	10.1	8.9	8.6	9.8
Eu	1.3	1.4	2.4	1.5	2.1	1.7	1.4	1.3	2.1
Tb	na	na	na	na	na	na	na	na	na
Yb	5.7	6.4	5.5	6.2	4.2	5.6	5.2	4.8	5.4
Lu	0.87	0.94	0.81	0.89	0.67	0.84	0.81	0.71	0.81
Hf	na	na	na	na	na	na	na	na	na
Ta	na	na	na	na	na	na	na	na	na
W	na	na	na	na	na	na	na	na	na

	Hells Mesa -- Fresh Whole Rock				Hells Mesa -- Altered Whole Rock			
SAMPLE	HM-TUFF	78-7-75	84-10-28	19-D	KM-54	KM-58	KM-59	KM-60
SiO2	75.46	69.50	73.90	69.84	72.79	72.80	74.96	72.36
TiO2	0.21	0.33	0.25	0.37	0.27	0.30	0.24	0.26
Al2O3	nr	14.83	13.50	15.12	13.26	14.47	14.03	13.53
Fe2O3	1.44	1.56	1.52	2.26	2.22	2.18	1.77	1.98
MnO	0.03	0.06	0.05	0.04	0.08	0.02	0.02	0.09
MgO	0.44	0.33	0.43	0.72	0.37	0.64	0.41	0.48
CaO	nr	0.83	0.90	1.84	0.79	0.36	0.28	1.79
Na2O	3.47	4.24	3.73	3.90	1.42	0.99	1.26	1.67
K2O	4.76	5.54	4.56	4.47	7.83	8.39	7.27	7.18
P2O5	0.06	0.08	0.07	0.11	0.05	0.05	0.04	0.05
LOI	nr	nr	nr	0.92	0.15	0.18	0.18	0.33
V	nr	nr	25	nr	na	na	na	na
Cr	nr	nr	0	nr	562	268	510	461
Ni	nr	nr	0	nr	na	na	na	na
Cu	1.8	nr	1.7	nr	na	na	na	na
Zn	24	nr	30.7	nr	33	74	52	30
Ga	na	nr	16	nr	na	na	na	na
As	2	nr	1.4	nr	9.2	16.1	13.0	6.2
Rb	195	169	193	144	424	310	341	335
Sr	180	178	235	384	120	16	77	92
Y	18	71	11	27	60	61	20	21
Zr	137	286	142	219	444	152	157	138
Nb	23	30	23	26	23	28	31	26
Mo	nr	nr	<1	nr	na	na	na	na
Ba	524	nr	593	1028	794	998	600	511
Pb	18	nr	5	nr	26	34	19	17
Th	39.6	20	24	18	19	27	30	26
U	4	6	4	3	4	5	10	9
FeO	nr	nr	na	nr	2.0	2.1	1.7	1.9
Sc	1.79	nr	1.68	nr	2.4	2.6	2.1	2.7
Co	nr	nr	41.0	nr	7.6	4.6	4.9	5.7
Br	0.3	nr	1	nr	0.12	0.16	0.03	0.06
Sb	0.30	nr	0.40	nr	0.54	0.55	3.0	0.48
Cs	4.0	nr	3.0	nr	8.3	20.0	10.5	10.3
La	42.4	nr	38.1	nr	39.5	41.4	42.7	39.1
Ce	71	nr	76	nr	69	77	76	67
Nd	25	nr	18	nr	21.4	26.6	22.2	19.6
Sm	3.0	nr	2.7	nr	3.3	4.6	3.4	3.3
Eu	0.55	nr	0.6	nr	0.7	0.8	0.6	0.7
Tb	0.32	nr	0.30	nr	0.38	0.51	0.38	0.4
Yb	2.0	nr	1.6	nr	2.1	2.4	2.6	2.5
Lu	0.36	nr	0.26	nr	0.34	0.35	0.42	0.41
Hf	4.7	nr	4.6	nr	4.9	5.8	5.4	4.7
Ta	2.2	nr	2.0	nr	1.8	1.6	2.1	1.8
W	nr	nr	340	nr	1.7	1.2	1.9	1.3

	Hells Mesa -- Altered Whole Rock							
SAMPLE	KM-61	KM-96	KM-102	KM-112	KM-113	KM-114	KM-115	KM-116
SiO2	75.90	74.52	73.03	73.38	71.18	71.81	73.33	73.51
TiO2	0.22	0.24	0.25	0.26	0.29	0.28	0.23	0.24
Al2O3	13.30	12.92	13.34	13.25	14.11	13.77	13.13	13.07
Fe2O3	1.85	1.61	1.62	1.99	2.11	2.01	1.55	1.85
MnO	0.06	0.01	0.01	0.05	0.05	0.04	0.05	0.05
MgO	0.35	0.23	0.21	0.33	0.29	0.28	0.27	0.25
CaO	0.61	0.17	0.22	0.27	0.46	0.43	0.20	0.44
Na2O	2.53	0.60	0.71	1.12	1.63	1.16	0.80	2.00
K2O	6.28	8.52	8.86	7.60	7.69	8.79	8.49	6.79
P2O5	0.04	0.06	0.06	0.07	0.08	0.08	0.06	0.07
LOI	0.06	1.06	1.21	1.73	1.59	1.78	1.56	1.36
V	na	22	28	35	42	30	27	35
Cr	641	26	19	144	165	134	137	151
Ni	na	<5	<5	6.7	6.3	<5	5	5.3
Cu	na	12.6	10.7	8.8	8.7	6.1	10	<5
Zn	45	104	52	69	56	59	44	39
Ga	na	16	15	16	16	16	16	16
As	10.3	4	11.1	17.6	7.8	8.1	10.4	4.5
Rb	305	335	311	372	328	375	419	340
Sr	117	88	98	75	144	111	74	110
Y	17	22	25	21	28	26	28	22
Zr	134	134	151	140	175	158	136	135
Nb	29	23	23	22	22	22	25	23
Mo	na	<3	<3	8.3	9.1	7.4	7.2	8.7
Ba	502	858	1187	773	1622	1586	1911	636
Pb	29	182	327	39	28	29	36	16
Th	29	25	22	25	22	20	30	27
U	9	8	5	6	5	4	7	6
FeO	1.7	na	na	na	na	na	na	na
Sc	2.1	na	na	na	na	na	na	na
Co	6.6	na	na	na	na	na	na	na
Br	0.13	na	na	na	na	na	na	na
Sb	0.57	3.2	1.4	0.9	0.4	0.5	0.8	0.7
Cs	12.3	4.0	4.0	21.0	6.0	8.0	14.0	9.0
La	36.7	45.9	54.4	42.1	45.3	45.1	45.6	45.3
Ce	66	69	74	71	89	75	70	71
Nd	17.4	21	23	20	24	24	20	19
Sm	2.6	2.8	3.2	3.0	3.9	3.8	2.9	2.9
Eu	0.5	0.6	0.8	0.8	0.8	0.7	0.7	0.5
Tb	0.30	na	na	na	na	na	na	na
Yb	2.3	2.4	2.5	2.4	2.6	2.7	2.5	2.7
Lu	0.37	0.35	0.36	0.40	0.43	0.44	0.46	0.44
Hf	5.0	na	na	na	na	na	na	na
Ta	2.0	na	na	na	na	na	na	na
W	2.1	na	na	na	na	na	na	na

	Hells Mesa -- Altered Whole Rock							
SAMPLE	KM-117	KM-118	KM-119	KM-120	KM-121	KM-153	KM-155	KM-158
SiO2	71.65	73.95	74.11	73.47	74.37	77.27	78.47	75.54
TiO2	0.41	0.22	0.22	0.25	0.21	0.16	0.15	0.21
Al2O3	13.41	12.91	13.00	13.78	12.87	11.33	11.88	13.00
Fe2O3	2.81	1.65	1.65	1.77	1.59	1.09	1.13	1.50
MnO	0.04	0.07	0.04	0.04	0.03	0.03	0.01	0.03
MgO	0.45	0.44	0.30	0.23	0.30	0.08	0.34	0.39
CaO	0.86	0.69	0.50	0.90	0.64	0.10	0.04	0.53
Na2O	2.29	2.85	2.18	3.14	2.66	0.83	0.11	2.61
K2O	6.23	5.82	6.37	5.70	5.62	8.74	5.83	5.10
P2O5	0.13	0.07	0.06	0.07	0.06	0.02	0.03	0.05
LOI	1.47	0.87	1.43	0.84	1.23	0.66	2.45	1.32
V	60	30	31	33	34	26	24	26
Cr	171	182	190	148	177	227	144	129
Ni	8.2	5	9.5	6.4	<5	6.2	<5	5.7
Cu	10.8	<5	5	6	7.7	7.3	10.2	<5
Zn	45	32	35	28	31	18	84	24
Ga	17	15	16	16	16	14	17	15
As	7.8	11.6	10.5	8.2	5.5	9	4.8	3
Rb	353	291	330	261	297	306	277	251
Sr	214	151	147	230	171	27	40	118
Y	27	18	22	21	20	64	18	19
Zr	159	127	129	155	126	155	108	119
Nb	19	24	23	24	24	28	22	24
Mo	8.3	10.5	9.7	9.1	10.7	10.7	8.4	6.9
Ba	1742	1044	2073	2274	1362	275	598	473
Pb	33	58	24	29	25	17	278	19
Th	21	29	28	26	29	22	29	30
U	6	5	5	5	6	6	8	5
FeO	na	na	na	na	na	na	na	na
Sc	na	na	na	na	na	na	na	na
Co	na	na	na	na	na	na	na	na
Br	na	na	na	na	na	na	na	na
Sb	1.0	0.7	0.4	0.5	1.0	7.0	1.7	0.3
Cs	22.0	11.0	10.0	5.0	18.0	3.0	8.0	4.0
La	46.6	43.3	44.0	49.2	44.7	32.4	47.0	41.4
Ce	73	64	65	76	69	62	69	59
Nd	20	17	16	23	19	26	20	15
Sm	4.3	2.2	2.5	3.1	2.5	5.4	2.8	1.9
Eu	1.0	0.6	<.5	0.8	0.3	0.5	0.6	0.5
Tb	na	na	na	na	na	na	na	na
Yb	2.7	1.9	2.2	2.5	2.0	5.0	1.9	2.0
Lu	0.45	0.34	0.39	0.43	0.35	0.74	0.33	0.32
Hf	na	na	na	na	na	na	na	na
Ta	na	na	na	na	na	na	na	na
W	na	na	na	na	na	na	na	na

Separated Upper Lemitar and Hells Mesa Samples

Analytical results for the separated samples are given in the subsequent tables. The average analytical errors for elements determined by INAA in the separated, altered plagioclase samples are based on counting statistics as determined by the TEABAGS analysis program. Duplicate and triplicate samples were not able to be used due to the extremely small amount of material obtained for the separated samples. The average analytical error is given below (oxide error given in wt. %, the remainder of elements in ppm):

Element	Error	Element	Error
Na_2O	±0.013	La	±0.25
CaO	±0.25	Ce	±0.64
FeO	±0.10	Nd	±2.1
Sc	±0.07	Sm	±0.05
Cr	±2.4	Eu	±0.02
Co	±0.13	Tb	±0.02
Zn	±3.8	Yb	±0.05
As	±0.7	Lu	±0.01
Se	±0.4	Hf	±0.07
Br	±0.13	Ta	±0.02
Rb	±9.3	Hg	±0.16
Sr	±32.5	Au	±0.0014
Ag	±0.16	W	±0.7
Sb	±0.04	Th	±0.08
Cs	±0.25	U	±0.07
Ba	±43.0		

In the following data tables, na=not analyzed and nd=not detected. All oxides are given in wt. % with all other elemental abundances expressed as parts per million (ppm).

	Separated Sample Chemistry							
SAMPLE	KJH-26	KM-31	KM-36	KM-41	KM-46	KM-51	KM-54	KM-55
Na2O	6.86	4.70	0.27	1.45	3.70	1.0	0.13	0.55
CaO	7.50	1	na	na	na	na	na	na
FeO	0.27	0.18	0.84	0.94	1.17	0.59	0.80	0.89
Sc	0.23	0.09	11.03	2.0	3.93	5.65	4.75	9.66
Cr	0.40	0.2	69.3	574.0	592.0	45.9	13.9	25.8
Co	0.14	0.11	3.48	5.25	6.05	2.17	8.49	3.33
Zn	5.9	nr	165	35.2	30.2	70.1	79.2	215
As	nd	1.24	5.86	1.49	3.10	0.82	6.61	108.0
Se	nd	nd	0.98	nd	nd	nd	nd	0.7
Br	0.26	0.10	0.40	0.35	1.17	2.25	0.21	0.10
Rb	1	110	510	512	187	211	382	519
Sr	na	na	na	na	na	na	na	na
Ag	na	na	na	na	na	na	na	na
Sb	0.01	0.10	0.32	0.19	0.10	0.06	0.12	9.74
Cs	0.08	0.22	23.9	8.7	4.7	13.6	25.4	12.4
Ba	664	112	3600	289	1259	262	747	3771
La	22.3	3.5	16.1	12.5	42.2	11.4	12.9	70.0
Ce	32.4	4.9	44.1	31.8	76.0	21.9	32.7	95.7
Nd	9.7	nd	18	7.4	26.78	7.72	8.2	44.3
Sm	1.15	0.23	3.9	1.6	4.3	1.5	2.0	6.2
Eu	1.73	0.74	0.80	0.34	1.11	0.44	0.65	1.00
Tb	0.11	0.05	0.55	0.23	0.48	0.23	0.32	0.76
Yb	0.45	0.33	1.34	0.95	1.86	1.35	1.40	2.50
Lu	0.08	0.04	0.16	0.15	0.28	0.22	0.20	0.37
Hf	1.31	0.57	1.75	2.09	4.05	5.27	2.85	4.47
Ta	0.10	0.06	0.17	0.32	0.64	1.36	0.66	0.71
Hg	na	na	na	na	na	na	na	na
Au	na	na	na	na	na	na	na	na
W	24.7	16.1	1.4	1.7	1.3	0.32	0.89	1.2
Th	4.2	0.78	2.4	5.2	11.3	6.2	13.8	10.6
U	0.2	0.5	1.0	1.0	1.9	1.1	1.5	1.2

	Separated Sample Chemistry							
SAMPLE	KM-56	KM-58	KM-59	KM-60	KM-61	KM-86	KM-90	KM-91
NaO	0.60	0.11	0.10	0.85	2.75	3.07	0.57	1.16
CaO	na	na	na	na	na	na	na	na
FeO	0.92	0.64	0.62	0.51	0.67	0.89	0.87	1.0
Sc	5.3	2.7	2.3	4.5	4.5	8.5	34.1	10.3
Cr	42.0	11.9	21.1	34.9	90.1	57.3	104.7	173.9
Co	2.6	2.2	1.4	1.7	2.1	2.0	3.6	3.5
Zn	204	98.5	114.6	103.7	116.6	87	184	167
As	69.0	40.1	32.1	2.95	8.9	5.55	108.6	5.0
Se	0.6	0.35	nd	nd	1.21	<1	nd	2.0
Br	0.22	0.08	0.08	0.06	0.34	0.72	1.93	0.78
Rb	483	411	294	223	309	420	662	617
Sr	na	na	na	na	na	141	nd	nd
Ag	na	na	na	na	na	nd	nd	nd
Sb	3.77	0.26	0.74	0.10	0.19	0.16	2.21	5.01
Cs	8.7	17.9	17.2	14.6	50.1	14.8	90.3	91.7
Ba	25051	257	4386	179	440	2416	641	1074
La	48.8	15.3	13.5	69.4	15.1	27.0	55.1	31.8
Ce	93.5	21.3	24.5	33.0	65.7	73.6	140.2	84.8
Nd	38.5	7.12	2.9	42.8	8.3	26.7	56.0	29.0
Sm	8.7	1.21	1.13	6.8	1.72	5.9	13.8	5.9
Eu	1.4	0.27	0.29	1.5	0.69	1.39	1.40	1.3
Tb	1.5	0.15	0.25	0.81	0.26	0.88	2.38	0.71
Yb	5.6	0.78	1.6	4.2	1.3	2.23	5.15	1.4
Lu	0.80	0.10	0.26	0.64	2.0	0.31	0.62	0.18
Hf	5.6	3.0	2.6	1.4	2.5	2.71	3.4	2.1
Ta	0.94	0.53	0.31	0.22	0.20	0.18	0.34	0.27
Hg	na	na	na	na	na	0.32	0.53	nd
Au	na	na	na	na	na	0.003	nd	nd
W	1.9	0.52	0.68	0.74	0.99	1.9	4.1	nd
Th	9.6	4.19	5.17	5.11	2.9	2.7	5.4	2.7
U	1.5	0.65	1.11	0.76	0.78	0.96	1.1	1.0

	Separated Sample Chemistry							
SAMPLE	KM-94	KM-95	KM-96	KM-102	KM-107	KM-111	KM-112	KM-113
NaO	0.30	0.36	0.16	0.19	1.65	4.53	0.24	0.36
CaO	na	na	na	na	na	na	na	na
FeO	0.80	0.99	1.34	1.31	0.84	0.46	0.59	0.68
Sc	11.6	23.4	3.4	5.1	1.7	3.5	1.2	1.8
Cr	124.9	152.6	51.9	48.4	391.0	66.8	188.6	193.0
Co	3.7	3.2	3.9	4.3	71.4	12.2	13.4	8.6
Zn	141	87	248	120	27	31	145	199
As	11.9	8.0	3.9	2.2	1.1	3.9	12.2	6.1
Se	nd	2.1	nd	1.30	0.10	nd	nd	nd
Br	3.2	0.68	1.31	0.68	1.26	0.91	0.94	0.67
Rb	552	517	508	421	475	205.0	346	219
Sr	nd	36	35	49	nd	586	45	108
Ag	nd	1.4	1.2	0.7	1.83	nd	nd	nd
Sb	0.72	2.5	8.6	1.07	0.14	0.09	0.26	0.29
Cs	25.1	24.4	13.2	16.3	3.1	5.0	10.9	6.8
Ba	4526	861	651	1566	1787	709	1336	6402
La	13.98	17.91	11.51	24.09	27.18	27.59	9.02	7.93
Ce	32.3	47.7	22.2	39.3	77.2	49.6	28.0	46.7
Nd	15.7	17.3	6.1	9.9	27.3	23.2	4.3	3.9
Sm	3.2	4.0	1.2	2.3	6.7	4.4	1.2	1.1
Eu	0.66	0.84	0.24	0.45	1.87	1.32	0.29	0.28
Tb	0.49	0.57	0.29	0.33	1.02	0.53	0.22	0.17
Yb	1.48	1.52	1.41	1.2	2.5	1.65	0.88	0.62
Lu	0.19	0.20	0.21	0.17	0.51	0.24	0.14	0.10
Hf	2.6	2.5	1.5	1.8	3.3	2.7	1.4	1.4
Ta	0.20	0.19	0.27	0.33	0.68	0.37	0.20	0.22
Hg	nd	nd	0.35	nd	0.36	nd	nd	nd
Au	nd	nd	0.004	0.003	9.13	0.01	0.004	0.005
W	3.4	6.7	<1	1.01	3.9	1.17	1.73	2.40
Th	2.9	2.3	4.9	7.2	6.7	6.7	3.7	2.2
U	0.76	0.81	1.65	1.95	0.93	1.11	0.85	0.59

	Separated Sample Chemistry							
SAMPLE	KM-114	KM-115	KM-116	KM-127	KM-128	KM-129	KM-131	KM-144
NaO	0.70	0.13	2.37	0.20	0.27	3.60	2.72	0.27
CaO	na	na	1.56	0.52	na	na	na	na
FeO	0.58	0.62	0.81	1.16	0.92	1.17	0.99	1.18
Sc	1.4	1.0	7.3	9.7	6.9	2.0	12.2	15.8
Cr	120.7	229.4	366.0	625.0	208.3	144.3	119.4	309.0
Co	9.74	14.47	44.8	37.3	10.77	1.657	7.17	3.95
Zn	132	126	158	61	143	42.6	113.4	121
As	9.11	26.57	6.77	3.70	3.20	20.80	7.50	8.91
Se	nd	nd	1.00	nd	nd	1.70	0.90	1.80
Br	0.79	0.90	0.84	0.73	0.87	nd	2.50	0.65
Rb	303	284	295	467	469	374	330	854
Sr	211	416	217	nd	86	157	465	68
Ag	nd	nd	nd	nd	nd	nd	nd	nd
Sb	0.18	0.20	0.29	0.36	0.19	0.33	0.31	0.35
Cs	5.5	11.1	20.8	19.1	22.8	2.1	20.1	146
Ba	8510	38899	991	950	935	481	926	594
La	10.0	9.8	11.9	15.1	20.9	32.2	26.1	23.6
Ce	23.9	20.2	31.8	57.9	63.7	91.0	53.8	67.8
Nd	8.1	3.8	5.8	17.5	20.5	33.5	22.0	24.6
Sm	1.4	1.6	1.4	3.7	4.2	7.4	4.7	5.3
Eu	0.44	0.48	0.51	0.82	0.81	1.32	1.7	0.78
Tb	0.30	0.63	0.32	0.54	0.53	1.16	0.72	0.69
Yb	1.3	2.3	1.91	1.29	1.28	3.87	2.2	1.60
Lu	0.19	0.30	0.29	0.16	0.18	0.57	0.30	0.21
Hf	1.7	2.09	2.7	1.6	2.2	4.8	2.5	2.6
Ta	0.18	0.23	0.24	0.13	0.18	1.16	0.40	0.22
Hg	nd	nd	nd	0.38	nd	nd	0.41	nd
Au	0.00	0.00	0.00	0.00	nd	nd	nd	0.00
W	nd	nd	nd	nd	2.9	0.5	35.8	2.5
Th	3.3	3.4	4.7	2.1	2.3	14.5	3.5	4.8
U	0.77	1.6	2.4	0.59	0.61	2.6	0.84	0.80

	Separated Sample Chemistry							
SAMPLE	KM-148	KM-149	KM-150	KM-152	KM-153	KM-154	KM-155	KM-156
NaO	4.86	3.77	2.83	4.95	1.65	0.35	0.43	0.82
CaO	na	2.40	na	0.75	na	na	na	na
FeO	1.44	1.26	1.38	0.84	0.67	1.65	1.46	0.96
Sc	2.91	2.71	3.70	5.05	0.80	6.18	1.78	4.67
Cr	302.0	428.0	513.0	98.7	507.0	3.4	351.0	257.2
Co	2.02	2.67	2.86	3.94	1.8	4.07	2.53	1.94
Zn	35.2	29	47.8	150	23.6	68.8	167	61.2
As	nd	10.90	9.20	7.40	14.20	8.50	16.78	26.00
Se	0.50	nd	nd	nd	3.60	nd	nd	2.80
Br	0.52	0.67	0.34	1.16	0.61	0.44	1.55	0.77
Rb	141	315	359	300	384	461	410	704
Sr	449	382	599	417	99	73	118	106
Ag	nd	nd	nd	nd	nd	0.70	0.33	nd
Sb	0.06	0.40	0.39	0.24	2.6	7.7	3.1	0.58
Cs	2.2	2.5	18.6	8.3	2.1	16.0	13.3	5.9
Ba	704	1068	894	829	1044	800	1256	1859
La	27.5	33.4	27.7	55.8	23.2	16.0	39.7	25.09
Ce	103.4	78.2	65.2	103.5	83.9	34.7	66.4	53.0
Nd	28.4	27.1	24.6	49.9	nd	15.2	16.9	20.4
Sm	7.6	5.9	5.3	10.8	7.1	4.4	3.5	4.5
Eu	1.6	2.0	1.7	2.6	0.96	1.06	0.62	1.12
Tb	1.4	1.0	0.8	1.7	1.6	1.5	0.39	0.59
Yb	5.0	3.3	2.5	4.0	5.6	5.1	1.2	1.9
Lu	0.74	0.47	0.34	0.54	0.72	0.71	0.18	0.27
Hf	6.5	3.0	3.3	3.7	1.8	3.3	2.4	4.8
Ta	1.5	0.60	0.86	0.23	0.42	0.45	1.09	0.39
Hg	nd	nd	nd	nd	nd	nd	nd	nd
Au	nd	0.01	0.01	0.00	0.01	0.00	0.03	0.09
W	11.8	16.1	45.0	2.2	6.4	3.6	4.0	3.6
Th	17.3	9.2	6.5	3.0	5.5	5.9	17.6	3.7
U	3.2	2.0	1.0	1.5	0.97	1.1	4.8	1.0

	Separated Sample Chemistry			
SAMPLE	KM-157	KM-158	KM-159	KM-160
NaO	1.69	5.36	0.59	0.60
CaO	1.39	na	na	na
FeO	0.84	0.63	1.0	1.1
Sc	10.9	2.16	7.21	6.0
Cr	40.1	95.2	297.4	61.4
Co	1.53	1.4	7.4	5.8
Zn	133.4	42	202	231
As	7.3	1.8	4.9	7.7
Se	nd	1.50	4.20	nd
Br	0.61	nd	0.89	0.95
Rb	263	93	662	588
Sr	166	491	45	168
Ag	nd	5.0	2.9	nd
Sb	0.43	0.23	1.8	2.9
Cs	67.8	13.9	23.8	48.2
Ba	415	674	2622	1385
La	27.1	19.7	20.6	37.8
Ce	59.9	31.2	55.8	94.1
Nd	21.6	7.4	22.5	34.5
Sm	5.3	1.3	5.0	7.8
Eu	1.2	0.68	1.0	1.7
Tb	0.79	0.18	1.0	1.1
Yb	2.2	1.0	3.9	3.6
Lu	0.31	0.15	0.56	0.53
Hf	3.0	2.4	2.7	2.7
Ta	0.39	0.39	0.30	0.33
Hg	nd	nd	nd	nd
Au	nd	nd	nd	0.003
W	1.9	0.90	4.9	2.7
Th	4.0	9.8	4.3	3.6
U	1.9	1.6	1.3	1.2

Appendix V

DELTAS TurboBasic Version 1987

This program calculates hypothetical igneous precursor compositions. It is based on the equations of F. G. Smith (1963) from Physical Geochemistry, p.377 along with linear relationships among the oxides of Daly's average igneous rock compositions (1933). The ratio of $Al_2O_3/(Al_2O_3 + Fe_2O_3t)$ is assumed to remain unchanged during alteration. Initial conditions are calculated from the following equations:

$$FeO = -0.7031 * Al_2O_3 + 0.6584 * (Al_2O_3 + Fe_2O_3t)$$
$$SiO_2 = \exp(1.247 * ratio + 3.264)$$
$$TiO_2 = \exp(3.590 - 5.482 * ratio)$$

The iteration process begins with calculations of cfm and alk from the equations:

$$cfm = 2.229 * (Al_2O_3 + Fe_2O_3t) - 2.383 * Al_2O_3$$
$$alk = 0.112 * (sil + cfm) - 0.1954 * cfm$$

where cfm is from a linear regression and alk is from Smith (1963). FeO is calculated again from the equation above and then SiL, TiO_2, Al_2O_3, Fe_2O_3t, cfm, and alk are recalculated to the original sum.

The iteration is then repeated until successive values of SiO_2 are within 0.1% tolerance. When iteration is complete, the remaining oxides are calculated from the equations

$$MgO = -21.70 * ratio + 18.79$$
$$MnO = -3644 * ratio + 0.3846$$
$$CaO = cfm - FeO - MnO - MgO$$
$$Na_2O = 0.3727 * Al_2O_3 - 0.111 * (Al_2O_3 + Fe_2O_3t)$$
$$K_2O = alk - Na_2O$$

The oxides are then recalculated to 100% and mass balance is calculated by ratioing the

hypothetical $Al_2O_3 + Fe_2O_3t$ to the analyzed concentrations and adjusting all the oxides by this ratio.

This thesis is accepted on behalf of the faculty of the New Mexico Institute of Mining and Technology by the following committee:

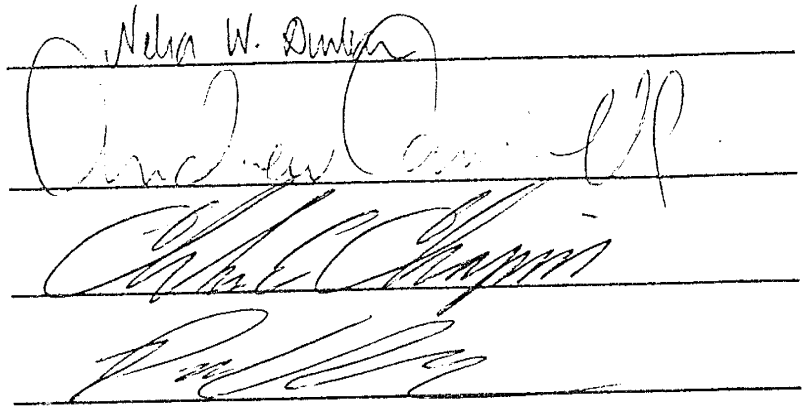

I release this document to the New Mexico Institute of Mining and Technology.

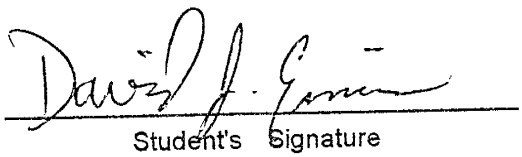

Student's Signature

Aug. 20, 1996

Date